

**STATUS REPORTS**

to the

**PAPERMAKING**

**PROJECT ADVISORY COMMITTEE**

VOLUME I

March 23, 1998

INSTITUTE OF PAPER SCIENCE AND TECHNOLOGY

Atlanta, Georgia

**ANNUAL PROGRAM REVIEW**

PAPERMAKING

VOLUME I

March 23, 1998





February 16, 1998

TO: MEMBERS OF THE PAPERMAKING PROJECT ADVISORY COMMITTEE

Attached for your review are the Status Reports for the projects to be discussed at the Papermaking Project Advisory Committee meeting being held at the Institute of Paper Science and Technology. The Program Review is scheduled for Monday, March 23, 1998, from 1:00 p.m. to 5:00 p.m. and the PAC Committee Meeting will meet on Tuesday, March 24, from 1:00 p.m. to 5:00 p.m.

We look forward to seeing you at this time.

Sincerely,

A handwritten signature in black ink that reads "David I. Orloff". The signature is written in a cursive, flowing style.

David I. Orloff, Ph.D.  
Professor of Engineering & Director  
Engineering and Paper Materials Division

DIO/map

Attachments

---

***Institute of Paper Science and Technology, Inc.***



**PAPERMAKING  
PROJECT ADVISORY COMMITTEE**

**IPST Liaison: Dr. David Orloff (404) 894-6649; FAX (404) 894-1496  
RAC Liaison: Mr. John Bergin (715) 422-2239; FAX (715) 422-2227**

Dr. Dwight E. Anderson \*(2001)  
Project Manager  
Weyerhaeuser Company  
WTC 2F39  
Post Office Box 2999  
Tacoma, WA 98477-2999  
(253) 924-6466  
(253) 924-6541 FAX

Mr. Jack Burke \*(1999)  
Principle Project Manager  
Radian International LLC  
1979 Lakeside Parkway  
Suite 800  
Tucker, GA 30084  
(770) 414-4522  
(770) 414-4919 FAX

Mr. William O. Burns \*(1999)  
Director, Manufacturing Technology  
Fort James Corporation  
1915 Marathon Avenue  
Post Office Box 899  
Neenah, WI 54957-0899  
(920) 729-8437  
(920) 729-8597 FAX

Dr. Partha S. Chaudhuri \*(1999)  
Senior Scientist, Papermaking  
Champion International Corporation  
Technical Center  
West Nyack Road  
West Nyack, NY 10994  
(914) 578-7123  
(914) 578-7474 FAX

Mr. Frank Cunnane \*(1999)  
Vice President, Technology  
Asten, Inc.  
4399 Corporate Road  
Post Office Box 118001  
Charleston, SC 29423  
(803) 747-7800  
(803) 747-3856 FAX

Mr. Marcel Dauth \*(1998)  
St. Laurent Paperboard Inc.  
630 Rene Levesque Blvd, West  
Suite 3000  
Montreal, Quebec H3B 5C7, CANADA  
(514) 864-5108  
(514) 861-9559 FAX

Dr. Christopher P. Devlin \*(2001)  
Process Engineering Manager  
Inland Eastex  
A Temple-Inland Company  
Post Office Box 816  
Silsbee, TX 77656  
(409) 276-3190  
(409) 276-3419 FAX  
cdevlin@iccnet.com

Mr. William Haskins \*(1998)  
Market Development Manager  
Specialty Minerals Inc.  
35 Highland Avenue  
Bethlehem, PA 18017  
(610) 882-8652  
(610) 882-8760 FAX

Mr. Neil E. Johnson \*(2000)  
Research Engineering  
Potlatch Corporation  
20 North 22nd Street  
Cloquet, MN 55720  
(218) 879-2321  
(218) 879-2375 FAX

Dr. Charles Kramer \*(1998)  
Director  
Albany International Research Company  
Post Office Box 9114  
Mansfield, MA 02048  
(508) 337-9541  
(508) 339-4996 FAX

Mr. David J. Lacz \*(2001)  
Technical Associate  
Eastman Kodak Company  
Paper Support Division B-319  
1669 Lake Avenue  
Rochester, NY 14652-3622  
(716) 477-6301  
(716) 588-2680 FAX  
dlacz@kodak.com

Mr. Joseph P. MacDowell \*(1999)  
Research Project Supervisor - Coated  
and Uncoated  
P.H. Glatfelter Co.  
228 South Main Street  
Spring Grove, PA 17362-1000  
(717) 225-4711  
(717) 225-7454 FAX  
jmacdowell@glatfelter.com

## **Papermaking PAC (cont.)**

Dr. Michael Marziale \*(1999)  
Technical Assistant to the Wickliffe Mill Manager  
Westvaco Corporation  
1724 Westvaco Road  
Post Office Box 278  
Wickliffe, KY 42087-0278  
(502) 335-4203  
(502) 335-4101 FAX

Dr. Franco Palumbo \*(1997)  
Riverwood International Corporation  
Post Office Box 35800  
West Monroe, LA 71294-5800  
(318) 362-2000  
(318) 362-2133 FAX

Dr. Paul R. Proxmire \*(2001)  
Research Associate  
Appleton Papers Inc.  
Post Office Box 359  
Appleton, WI 54912-0359  
(920) 730-7254  
(920) 991-7243 FAX

Mr. Thomas E. Rodencal \*(Alternate)  
Sr. Paper Mill Staff Engineer  
Georgia-Pacific Corporation  
133 Peachtree Street, NE  
18th Floor  
Atlanta, GA 30303  
(404) 652-4514  
(404) 584-1466 FAX

Dr. Jay A. Shands \*(2001)  
Manager, Forming Systems  
Beloit Corporation  
Rockton Research Center  
1165 Prairie Hill Road  
Rockton, IL 61072-1595  
(608) 364-8501  
(608) 364-8600 FAX

Mr. Jay Thiessen \*(2000)  
Consolidated Papers, Inc.  
Post Office Box 8050  
Wisconsin Rapids, WI 54495-8050  
(715) 422-1616  
(715) 422-1639 FAX

Mr. Vic Nisita \*(2001)  
Operations Superintendent  
Wisconsin Tissue Mills  
Chicago Operations  
13101 S. Polaski Road  
Alsip, IL 60658  
(708) 824-4397  
(708) 389-4901 FAX

Mr. Jason R. Panek \*(2001)  
Technical Director  
Manistique Papers  
453 S. Mackinac Avenue  
Manistique, MI 49854  
(906) 341-2175  
(906) 341-5635 FAX

Mr. Jeffrey R. Reese \*(2001)  
Consultant, Paper Mill  
Georgia-Pacific Corporation  
133 Peachtree Street, NE  
18th Floor  
Atlanta, GA 30303  
(404) 652-4880  
(404) 584-1466 FAX  
JReese@GAPAC.com

Mr. John Rogers \*(1997)  
Technical Director  
Sandusky International Inc.  
Post Office Box 5012  
Sandusky, OH 44870-8012  
(419) 626-5340  
(419) 626-8674 FAX

Mr. Stephen G. Simmons \*(1998)  
Technical Manager, Fiber Development  
The Mead Corporation  
Mead Central Research Laboratories  
232 Eighth Street  
Chillicothe, OH 45601-5700  
(614) 772-3051  
(614) 772-3595 FAX  
stephen\_simmons@mead.com

Mr. David G. Thurman \*(Alternate)  
Project Leader, Board  
EKA Chemicals Inc.  
2211 Newmarket Parkway  
Suite 106  
Marietta, GA 30067

***Papermaking PAC (cont.)***

Mr. Thomas K. Toothman \*(Alternate)  
Paper Mill Superintendent  
Wisconsin Tissue Mills Inc.  
Third & Tayco Streets  
Post Office Box 489  
Menasha, WI 54952  
(920) 725-2431  
(920) 727-2940 FAX

Mr. Lloyd O. Westling \*(1999)  
Vice President, Production Planning  
Longview Fibre Company  
Post Office Box 639  
Longview, WA 98632  
(360) 425-1550  
(360) 575-5925 FAX

Mr. Jim Watson \*(2001)  
Sr. Technical Sales Representative  
EKA Chemicals Inc.  
2211 Newmarket Parkway  
Suite 106  
Marietta, GA 30067

Dr. David E. White \*(2001) (Chairman)  
Research Associate  
Union Camp Corporation  
Post Office Box 3301  
Princeton, NJ 08543-3301  
(609) 844-7249  
(609) 844-7366 FAX  
Dave\_E.\_White@ucamp.com



**PAPERMAKING  
PROJECT ADVISORY COMMITTEE MEETING**

*March 23, 1998*

**Institute of Paper Science and Technology  
Atlanta, Georgia**

**PROGRAM REVIEW AGENDA**

**Seminar Room 114**

1:00 p.m. - 1:10 p.m.	Opening Remarks Review Antitrust Statement Confidentiality Statement	David White
1:10 p.m. - 1:25 p.m.	Welcome from Vice President of Research	Gary Baum
1:25 p.m. - 1:35 p.m.	Overview of IPST Papermaking Research	David Orloff
1:35 p.m. - 2:10 p.m.	Project F004 Approach Pipe Systems	Xiaodong Wang
2:10 p.m. - 2:55 p.m.	Project F005 Headbox and Forming Hydrodynamics	Cyrus Aidun
2:55 p.m. - 3:10 p.m.	Break	
3:10 p.m. - 3:40 p.m.	Project F003 Fundamentals of Coating Systems	Cyrus Aidun
3:40 p.m. - 4:10 p.m.	Project F002 Fundamentals of Web Heating	Tim Patterson
4:10 p.m. - 5:10 p.m.	Project F001 Status of Impulse Drying Commercialization	David Orloff
5:10 p.m. - 6:00 p.m.	Sub Committee Discussions of Projects	



**PAPERMAKING  
PROJECT ADVISORY COMMITTEE MEETING**

*March 24, 1998*

**Institute of Paper Science and Technology  
Atlanta, Georgia**

**COMMITTEE DISCUSSIONS AGENDA**

**Room 177**

1:00 p.m. - 1:10 p.m.	Convene - Antitrust Statement - Confidentiality Statement - New Members - Acceptance of Fall, 1997 minutes - Review of agenda	White
1:10 p.m. - 1:40 p.m.	RAC Report Research Roadmap	John Bergin David White, David Orloff
1:40 p.m. - 2:00 p.m.	Project F022 Flow Through Porous Media presentation	Seppo Karrila
2:00 p.m. - 2:20 p.m.	Project F021 Drying presentation	Fred Ahrens
2:20 p.m. - 2:50 p.m.	Approach Flow Systems (F004- Wang)	<b><u>Johnson</u></b> , Westling, Marziale, Thiessen
2:50 p.m. - 3:00 p.m.	Break	
3:00 p.m. - 3:30 p.m.	Headbox and Forming Hydrodynamics (F005- Aidun)	<b><u>Shands</u></b> , Anderson, Burns, Devlin, Panek
3:30 p.m. - 4:00 p.m.	Fundamentals of Coating Systems (F003-Aidun)	<b><u>Simmons</u></b> , Proxmire, Bergin
4:00 p.m. - 4:30 p.m.	Web Heating and Pressing of Heated Webs (F002-Patterson)	<b><u>Cunnane</u></b> , MacDowell, Lacz
4:30 p.m. - 5:00 p.m.	Impulse Drying (F001- Orloff)	<b><u>Kramer</u></b> , Rogers, Haskins
5:00 p.m. - 5:30 p.m.	Pressing, Drying (F021, F022)	<b><u>Chaudhuri</u></b> , Palumbo, Nisita, White, Reese



## TABLE OF CONTENTS

		<b>Page</b>
<b><u>Volume I:</u></b>		
Project F001	Fundamentals of Drying	1
Project F002	Fundamentals of Web Heating	129
<b><u>Volume II:</u></b>		
Project F003	Fundamentals of Coating Systems	171
Project F004	Approach Flow Systems	185
Project F005	Fundamentals of Headbox and Forming Hydrodynamics	269



FUNDAMENTALS OF DRYING

STATUS REPORT

FOR

PROJECT F001

David I. Orloff (PI)  
P. Phelan, T. Patterson, I. Rudman,  
F. Bloom, A. Woods, A. Dowdell

March 23-24, 1998

Institute of Paper Science and Technology  
500 10th Street, N.W.  
Atlanta, Georgia 30318



**PROJECT SUMMARY**

**Project Title:** FUNDAMENTALS OF DRYING

**Project Code:** DRYING

**Project Number:** F001

**PAC:** Papermaking

**Division:** Engineering

**Project Staff**

**Faculty/Senior Staff:** D. Orloff  
**Staff:** P. Phelan, T. Patterson, I. Rudman,  
F. Bloom, A. Woods, A. Dowdell

**FY 97-98 Budget:** \$190,200

**Allocated as Matching Funds:** \$0

**Time Allocation**

**Faculty/Senior Staff:** 0.20 man-yrs  
**Support:** 2.00 man-yrs

**Supporting Research**

**M.S. Students:** none  
**Ph.D. Students:** A. Woods (Northern Illinois University)  
**External:** U.S. DOE: Project 3595: FY'97-98 \$212,800

**RESEARCH LINE/ROADMAP:** Increase paper-machine productivity by 30% over '97 levels via focus on breakthrough forming, dewatering, and drying concepts. Develop technologies for increased press solids, improved runnability, and methods to control sheet properties and structure.

**PROJECT OBJECTIVE:** To develop an understanding and a database for commercialization of advanced water removal systems based on high intensity drying principles. This new technology will reduce capital costs, increase machine productivity, reduce virgin fiber use, reduce the amount of energy used, and improve paper physical properties.

**PROJECT BACKGROUND:** The Institute's impulse drying project has focused on developing and demonstrating the technology for board grades of paper. In recent years this has resulted in the invention of a new ramp decompression concept that shows promise for increasing the operating window of the technology to a wider range of furnishes, grades, and refining levels.

**SUMMARY OF RESULTS:** Work on the dues-funded (No. F001) project and on the separate DOE funded (No. 3595) project are behind on schedule as a result of the need for additional process development work. The dues-funded work has focused on evaluating nip decompression and post-nip depressurization techniques as used on the Beloit X2 pilot paper machine and developing a theoretical framework for the design of plasma sprayed press roll surfaces. The DOE-funded work (in collaboration with and partially funded by Beloit) has concentrated on implementing IPST impulse drying technology on Beloit's No. 4 and No. 2 pilot paper machines. The key accomplishments of this period are summarized in this section.

- Patents: A U.S. patent on the use of a ramped decompression to eliminate delamination was issued on September 23, 1997, as U.S. Patent number 5,669,159. Beloit has funded the foreign filing of this patent. An apparatus patent will issue on March 3, 1998 as U.S. Patent number 5,722,183.
- Publications: Members of the Impulse Drying team presented four papers at the 1997 TAPPI Engineering & Papermakers Conference, three of these have been accepted for publication in TAPPI Journal.
  1. "High-Speed Infrared Detection of Coated Roll Surface Defects," TAPPI Proceedings 1997, Engineering & Papermakers: Forming Bonds for Better Papermaking, Book 2, pp. 971-987.
  2. "Opening the Operating Window of Impulse Drying: III. Controlled Decompression Experiments," TAPPI Proceedings 1997, Engineering & Papermakers: Forming Bonds for Better Papermaking, Book 3, pp. 1489-1500.
  3. "Opening the Operating Window of Impulse Drying: II. Pressure Differential as a Source of Delamination," TAPPI Proceedings 1997, Engineering & Papermakers: Forming Bonds for Better Papermaking, Book 3, pp. 1467-1488.
  4. "Opening the Operating Window of Impulse Drying - I. The Effect of Ambient Pressure at Nip Opening," TAPPI Proceedings 1997, Engineering & Papermakers: Forming Bonds for Better Papermaking, Book 3, pp. 1457-1466.
- Experiments on the Beloit X4 pilot paper machine demonstrated that an earlier roll coating durability problem has been solved. They also showed that further development work on sheet picking, implementation of delamination suppression techniques and CD temperature control are necessary in order to ensure success on the X4 machine.

- Experiments on the Beloit X2 pilot paper machine were carried out to resolve issues identified on the X4 machine. Two methods of implementing the IPST press nip decompression were investigated. The results confirmed that the IPST technology can be used to increase impulse drying operating temperatures. The work also led to the development of techniques to minimize picking.
- A proposal, titled "Press and Dryer Roll Surfaces and Web Transfer Systems For Ultra High Paper Machine Speeds," was submitted to the DOE Agenda 2020 capital effectiveness initiative and is included in this report.
- A report titled "Delamination Bucking and Spalling of Plasma Sprayed Thermal Barrier Coating for Impulse Drying", was completed and is included in this report.

### **GOALS FOR FY 98-99:**

- Conduct experiments on the Beloit X2 pilot paper machine at higher basis weights and higher ingoing solids to match those required to produce 26 lb/1000 ft<sup>2</sup> linerboard where the impulse dryer is operating at typical ingoing solids of a third press. These experiments will seek to optimize press shoe pressure profile, blanket groove geometry, felt, and post-nip decompression.
- Conduct experiments on the Beloit X4 pilot paper machine at a basis weight of 42 lb/1000 ft<sup>2</sup> at an ingoing solids typical of current third press applications. The objective of these experiments will be to set up the machine for a long demonstration run.
- Demonstrate impulse drying of 42 lb/1000 ft<sup>2</sup> linerboard on the Beloit X4 pilot paper machine. Produce sufficient number of rolls of paper for converting trials.
- Conduct converting trials and report results.

### **DELIVERABLES:**

- Report on the optimization of the press shoe pressure profile, blanket groove geometry, felt, and post-nip decompression for production of 26 lb/1000 ft<sup>2</sup> linerboard.
- Report on the runnability and drying efficiency of the Beloit X4 pilot paper machine during the impulse drying of linerboard. The report will also include a discussion of the physical properties of the linerboard as well as a discussion of the convertibility and physical properties of the containerboard produced from that linerboard.

**SCHEDULE** (dates depend on availability of Beloit pilot paper machines):

TASKS	1st Qtr'98	2nd Qtr'98	3rd Qtr'98	4th Qtr'98
Beloit X2 experiments to optimize conditions to produce 26 # linerboard where impulse dryer is a third press.	-----X			
Shakedown trial on Beloit X4; using Beloit G roll, hover press, adjustable shoe ramp, enclosed inductors, loaded Teflon doctor, and shower temperature profile control. Produce 42# linerboard for physical testing.		--X		
XPM#4: Produce 42# linerboard for physical testing and in quantities required for converting trials.		--X		
Double-back corrugating trial.		--X		
Post-printing printability trial.		--X		
Box making and testing		--X		
Analysis of results and report writing			-----X	

**DISCUSSION****A. Overview**

In January 1997 the Beloit X4 pilot paper machine was started up in a single-felted wet pressing mode to verify that 205 gsm linerboard could be produced at machine speeds of 1250 ft/min. The machine has a vertical twin wire forming section, while the press section was configured with a bi-nip roll press followed by a 10-inch-long shoe press (ENP). The bi-nip was set at a press loading of 400 pli on the first press and 600 pli on the second press. The ENP was configured with a post-nip roll wrap and set at 6000 pli. The press roll of the ENP was coated with Beloit "E" coating, while an Albany International "CSX" press felt was used. Employing a once-dried Kraft (composed of mixed softwood, hardwood, and OCC) repulped to a freeness of 670 ml CSF, press dryness of between 48 to 50% was achieved at a basis weight of 209 gsm. Samples from the reel were tested yielding an average caliper of 346  $\mu\text{m}$  and an average apparent density of 0.605  $\text{g}/\text{cm}^3$ .

Also in January 1997, the ENP roll on the Beloit X4 pilot paper machine was heated to 325°F and an attempt was made to thread a paper web through the press section. The paper stuck to the roll before the web could be broken back to the former. Attempts to clean the roll failed and it was decided to cool the roll down to facilitate cleaning. After cleaning the paper off the roll, two areas of cover failure were noticed. The failure occurred towards the bottom surface of the coating and not in the bond coat or at the steel surface of the roll. This event ended the scheduled impulse drying experiments. Co-current roll coating durability testing at IPST had shown that a coating of similar composition (but reduced thickness) had been exposed to nearly 5 million thermal and mechanical cycles without failure. Based on these results, and a comparison of the

coating thickness on the ENP roll and the IPST roll, it was decided to go ahead with the March X4 experiments with a roll coated with a thinner coating of Beloit "E".

Also in January 1997, low-speed heated roll press experiments, performed at Beloit, suggested that a post-nip roll wrap does help to inhibit sheet delamination during impulse drying.

In February 1997, an investigation was begun on what mechanisms could cause such a failure. A literature search was performed and development of an analytical model and experimental data were begun by IPST. To confirm IPST roll durability results, the IPST press roll on the roll durability test facility was thoroughly cleaned and the coating was examined under 30X magnification. This magnification makes it possible to identify defects on the order of 5-10 mm in width, which were typical crack widths observed on the failed X4 roll. An examination did not reveal any cracking.

In March 1997, experiments were continued on the Beloit X4 machine. The thinner roll coating survived, felt performed above expectations, and threading was accomplished at high temperature. Linerboard, at a basis weight of 205 gsm, was produced at speeds of 1250 to 1500 ft/min. No roll coating cracking or spalling was noted after two weeks of operation at speed, load, and temperature. The Albany International CSX felt operated to 500°F, at a speed of 1500 ft/min and a press load of 6000 pli. The machine could be threaded at a roll temperature of 400°F. CD temperature uniformity, basis weight, and load are important at thread-up.

The control of CD roll surface temperature specifically during initial roll heating, threading, and steady state operation is important and required additional development. Sheet picking was observed at higher roll temperatures than were previously observed on Beloit's heated roll press and IPST's MTS. This made CD roll surface control critical during attempts to set the roll temperature between the sticking temperature and the critical impulse drying temperature. The available post-nip felt wrap yielded a pressure of 20 kPa, which was insufficient to prevent sheet delamination even for high freeness. As a result, the picking temperature was higher than expected and the critical temperature was lower than expected, resulting in a nonexistent operating window. It was observed during the trial that Teflon blocks holding thermocouples to the heated roll surface yielded MD streaks in the web where there was no picking while adjacent areas of the sheet showed picking. This suggested two courses of action: either include Teflon in the roll surface coating or apply it continuously, with a Teflon doctor, during normal roll operation.

In April 1997, it was decided to continue the shakedown work on Beloit's, more readily available, X2 pilot paper machine. In order to address the sticking problem, Beloit initiated development of a new roll coating, Beloit G, in preparation for June roll sticking experiments on the X2 machine. That trial used two different furnishes, the furnish used in the March '97 trial and a once dried Virgin softwood Kraft furnish from a different source. The objective of the trial was to evaluate the roll coating susceptibility to sticking under wet pressing conditions and under impulse drying conditions at temperatures of 300 °F to 450 °F. Beloit also scheduled time in July to optimize the decompression ramp of the press shoe pressure profile. IPST began supporting the development of an optimized shoe profile by conducting MTS simulations.

In May 1997, a laboratory investigation to determine a range of ramp profiles which are both physically possible on a shoe press and which provide a reasonable increase in critical temperature was performed at IPST. The work was done using the same furnish as was used during the March '97 X4 trial and was performed on the MTS hydraulic

press. The results were evaluated and suggested ramp profiles were communicated to Beloit. During that time, Beloit began building the new shoe which was designed to incorporate a ramp on the end of a shortened ENP shoe. The design allowed for the start pressure and duration of the ramp to be adjustable when the shoe is taken out of the machine.

Additional roll durability testing brought the IPST press roll, with the four coatings to approximately 10 million thermal/mechanical cycles. The roll was cleaned and examined under 100X magnification. There were no new cracks observed (when the roll was delivered to IPST, one coating had some small (< 5 mm long) cracks along the edges of the coating; these have not changed in size or appearance). Some pitting (< 1 mm diameter) was observed in the Beloit A coating. The Beloit E coating showed only one or two pits over its entire surface.

In June 1997, the furnish used in March '97 was run on the X2 machine equipped with the new Beloit "G" press roll coating. The shoe used was a standard shoe with no ramp. The intent of this trial was solely to investigate sticking. The new roll coating was successful in preventing sticking at roll temperatures of 180 to 210°C. This range was chosen as it caused considerable sticking during the March trial. As a last step, the 100% Virgin Kraft was run. There was also no sticking with that furnish in the temperature range of 356 to 410°F.

In July 1997, an X2 machine trial took place as planned. This trial used a once-dried Virgin softwood Kraft furnish at 550 ml CSF, 30% ingoing solids, and at a machine speed of 1250 fpm. As with all previous X2 trials, sheet weight was limited to 100 gsm. The purpose of this trial was to evaluate recent shoe modifications and determine an optimized ramp for the operating conditions. The shoe evaluated was a 6-inch-long shoe with an 8-inch extension designed to produce a ramp at the end of the main profile. The extension was adjustable when taken out of the machine. This allowed limited but time consuming modification of the ramp characteristics. This preliminary work showed the ramp could be used to increase the critical temperature by at least 40 to 70°F.

In August 1997, an X2 machine trial took place as planned. This trial used the same once dried Kraft, at 550 ml CSF, at an ingoing solids of 30%, 100 gsm, and at a continuous machine speed of 1250 fpm. The purpose of this trial was to continue the work begun during the July X2 trial, specifically optimization of the trailing ramp portion of the pressure pulse. The shoe evaluated was the same as was used in July 1997. During the trial a profile was found which made it possible to impulse dry the sheet with a roll temperature in excess of 405°F. In addition to this work it was also shown that by applying a Teflon doctor blade to the heated roll surface, with sufficient pressure, picking can be significantly reduced. Physical testing of samples from the August X2 trials showed a 100°F increase in critical temperature, and a 6% increase in dryness, and up to a 20% increase in STFI.

The shoe used in the trial had the disadvantages of requiring that it be removed from the ENP in order for the ramp profile to be adjusted and that the short shoe resulted in peak loads that induced picking. To rectify these shortcomings, a standard 10-inch shoe would be used with two newly designed modifications. One was a more "user friendly" shoe that could also be used on the X4 machine. The other was a mechanism for applying air pressure to the web just as it exits the nip. The mechanism would apply air pressure (~30 psi max.) over an area the full CD width of the machine and about 4 to 7 inches in the MD direction. It can best be thought of as a stationary hover craft. A preliminary version of the device was tested on Beloit's heated roll press using large hand sheets. A

version of the device which could be used on both the X2 and the X4 was jointly designed by Beloit and IPST. The geometry of the two machines requires that each use a slightly different design. Specifically, IPST personnel performed an analysis to determine the air flow requirements for such a device. The air flow required is such that a high flow rate compressor is required.

In September 1997, preliminary tests of a prototype "hover press" on Beloit's slow speed heat roll press indicated that there was no decrease in outgoing solids resulting from the applied air pressure. Additionally, the process appeared to inhibit delamination.

In October 1997, meetings were held between Beloit and IPST to scope out X2 experiments planned for December 1997. It was agreed to use a standard 10-inch shoe with a 4-inch ramp extension as well as a "hover press." Beloit designed the ramp extension so that the applied pressure, and the resultant ramp profile can be adjusted while the machine is running. This provides a significant advantage over the previous design. The "hover press" was designed with chambers allowing for progressive decreases in applied air pressure as distance from the nip exit increases. The peak applied air pressure was 30 psig. IPST arranged to have a large capacity (600 CFM at 30 psig) air compressor available for the test to supply air to the "hover press."

In December 1997 and early January 1998, impulse drying experiments were conducted on the Beloit X2 pilot paper machine. In December, the research team concentrated on installing the equipment and determining optimum operating conditions for both the new press shoe and the "hover press." A full week of experiments were conducted in early January, in which the optimum internal ramp and external hover press combinations were evaluated for a range of freeness and over a range of machine speeds. In addition, two blanket drainage geometries were also investigated. The results of these experiments are detailed in section B of this report.

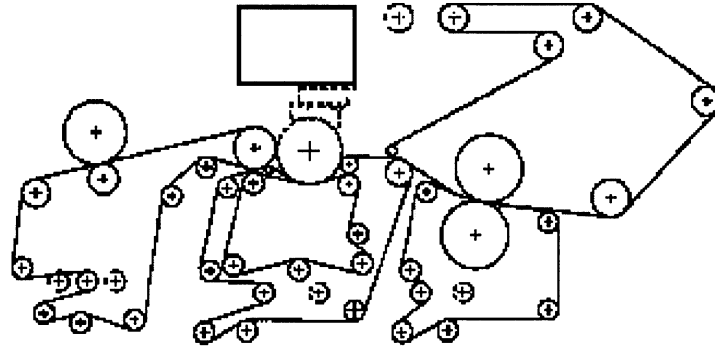
#### B. X2 Pilot Paper Machine Experiments.

This section will review two sets of experiments performed on the Beloit X2 pilot paper machine, those performed in July and August 1997, and those performed in January 1998.

##### ***The Summer Experiments:***

The purpose of the experiments, conducted in July and August 1997, was to verify that the ramp decompression concept could be used to extend the temperature operating window of high-speed continuous impulse drying and that sheet/roll surface picking could be eliminated by proper choice of press roll surface and/or by Teflon doctoring.

These and later experiments were conducted on Beloit's X2 pilot paper machine. While the machine has certain limitations with regard to basis weight, ingoing solids and width, it has the advantages of having an induction heated open extended nip press and was readily available. The open extended nip press was desirable as it did not significantly limit press shoe length and geometry. An overall schematic and diagram of the X2 machine is shown in Figure 1 and a close-up showing the location of the hover press is shown in Figure 2.



Schematic Diagram Of Beloit X2 Pilot Paper Machine

Figure 1. X2 Pilot Paper Machine.

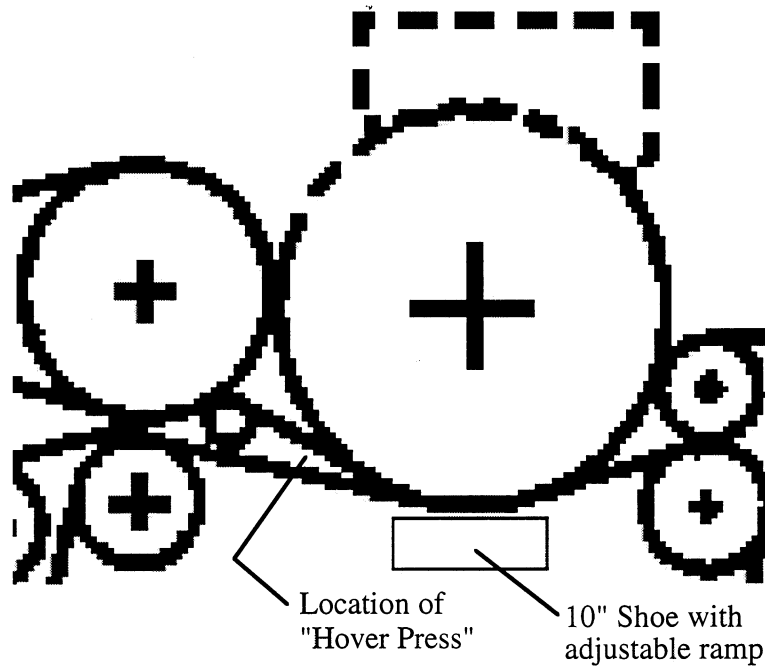
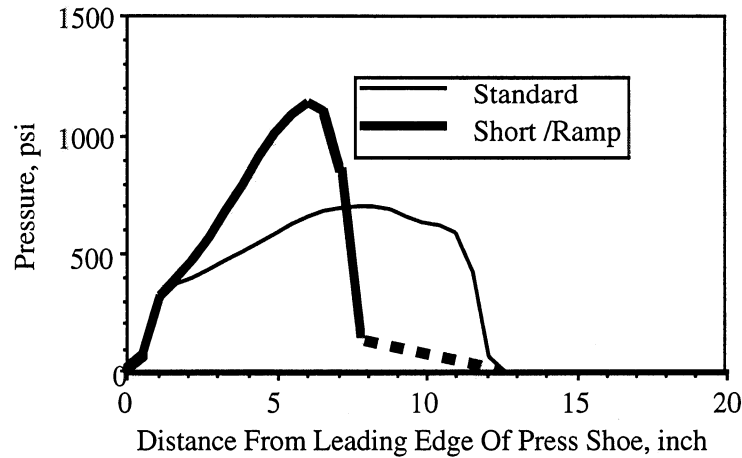


Figure 2. Close-up of January 1998 configuration of impulse dryer on the Beloit X2 pilot paper machine.

As the shape of the pressure profile, generated by the press shoe and the “hover press” were major variables of the experiments, its measurement was considered to be of importance. To this end, the Institute purchased and utilized a TechScan pressure measurement system to both statically and dynamically measure pressure profiles. Typical profiles at a press load of 6000 pli, used during the July and August experiments are shown in Figure 3. The “standard” profile corresponds to the pressure distribution resulting from a commercial Beloit 10-inch shoe. The “Short/Ramp” profile corresponds to the profile obtained from a 7-inch shoe followed by a 7-inch adjustable ramp. The specific ramp profiles

investigated during the July and August experiments are shown in Figure 4. Note that the ramps used in July and August each followed the short shoe as indicated in Figure 3.



**Figure 3.** Measured pressure profiles of the standard 10" and "short shoe" used in the July and August 1997 experiments on the Beloit X2 pilot paper machine.

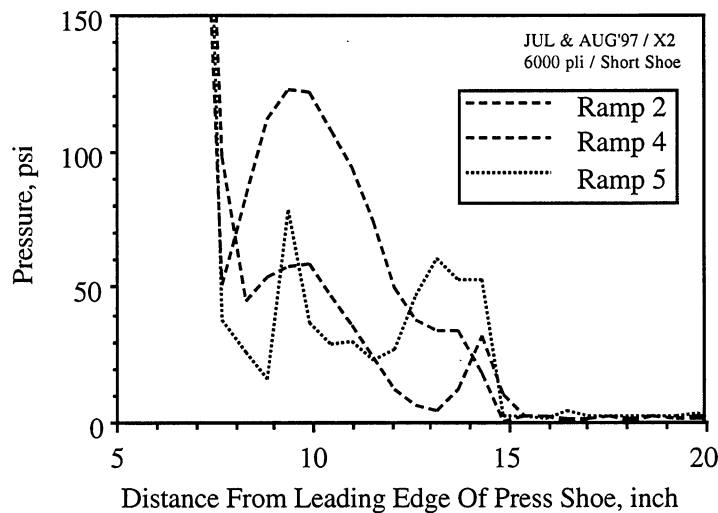


**Figure 4.** Measured pressure profiles of various ramp decompression profiles used in the July and August 1997 experiments on the Beloit X2 pilot paper machine.

The first objective of the July experiment was to characterize the performance of the standard 10-inch shoe with and without the use of a steambox just prior to the impulse dryer. Under both conditions of ingoing temperature, the roll surface

temperature increased over a range of temperatures from 300 to 400°F. Samples of paper produced at these conditions were then finish dried on a cylinder dryer and tested. Figure 5 reports the zd-specific elastic modulus as a function of roll surface temperature, while Figure 6 shows the corresponding coefficients of variation. Based on these test results, the critical impulse drying temperature of the unheated web was about 330°F, while that of the preheated web was less than about 310°F. As web preheating added an extra complication to the experiments and is generally ineffective at low freenesses, it was decided to delete the steam box from future experiments.

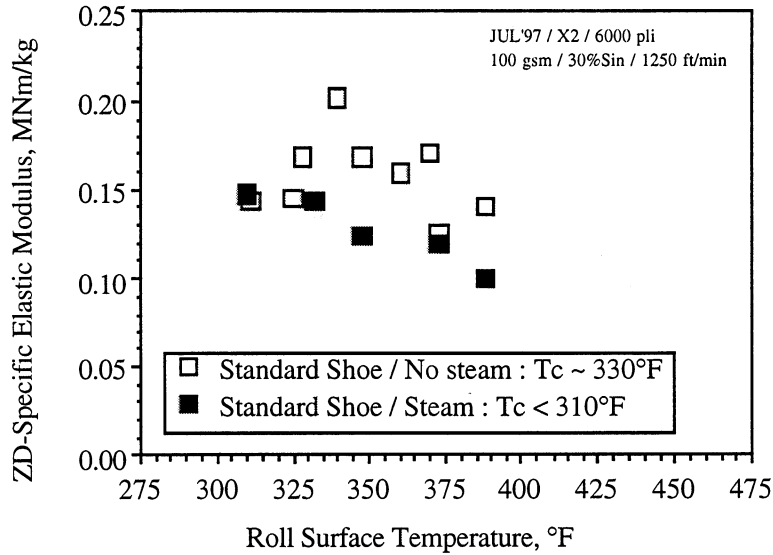


Figure 5. Out-of-plane specific elastic modulus as a function of press roll surface temperature for impulse drying using a standard 10-inch press shoe with and without steam preheating.

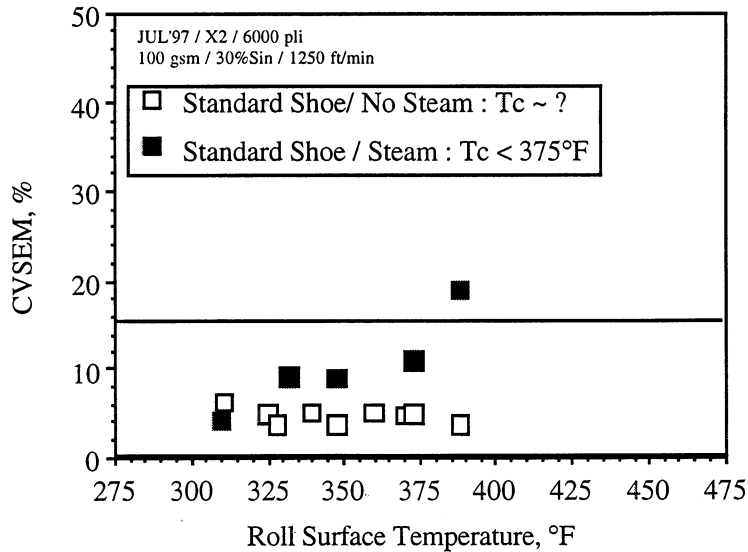


Figure 6. Coefficient of variation of the out-of-plane specific elastic modulus as a function of press roll surface temperature for impulse drying using a standard 10-inch press shoe with and without steam preheating.

The second objective was to determine whether the use of the short shoe with the ramp could be used to increase the critical impulse drying temperature above that obtained using the standard 10-inch shoe. The short shoe with the ramp was so designed as to generate the same impulse (area under the pressure - time curve) as the standard shoe. These experiments were conducted without the use of the steam box. Figure 7 reports the  $z_d$  - specific elastic modulus as a function of roll surface temperature for ramp #2. The corresponding coefficients of variation of the elastic modulus are shown in Figure 8. Based on these measurements, a critical impulse drying temperature of 400°F was obtained. Hence it was concluded that the modified profile resulted in an increase in the window of operation of about 70°F.

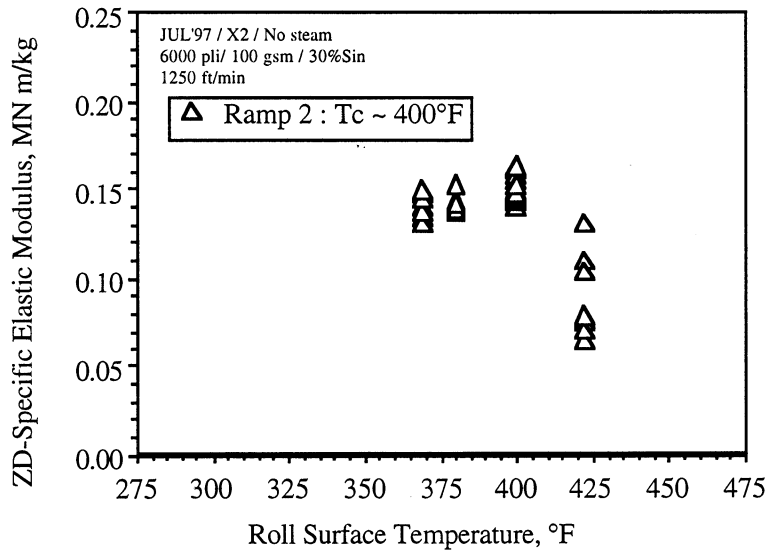
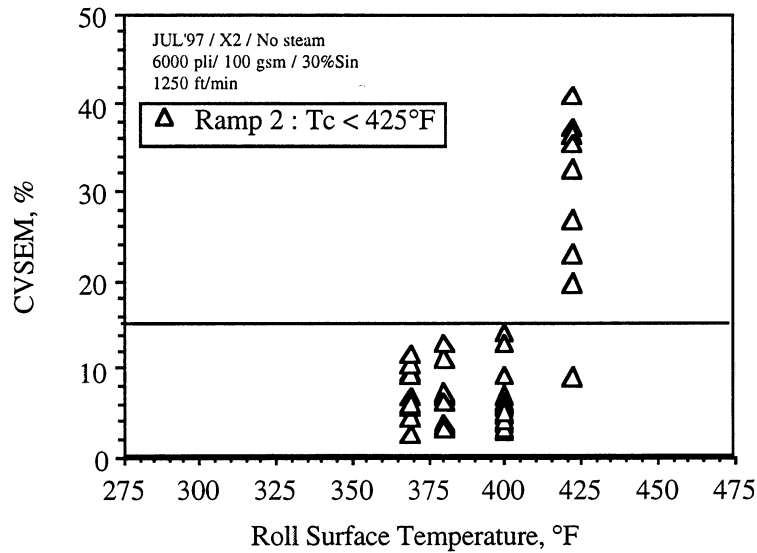


Figure 7. Out-of-plane specific elastic modulus as a function of press roll surface temperature for impulse drying using a “short shoe” with ramp #2 without steam preheating.



**Figure 8.** Coefficient of variation of the out-of-plane specific elastic modulus as a function of press roll surface temperature for impulse drying using a “short shoe” with ramp #2 without steam preheating.

Additional, more detailed, experiments were conducted in August. In these experiments, attempts were made to adjust the ramp profile shapes more closely to those of laboratory simulations. The resulting ramps (#4 and #5) were generally of lower pressure than ramp #2 but were still jagged in shape. Table 1 shows the setup conditions of the gap former and the impulse dryer. The furnish used for this as well as the July and January experiments was a once-dried Virgin unbleached softwood Kraft. The furnish was repulped and minimally refined to a freeness of 570 ml CSF for the August experiments. The ingoing solids to the impulse dryer was maintained between 31.5 and 32.2% solids while the basis weight was set at a nominal 100 gsm. Permeability testing of the wet web showed that the specific surface was between 3.2 and 4.1 m<sup>2</sup>/g as shown in Table 2. The machine was operated at 1250 ft/min.

Table 1. Comparison of Operating Conditions in August 1997 and January 1998

Section Of P.M.	Operating Condition	August 1997 (570 ml CSF Case)	January 1998 (540 ml CSF Case)
Forming	#1 Wire	145 x 104 , 507 CFM	152 x 68/34, 503 CFM
	#2 Wire	182 x 145	161 x 110, 471 CFM
	Pressure	145 in H <sub>2</sub> O	130 in H <sub>2</sub> O
	Flowrate	905 gpm	600 gpm
	Thick Stock	148 gpm	140 gpm
	Temperature	47 °C	43 °C
	pH	7.7	NA
Pressing	Solids In	32%	25%
	Press Shoe	6-inch with ramp extension	10-inch with adjustable ramp
	Felt	AI 289250 CSX	AI 289249 CSX
	Wrap Roll	inside link	outside link
	Blanket	grooved	op. side- blind drilled/ dr. side- grooved

Table 2. Ingoing Web Properties

Case Date - Ramp # P.M. Speed	Freeness, ml CSF	Ingoing Solids, %	Specific Surface, m <sup>2</sup> /g	Specific Volume, g/m <sup>3</sup>	OD Basis Weight, g/m <sup>2</sup>
			Average Std. Dev.	Average Std. Dev.	Average Std. Dev.
Aug'97- Ramp 4 1250 ft/min	570	32.2	3.20 0.03	1.16 0.02	105.5 6.8
Aug'97- Ramp 5 1250 ft/min	570	31.5	4.07 0.87	1.10 0.03	105.5 6.8
Jan'98 - Ramp 8 1250 ft/min	540	24.6	6.60 1.43	1.84 0.09	98.5 4.9
Jan'98 - Ramp 8 1250 ft/min	458	27.5	11.16 1.28	1.75 0.09	97.6 2.9
Jan'98 - Ramp 8 2500 ft/min	460	26.1	14.97 1.71	1.77 0.01	97.9 2.6

Using the short shoe with ramps #4 and #5, impulse drying experiments were conducted at a press load of 6000 pli over a range of press roll surface temperatures between 375 and 475°F. As shown in the zd-elastic modulus plot of Figure 9 and the coefficient of variation plots of Figure 10, the critical impulse drying temperature was about 424°F for ramp #4 and 408°F for ramp #5. In Figures 11 through 16 important paper physical properties are compared at the various critical temperatures and to corresponding wet pressing controls. In particular it is noted that impulse drying yielded a 5-point increase in press dryness, increased sheet smoothness and Gurley as well as improvements in STFI compression strength and ring crush.

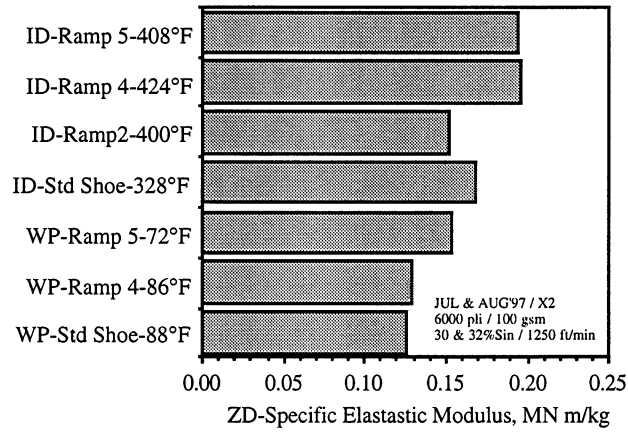


Figure 11. Out-of-plane specific elastic modulus of paper impulse dried at the critical temperature as compared to that paper wet pressed under the same pressing conditions.

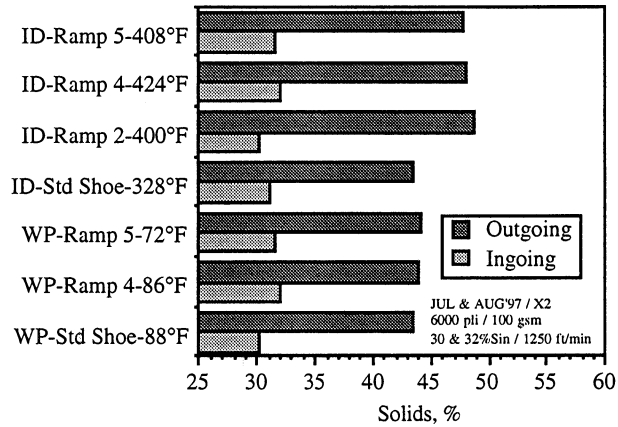


Figure 12. Ingoing and outgoing solids of paper impulse dried at the critical temperature as compared to that paper wet pressed under the same pressing conditions.

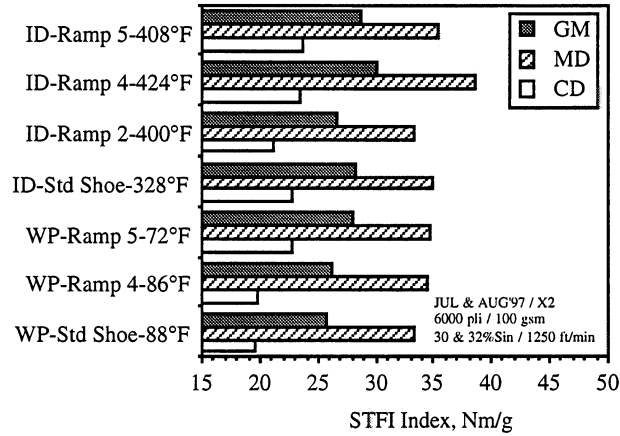


Figure 13. CD, MD, and GM STFI compression index of paper impulse dried at the critical temperature as compared to that paper wet pressed under the same pressing conditions.

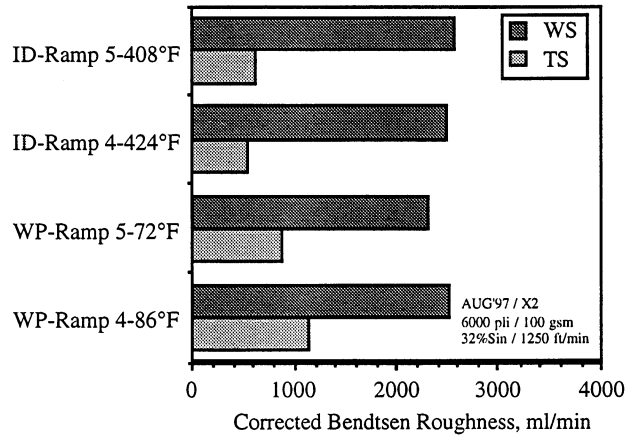


Figure 14. Corrected Bendtsen Roughness of paper impulse dried at the critical temperature as compared to that paper wet pressed under the same pressing conditions.

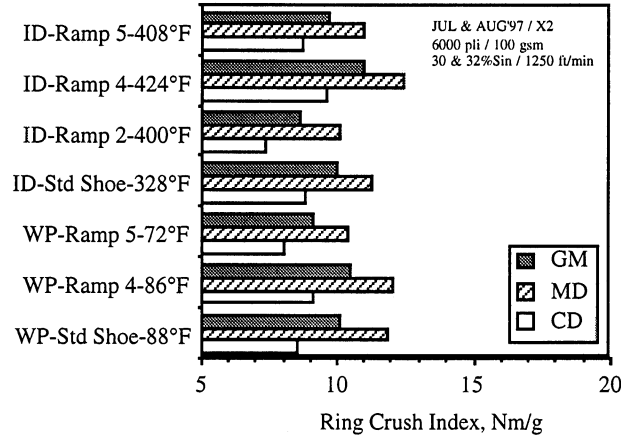


Figure 15. CD, MD, and GM Ring Crush index of paper impulse dried at the critical temperature as compared to that paper wet pressed under the same pressing conditions.

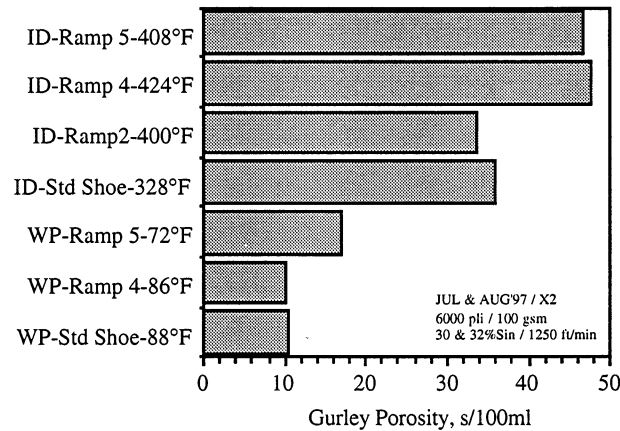


Figure 16. Gurley Porosity of paper impulse dried at the critical temperature as compared to that paper wet pressed under the same pressing conditions.

In addition to demonstrating the usefulness of modifying the press shoe, the August experiments also demonstrated the usefulness of using a heavily loaded Teflon doctor to minimize and, under some conditions, eliminate sheet/press roll picking. To further explore the variables influencing picking, a side experiment was conducted at various press loads while maintaining the press roll surface temperature at 400°F. It was found that picking decreased with decreasing press load. The experiments were also useful in showing the minimum press load that would be required for impulse drying performance to surpass that of 6000 pli wet pressing. Figure 17 to 23 show these comparisons. It was observed that an impulse dryer operating at 3000 pli would be superior to a similarly configured wet press operating at a press load of 6000 pli, see in particular Figures 19 and 20.

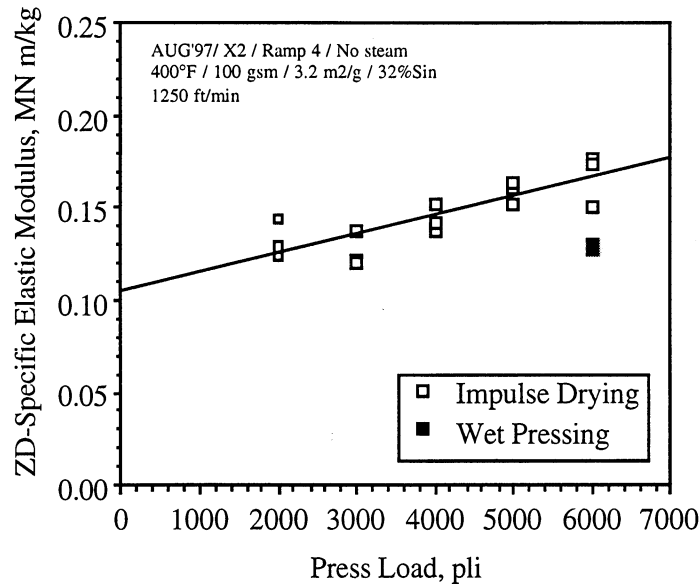


Figure 17. Out-of-plane specific elastic modulus of impulse dried paper as a function of press load at a fixed press roll surface temperature of 400°F using a “short shoe” with ramp #4 without steam preheating.

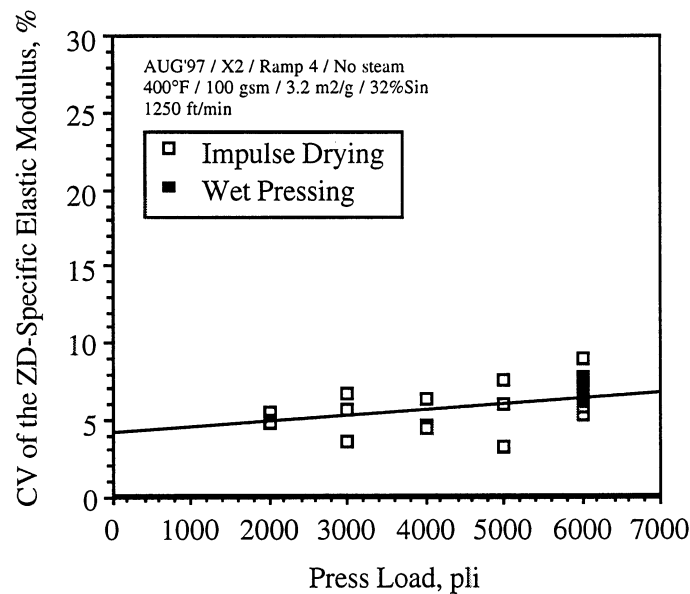


Figure 18. Coefficient of variation of the out-of-plane specific elastic modulus of impulse dried paper as a function of press load at a fixed press roll surface temperature of 400°F using a “short shoe” with ramp #4 without steam preheating.

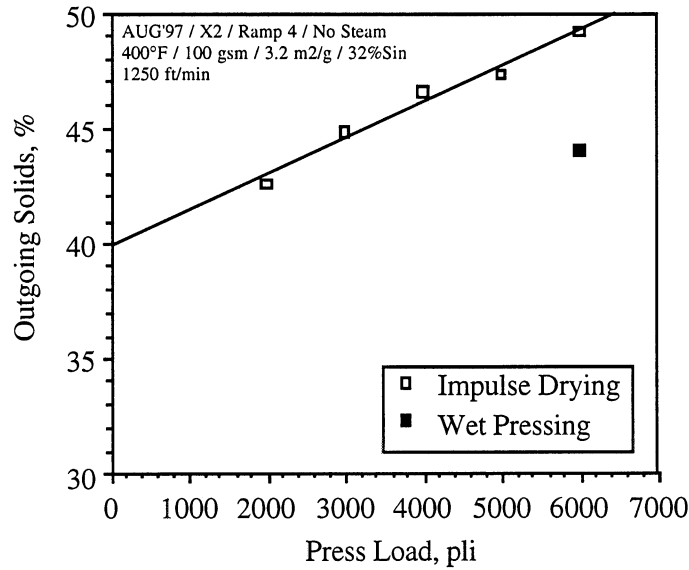


Figure 19. Outgoing solids of impulse dried paper as a function of press load at a fixed press roll surface temperature of 400°F using a “short shoe” with ramp #4 without steam preheating.

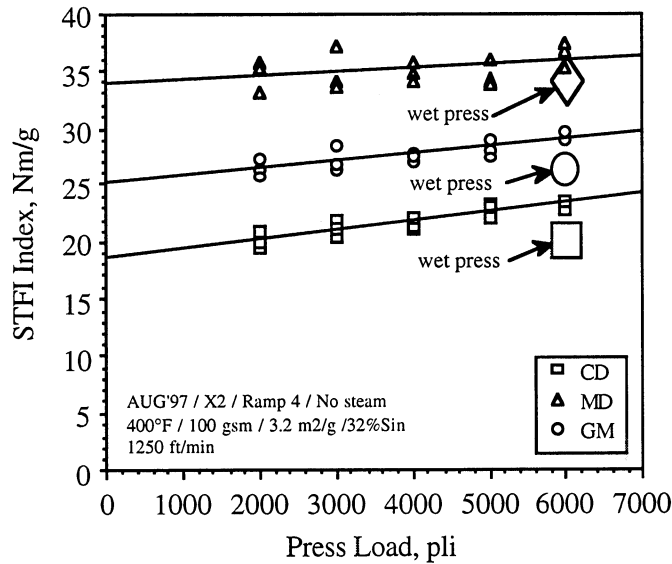


Figure 20. CD, MD, and GM STFI compression index of impulse dried paper as a function of press load at a fixed press roll surface temperature of 400°F using a “short shoe” with ramp #4 without steam preheating.

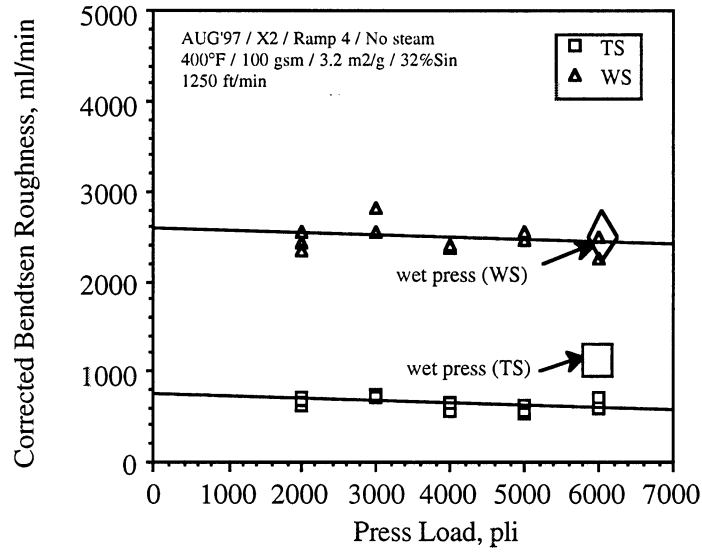


Figure 21. Corrected Bendtsen Roughness of impulse dried paper as a function of press load at a fixed press roll surface temperature of 400°F using a “short shoe” with ramp #4 without steam preheating.

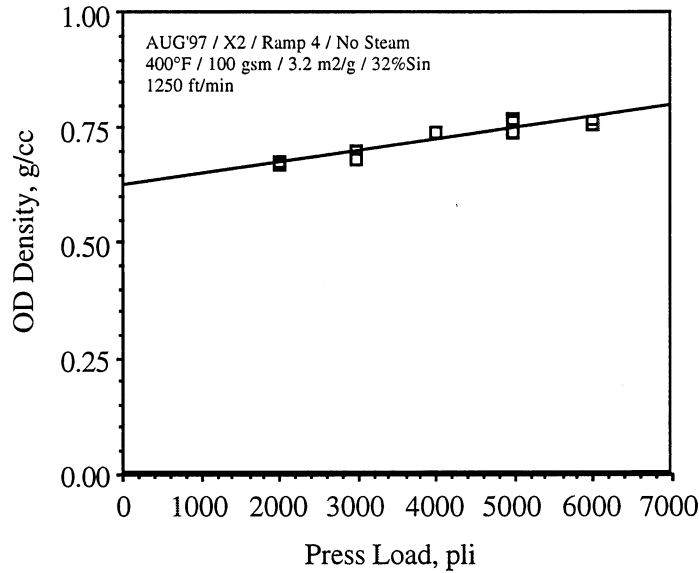
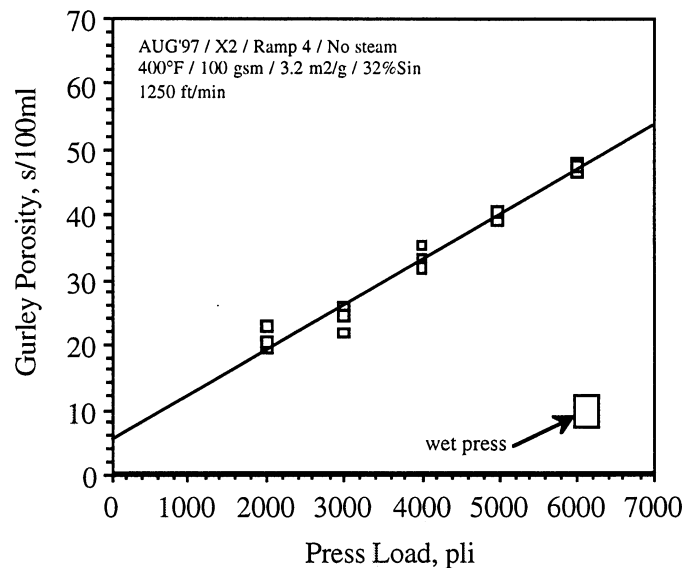


Figure 22. Oven-dried density of impulse dried paper as a function of press load at a fixed press roll surface temperature of 400°F using a “short shoe” with ramp #4 without steam preheating.



**Figure 23.** Gurley Porosity of impulse dried paper as a function of press load at a fixed press roll surface temperature of 400°F using a “short shoe” with ramp #4 without steam preheating.

### ***The Winter Experiments:***

There were a number of objectives of the January experiments. These included the evaluation of an improved adjustable (on-the-fly) press shoe ramp and the evaluation of an initial version of the “hover press.” It was also desirable to determine the effect of refining and machine speed on critical impulse drying temperature and runnability (sheet/press roll surface picking).

The August experiments had indicated that picking could be reduced by reducing the press load. This was interpreted to mean that the press shoe profile should be designed in such a way as to minimize the peak pressure while maximizing the impulse. Hence, the improved adjustable ramp was designed to follow a standard 10-inch shoe. To contain the shoe and ramp within the existing open extended nip press, the new adjustable ramp length was limited to a length of 4 inches. Figure 24 shows three press shoe pressure profiles that were investigated during the January experiments. The following nomenclature was used:

- Ramp 8 Off - Hover Off, signifies that the ramp as well as the “hover press” were installed but not pressurized.
- Ramp 8 On - Hover Off, signifies that the ramp was pressurized while the “hover press” was not pressurized.
- Ramp 8 On - Hover On, signifies that both the ramp and the “hover press” were pressurized.

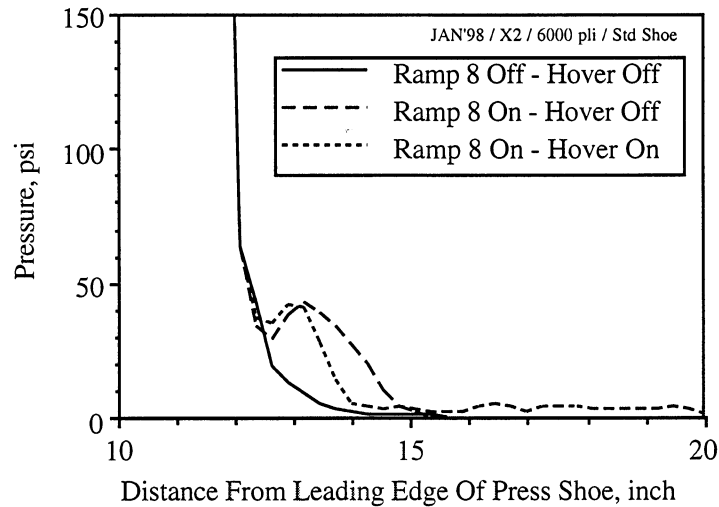


**Figure 24.** Measured pressure profiles of various ramp decompression profiles used in the January 1998 experiments on the Beloit X2 pilot paper machine.

The January experiments also provided an opportunity to explore whether blanket design would influence impulse drying. To accomplish this, the drive side of the blanket was grooved while the operator side was blind-drilled. Table 1 documents the forming and pressing conditions that were employed in January.

The same furnish used in the July and August experiments was also used in the January experiment. The ingoing solids, hydrodynamic specific surface and freeness of cases investigated are shown in Table 2.

The January experiments were conducted over a three-day period. At the start of each day, wet pressing controls were run for each of the three press shoe profiles. Afterwards, the press roll was heated to a range of temperatures and impulse drying samples were taken. The X2 machine was run at a speed of 1250 ft/min during the first two days and increased to 2500 ft/min on the third day. To investigate the effect of refining, the furnish was refined to 540 ml CSF on the first day and 460 ml CSF on the second and third day.

Figures 25 through 27 show the  $z_d$ -specific elastic modulus as a function of press roll surface temperature for each of the press shoe pressure profiles at a freeness of 540 ml CSF and a machine speed of 1250 ft/min. As in previous studies, the drop off of the modulus is an indicator of the critical impulse drying temperature. It was observed that the grooved blanket consistently resulted in a higher modulus than did the blind-drilled blanket. This suggests that felt drainage may be a more important factor in impulse drying than had been previously realized. It also suggests that the blanket groove geometry should be optimized. Based on Figures 25 through 27 the critical temperature were determined and outgoing solids and paper physical properties reported at these conditions.

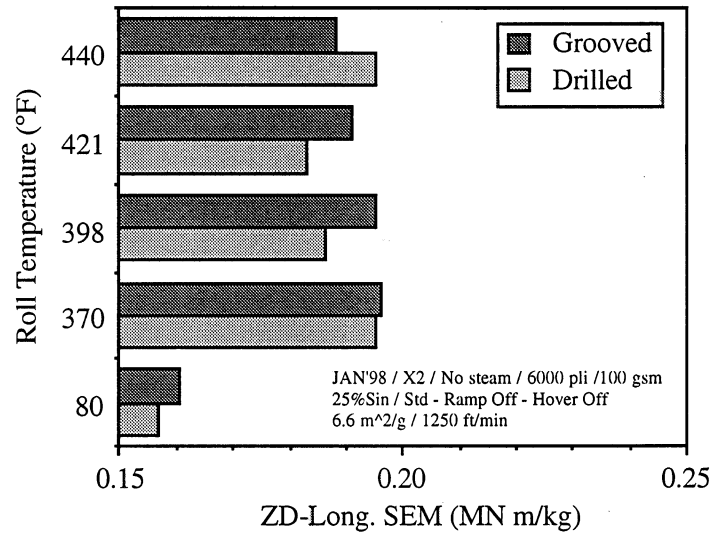


Figure 25. Out-of-plane specific elastic modulus as a function of press roll surface temperature for impulse drying using the standard 10-inch shoe with ramps #8 off and with the post-nip “hover press” off for both a drilled and a grooved blanket and without steam preheating.

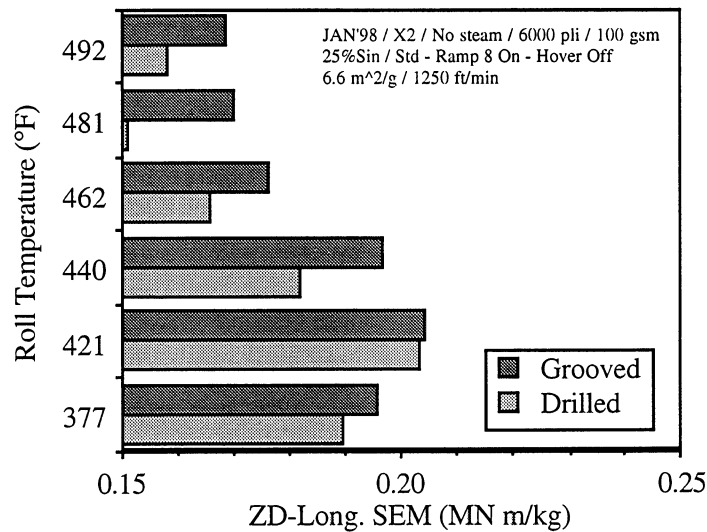
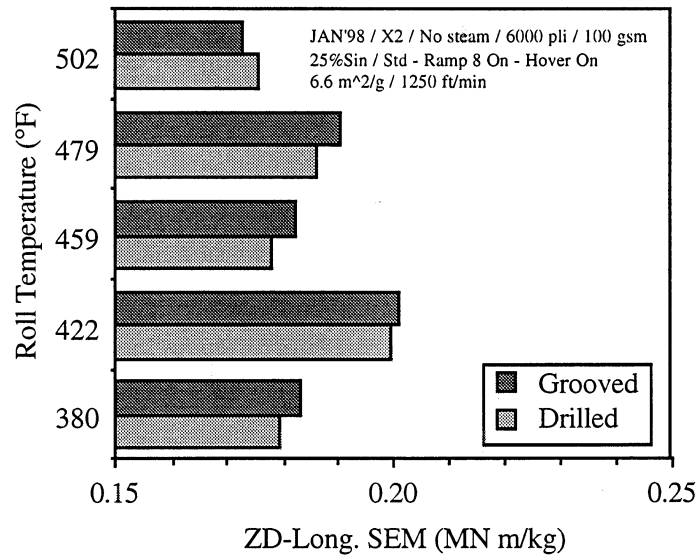


Figure 26. Out-of-plane specific elastic modulus as a function of press roll surface temperature for impulse drying using the standard 10-inch shoe with ramps #8 on and with the post-nip “hover press” off for both a drilled and a grooved blanket and without steam preheating.



**Figure 27.** Out-of-plane specific elastic modulus as a function of press roll surface temperature for impulse drying using the standard 10-inch shoe with ramps #8 on and with the post-nip “hover press” on for both a drilled and a grooved blanket and without steam preheating.

Figures 28 through 31 show these values as compared to the wet pressing controls. It was observed that ramp #8 resulted in an increase of critical temperature of about 23°F over the ramp off case. It is also observed that the “hover press” encouraged rewetting, see Figure 28. The increase in press dryness of impulse drying over wet pressing was only about 2 percentage points compared to the 5 percentage points observed during the August experiment. This point will be discussed in more detail in the conclusions. Comparing the paper physical properties of the impulse dried samples to the wet pressed controls, a smoother sheet at marginally better STFI compression strength is produced.

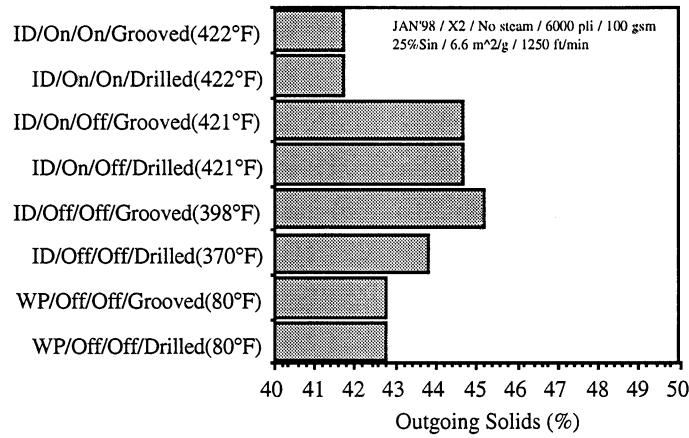


Figure 28. Outgoing solids of paper impulse dried at the critical temperature as compared to that paper wet pressed under the same pressing conditions using the standard 10-inch shoe and various ramp profiles for both a drilled and a grooved blanket and without steam preheating.

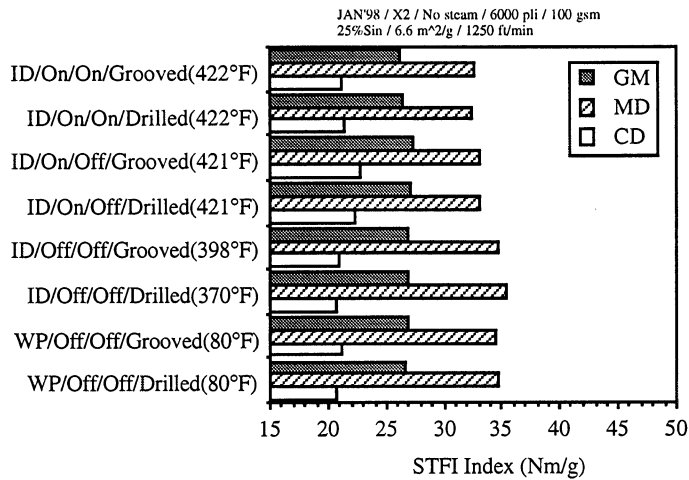
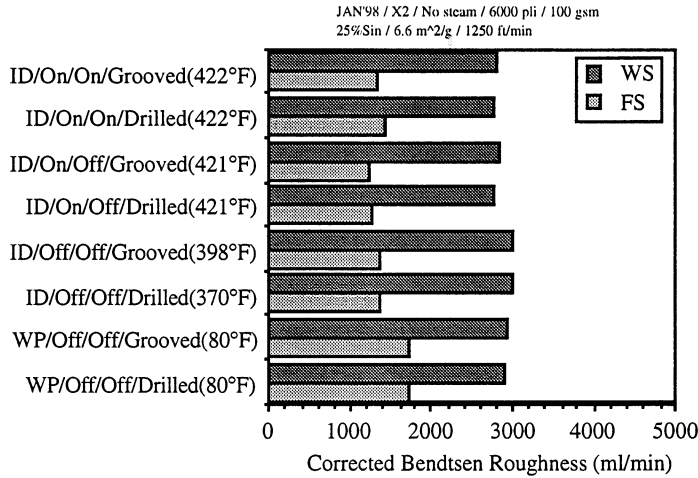
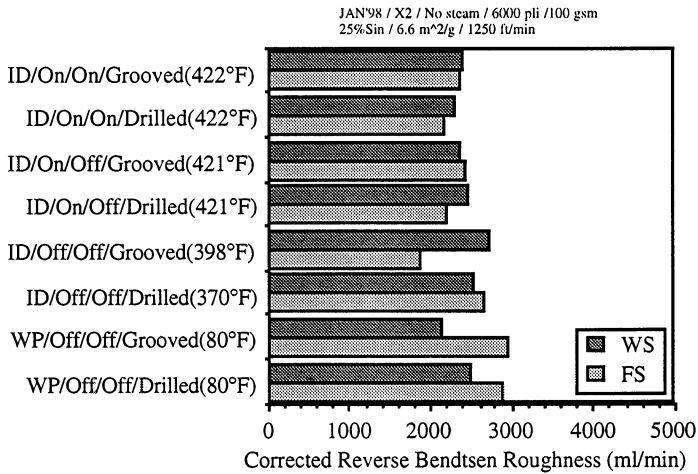


Figure 29. CD, MD, and GM STFI compression index of paper impulse dried at the critical temperature as compared to that paper wet pressed under the same pressing conditions using the standard 10-inch shoe and various ramp profiles for both a drilled and a grooved blanket and without steam preheating.



**Figure 30.** Corrected Bendtsen Roughness of paper impulse dried at the critical temperature as compared to that paper wet pressed under the same pressing conditions using the standard 10-inch shoe and various ramp profiles for both a drilled and a grooved blanket and without steam preheating.



**Figure 31.** Corrected Reverse Bendtsen Roughness of paper impulse dried at the critical temperature as compared to that paper wet pressed under the same pressing conditions using the standard 10-inch shoe and various ramp profiles for both a drilled and a grooved blanket and without steam preheating.

Figures 32 through 34 show the zd-specific elastic modulus as a function of press roll surface temperature for each of the press shoe pressure profiles at a freeness of 458 ml CSF and a machine speed of 1250 ft/min. As in the previous case, the grooved blanket consistently resulted in a higher modulus than did the blind-drilled blanket. Based on Figures 32 through 34, the critical temperature were determined and outgoing solids and paper physical properties reported at these conditions.

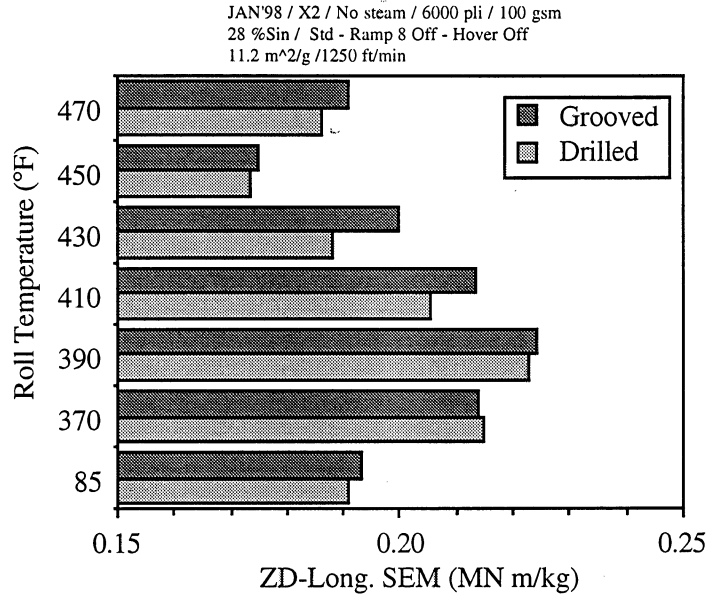


Figure 32. Out-of-plane specific elastic modulus as a function of press roll surface temperature for impulse drying using the standard 10-inch shoe with ramps #8 off and with the post-nip “hover press” off for both a drilled and a grooved blanket and without steam preheating.

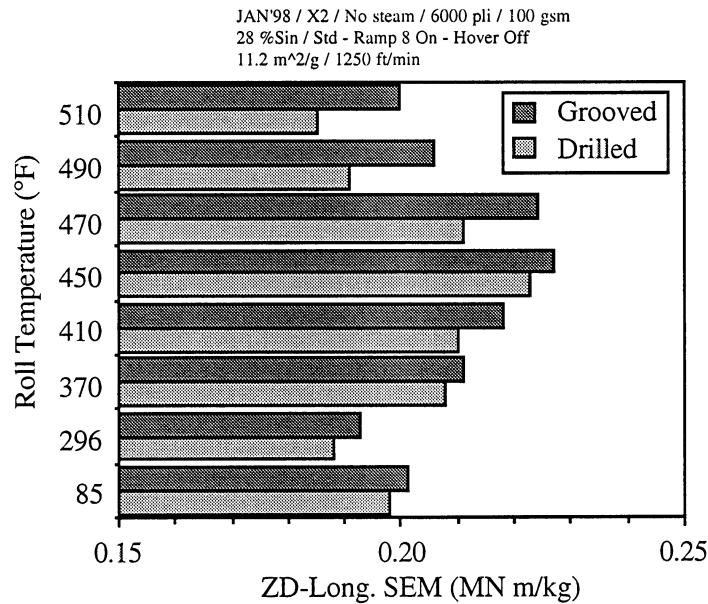
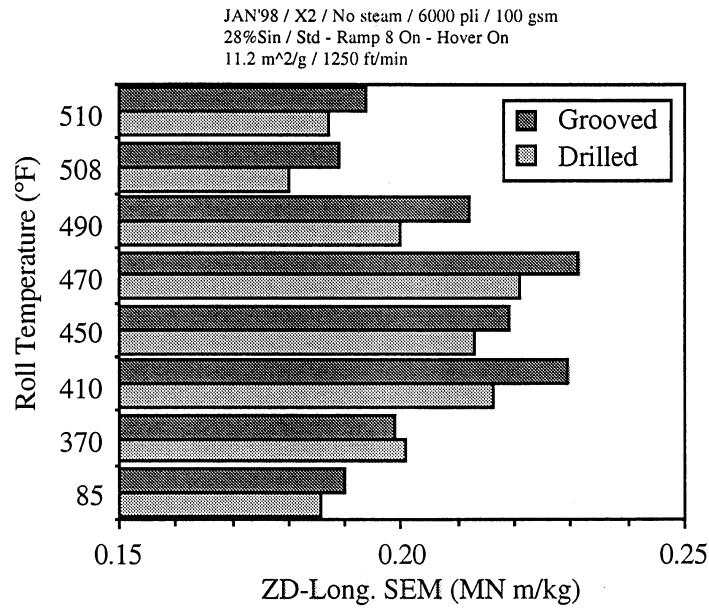
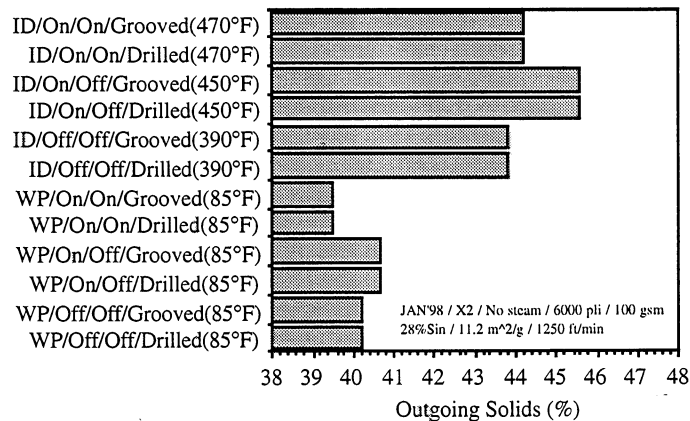


Figure 33. Out-of-plane specific elastic modulus as a function of press roll surface temperature for impulse drying using the standard 10-inch shoe with ramps #8 on and with the post-nip “hover press” off for both a drilled and a grooved blanket and without steam preheating.



**Figure 34.** Out-of-plane specific elastic modulus as a function of press roll surface temperature for impulse drying using the standard 10-inch shoe with ramps #8 on and with the post-nip “hover press” on for both a drilled and a grooved blanket and without steam preheating.

Figures 35 through 38 show these values compared to the wet pressing controls. At this freeness, ramp #8 resulted in an increase of critical temperature of about 60°F over the ramp off case. As at the higher freeness, the “hover press” seemed to encourage rewet, see Figure 35. The increase in press dryness of impulse drying over wet pressing was about 6 percentage points. Comparing the paper physical properties of the impulse dried samples to the wet pressed controls, the impulse dried samples have marginally better properties.



**Figure 35.** Outgoing solids of paper impulse dried at the critical temperature as compared to that paper wet pressed under the same pressing conditions using the standard 10-inch shoe and various ramp profiles for both a drilled and a grooved blanket and without steam preheating.

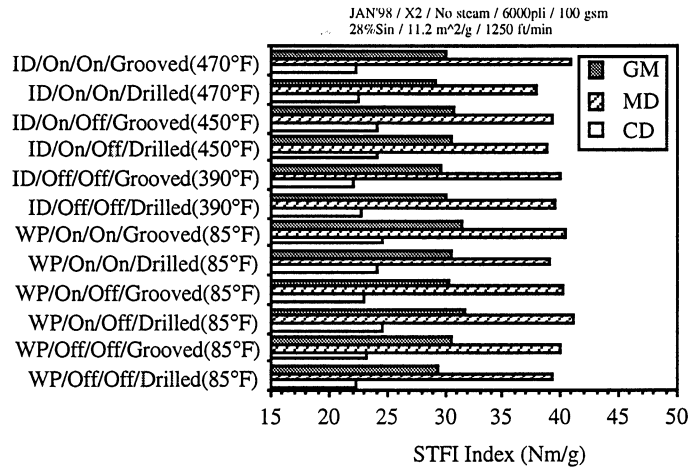


Figure 36. CD, MD, and GM STFI compression index of paper impulse dried at the critical temperature as compared to that paper wet pressed under the same pressing conditions using the standard 10-inch shoe and various ramp profiles for both a drilled and a grooved blanket and without steam preheating.

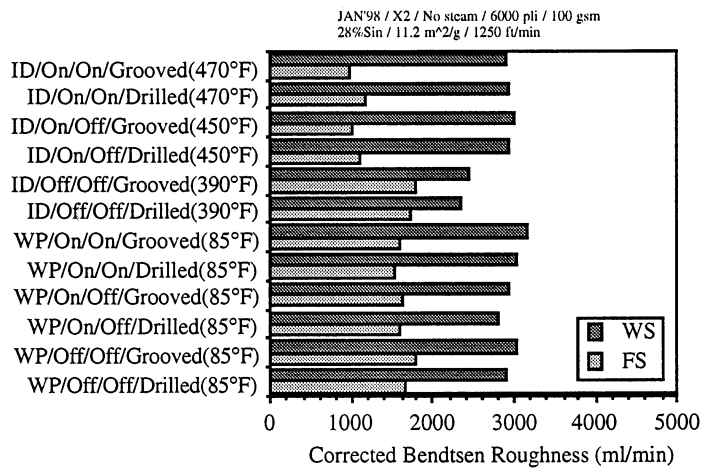
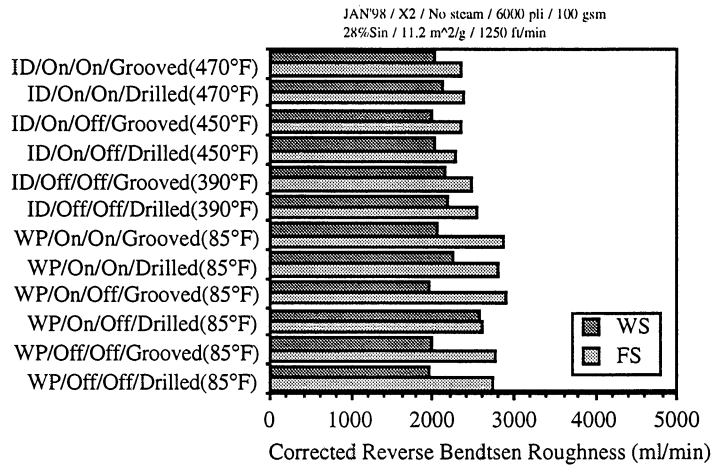


Figure 37. Corrected Bendtsen Roughness of paper impulse dried at the critical temperature as compared to that paper wet pressed under the same pressing conditions using the standard 10-inch shoe and various ramp profiles for both a drilled and a grooved blanket and without steam preheating.



**Figure 38.** Corrected Reverse Bendtsen Roughness of paper impulse dried at the critical temperature as compared to that paper wet pressed under the same pressing conditions using the standard 10-inch shoe and various ramp profiles for both a drilled and a grooved blanket and without steam preheating.

Figures 39 and 40 show the zd-specific elastic modulus as a function of press roll surface temperature for two of the press shoe pressure profiles at a freeness of 460 ml CSF and a machine speed of 2500 ft/min. As in the two previous cases, the grooved blanket consistently resulted in a higher modulus than did the blind-drilled blanket. Based on Figures 39 and 40, the critical temperatures were determined and outgoing solids and paper physical properties reported at these conditions.

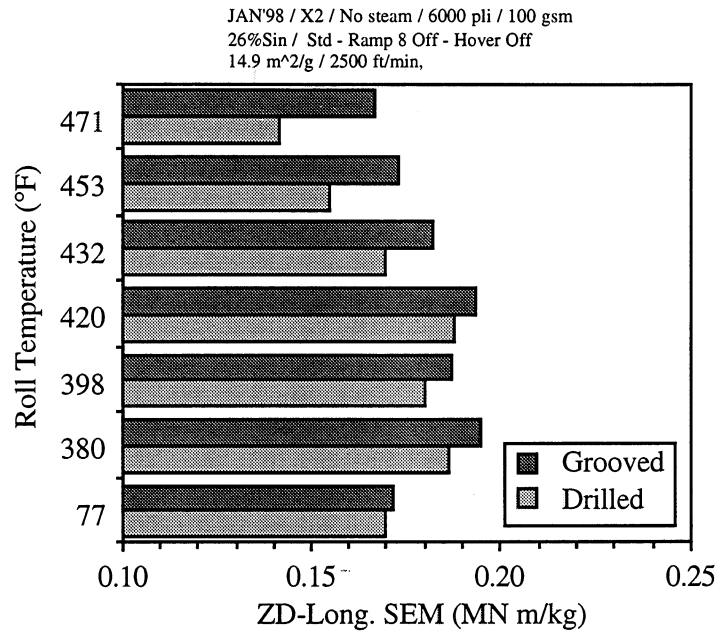


Figure 39. Out-of-plane specific elastic modulus as a function of press roll surface temperature for impulse drying using the standard 10-inch shoe with ramps #8 off and with the post-nip “hover press” off for both a drilled and a grooved blanket and without steam preheating.

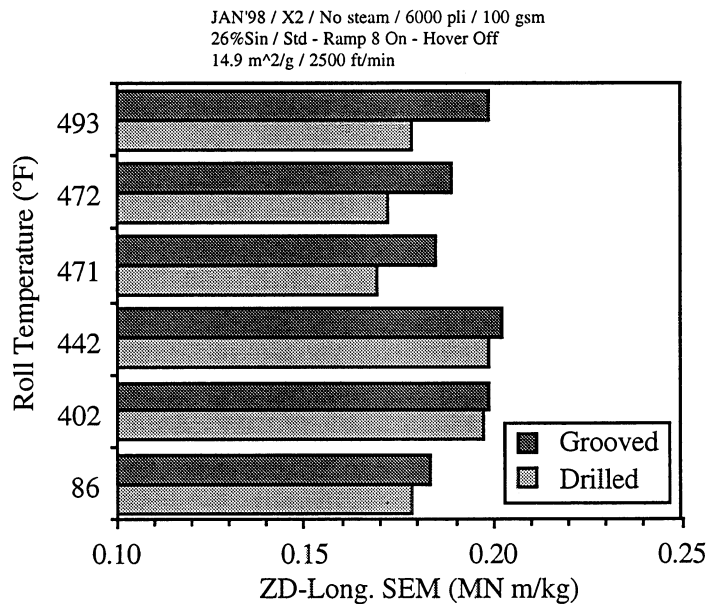


Figure 40. Out-of-plane specific elastic modulus as a function of press roll surface temperature for impulse drying using the standard 10-inch shoe with ramps #8 on and with the post-nip “hover press” off for both a drilled and a grooved blanket and without steam preheating.

Figures 41 through 44 show these values as compared to the wet pressing controls. At this increased machine speed, the ramp #8 resulted in an increase of critical temperature of about 22°F over the ramp off case. The increase in press dryness of impulse drying over wet pressing was about 3 percentage points. Comparing the paper physical properties of the impulse dried samples to the wet pressed controls, produced sheets of marginally better properties.

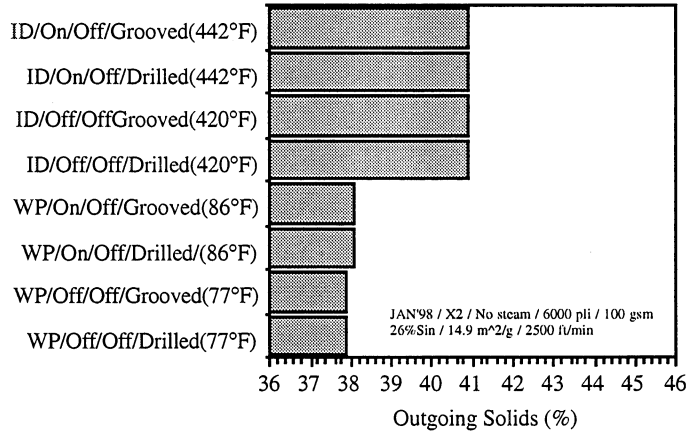


Figure 41. Outgoing solids of paper impulse dried at the critical temperature as compared to that paper wet pressed under the same pressing conditions using the standard 10-inch shoe and various ramp profiles for both a drilled and a grooved blanket and without steam preheating.

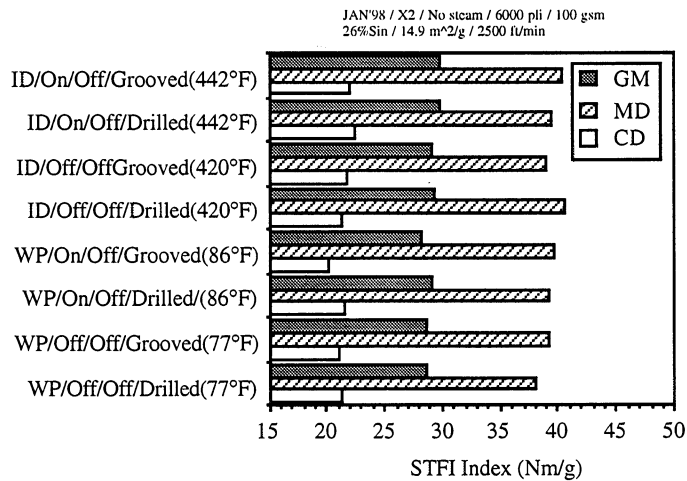
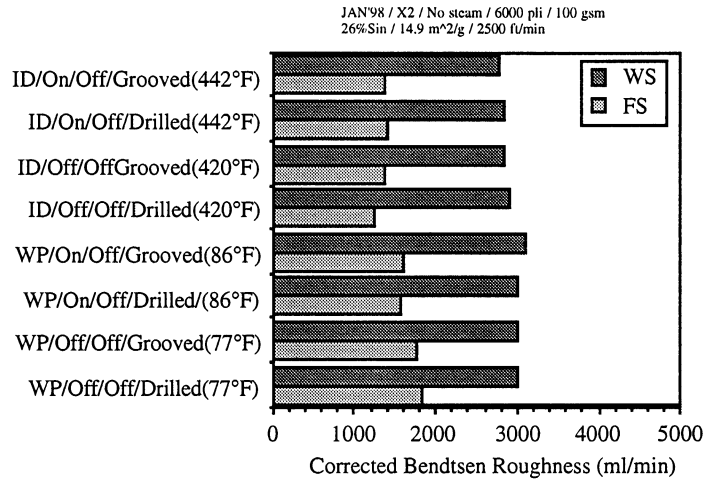
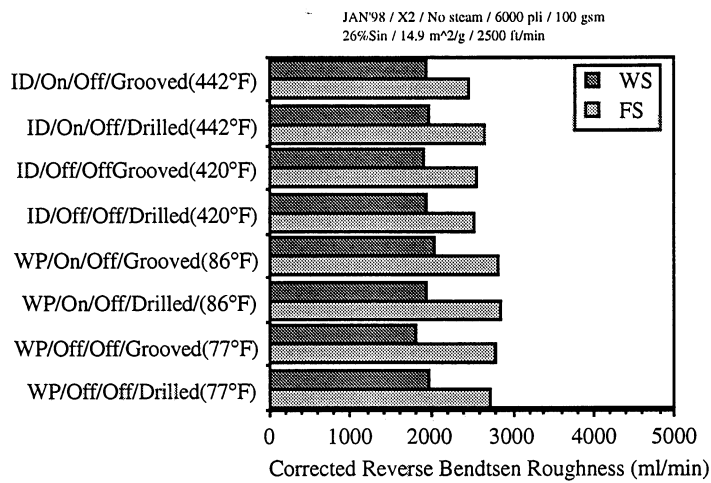


Figure 42. CD, MD, and GM STFI compression index of paper impulse dried at the critical temperature as compared to that paper wet pressed under the same pressing conditions using the standard 10-inch shoe and various ramp profiles for both a drilled and a grooved blanket and without steam preheating.



**Figure 43.** Corrected Bendtsen Roughness of paper impulse dried at the critical temperature as compared to that paper wet pressed under the same pressing conditions using the standard 10-inch shoe and various ramp profiles for both a drilled and a grooved blanket and without steam preheating.



**Figure 44.** Corrected Reverse Bendtsen Roughness of paper impulse dried at the critical temperature as compared to that paper wet pressed under the same pressing conditions using the standard 10-inch shoe and various ramp profiles for both a drilled and a grooved blanket and without steam preheating.

**Comparison Of Summer and Winter Experiments**

Table 3 summarizes the impulse drying critical temperatures that were determined in the pilot experiments that were conducted in the Summer of 1997 and the Winter of 1998. A

few differences are particularly interesting. It is noted that the critical impulse drying temperature of the July 1997 Standard 10-inch shoe (with no ramp) was about 70°F lower than the critical impulse drying temperature for the January 1998 Standard 10-inch shoe with Ramp #8 and the "hover press" both being unpressurized. There are a number of factors that contribute to these differences. These are differences in ingoing solids, freeness (and hydrodynamic specific surface), and small differences in the pressure profiles. Based on previous laboratory simulations, it is expected that a decrease in ingoing solids would decrease the critical impulse drying temperature. Likewise, an increase in hydrodynamic specific surface and a corresponding decrease in freeness would also result in a decrease in critical impulse drying temperature. As these trends were not observed, the differences in pressure profile were considered. Referring to Figure 3, the Standard 10 inch shoe pressure dropped the last 100 psi in less than 1 inch. Referring to Figure 24, the Standard 10-inch shoe with the unpressurized Ramp and hover dropped the last 100 psi in just over 2 inches. Hence, the unpressurized Ramp and hover profiles would be expected to result in some reduction in the net pressure difference between the inside and outside of the web as it leaves the impulse dryer. This effect could have resulted in the observed increase in critical impulse drying temperature. As the ingoing temperatures for all cases were about the same (105°F), the pressure profile was most probably the cause of the observed difference. Hence, an attempt to impulse dry the January 1998 furnishes with a standard 10-inch shoe, would have produced an even lower critical temperature than was observed in August 1997.

The remaining critical impulse drying temperature data appears to be internally consistent. Based on the analysis in the previous paragraph, it is concluded that the 4-inch long ramp is probably adequate in length for future experiments on the Beloit X4 pilot paper machine.

Table 3. Critical Impulse Drying Temperatures

Case Date, Freeness, P.M. Speed	Specific Surface, m <sup>2</sup> /g	Ingoing Solids, %	Shoe Press Configuration	Critical Impulse Drying Temperature, °F	
				Blind Drilled	Grooved
Jul'97 570 ml CSF 1250 ft/min	na	30.0	Std - No Ramp	na	328
Aug'97 570 ml CSF 1250 ft/min	3.20	32.2	Short -Ramp 4	na	424
	4.07	31.5	Short -Ramp 5	na	408
Jan'98 540 ml CSF 1250 ft/min	6.63	24.6	Std - Ramp 8 Off -Hover Off	370	398
			Std - Ramp 8 On -Hover Off	421	421
			Std - Ramp 8 On -Hover On	422	422
Jan'98 458 ml CSF 1250 ft/min	11.16	27.5	Std - Ramp 8 Off -Hover Off	390	390
			Std - Ramp 8 On -Hover Off	450	450
			Std - Ramp 8 On -Hover On	470	470
Jan'98 460 ml CSF 2500 ft/min	14.97	26.1	Std - Ramp 8 Off -Hover Off	420	420
			Std - Ramp 8 On -Hover Off	442	442

In the January 1998 experiments, there was a consistent difference between the specific elastic modulus of paper produced with the grooved blanket and the blind drilled blanket. In almost all cases (see Figures 27, 32, and 39), paper wet pressed or impulse dried on the grooved side was stronger than those wet pressed or impulse dried on the blind drilled side. This was interpreted as resulting from higher amounts of rewet or lower press solids on the blind drilled side which would reduce web densification and strength. This would be consistent with the hypothesis that the blind drilled blanket did not provide as much of a path for loss of water from the felt while the paper web and felt are in the nip. With this in mind, physical property development will be compared between the various cases based entirely on data from the grooved blanket side of the web. Tables 4 and 5 list the outgoing solids, Bendtsen roughness of the heated side, as well as the CD and GM STFI compression indices for the wet pressed controls as well as the impulse dried samples at the appropriate critical temperatures. It should be noted that samples for outgoing solids measurements were always taken across the entire web. Hence, for the January 1998 experiments, the tabulated outgoing solids slightly overstates the outgoing solids for the blind drilled blanket side of the web and understates the outgoing solids for the grooved blanket side of the web.

Referring to Table 4, attention is focused on the following cases: Short-Ramp 4, Short-Ramp 5, and Std-Ramp 8 On-Hover Off. In these cases, outgoing solids was improved over wet pressing by between 4 and 13%. Similarly, surface smoothness improved by between 22 and 51%. Examination of Table 5 shows corresponding improvements to CD STFI Index of between 3 and 20%, and improvements to GM STFI Index of between 0.7 and 17%. Clearly, impulse drying was beneficial.

**Table 4. Outgoing Solids and Bendtsen Roughness: Improvement of Impulse Drying Compared to Wet Pressing with a Standard 10-Inch Press Shoe.**

Case Date, Freeness, P.M. Speed	Shoe Press Configuration	Outgoing Solids, %			TS-Bendtsen Roughness, ml/min		
		WP	ID	% incr.	WP	ID	% decr.
JUL'97 570 ml CSF 1250 ft/min	Std - No Ramp	43.4	43.5	+0.2	1135	632	+44.3
Aug'97 570 ml CSF 1250 ft/min	Short -Ramp 4	44.0	48.1	+10.8	1140	550	+51.5
	Short -Ramp 5	44.2	47.8	+10.1	870	620	+45.4
Jan'98 540 ml CSF 1250 ft/min	Std - Ramp 8 Off -Hover Off	42.8	45.2	+5.6	1740	1340	+23.0
	Std - Ramp 8 On -Hover Off	na	44.7	+4.4	na	1250	+28.2
	Std - Ramp 8 On -Hover On	na	41.7	-2.6	na	1330	+23.6
Jan'98 458 ml CSF 1250 ft/min	Std - Ramp 8 Off -Hover Off	40.2	43.8	+9.0	1780	1780	+00.0
	Std - Ramp 8 On -Hover Off	40.7	45.6	+13.4	1600	1000	+43.8
	Std - Ramp 8 On -Hover On	39.5	44.2	+10.0	1580	990	+44.4
Jan'98 460 ml CSF 2500 ft/min	Std - Ramp 8 Off -Hover Off	37.9	40.9	+7.9	1770	1370	+22.6
	Std - Ramp 8 On -Hover Off	38.1	40.9	+7.9	1600	1380	+22.0

**Table 5. CD and GM STFI Compression Strength Indices: Improvement of Impulse Drying Compared to Wet Pressing with a Standard 10-Inch Press Shoe.**

Case Date, Freeness, P.M. Speed	Shoe Press Configuration	CD STFI Index, Nm/g			GM STFI Index, Nm/g		
		WP	ID	% incr.	WP	ID	% incr.
Jul'97 570 ml CSF 1250 ft/min	Std - No Ramp	19.7	22.8	+15.7	25.6	28.2	+10.2
Aug'97 570 ml CSF 1250 ft/min	Short -Ramp 4	19.9	23.4	+18.8	26.1	30.1	+17.6
	Short -Ramp 5	22.7	23.7	+20.3	28.0	28.9	+12.9
Jan'98 540 ml CSF 1250 ft/min	Std - Ramp 8 Off -Hover Off	21.2	21.0	-0.9	27.0	26.9	-0.4
	Std - Ramp 8 On -Hover Off	na	22.8	+7.5	na	27.4	+1.5
	Std - Ramp 8 On -Hover On	na	21.1	-0.5	na	26.2	-3.0
Jan'98 458 ml CSF 1250 ft/min	Std - Ramp 8 Off -Hover Off	23.4	22.1	-5.6	30.6	29.7	-2.9
	Std - Ramp 8 On -Hover Off	23.0	24.2	+3.4	30.4	30.8	+0.7
	Std - Ramp 8 On -Hover On	24.5	22.2	-5.1	31.4	30.1	-1.6
Jan'98 460 ml CSF 2500 ft/min	Std - Ramp 8 Off -Hover Off	21.1	21.8	+3.3	28.8	29.1	+1.0
	Std - Ramp 8 On -Hover Off	20.1	22.0	+4.3	28.2	29.8	+3.5

### C. Press and Dryer Roll Surfaces and Web Transfer Systems for Ultra-High Paper Machine Speeds.

#### *Abstract:*

In order to significantly increase current paper-machine speeds, new technology will need to be developed to allow ultra-high-speed web transfer from press rolls and dryer cylinders. Research is proposed that will provide the fundamental knowledge and diagnostic tools needed to design these new technologies. The research will deliver a database and understanding of the mechanisms of deposition of contaminants on roll surfaces, experimental results that demonstrate how surface chemistry and surface topology influence the fracture of water films between wet webs and roll surfaces during peeling, verification of improved web transfer models at ultra-high speeds, and development of an improved roll surface conditioning technology.

The benefits to the industry will include improved paper-machine runnability that will be seen by the paper producer as less breaks per day, increased machine uptime that favorably impacts capital effectiveness, improved utilization of the first dryer section that will improve machine efficiency and energy usage, the achievement of higher machine operating speeds, and improved paper sheet surface properties as a result of reduced sheet picking.

*Background:*

In the coming decade, there will be increasing pressure to substantially increase paper-machine speeds. One of the most important challenges to be faced by paper-machine builders and paper producers will be overcoming barriers to higher speeds. The most difficult of these challenges will be in the area of web transfer from press rolls and dryer cylinders. To help illustrate the problem, consider a single felted enclosed shoe press that is positioned in a second press position on a newsprint machine, as shown in Figure 1. The moist web at a dryness of about 41% is pulled from the press roll surface, in an open draw, by action of a vacuum roll. The tension applied to the web,  $T$ , is fixed at 60 N/m while the peel angle,  $\phi$ , is free to float to an equilibrium value as the machine speed,  $V$ , is increased. Based on the geometry, as shown in Figure 1, there are physical limits on the upper and lower bounds of the peel angle. The location of the doctor limits its maximum value, while the location of the felt roll limits its minimum value.

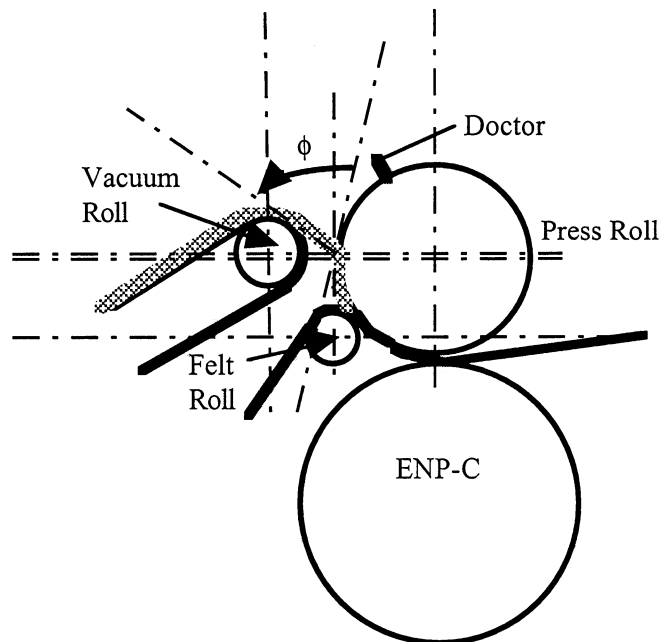


Figure 1. Schematic Diagram of Web Transfer from an Enclosed Shoe Press.

For simplicity, the web strain term in the Mardon Equation, is neglected, see appendix, and obtain the following relationship.

$$[(T-mV^2)/W] = [1/(1-\cos \phi)]$$

Where  $T$  is the tension required to peel the web from the roll,  $m$  is the mass of the wet web,  $V$  is the machine speed,  $W$  is the work of adhesion between the wet web and the roll surface, and  $\phi$  is the peel angle.

By plotting  $[1/(1-\cos \phi)]$  versus  $\phi$  and cross plotting  $[(T-mV^2)/W]$  for various machine speeds, the equilibrium peel angle at the intersection of the curves can be determined. Generally there will be two solutions. Typically solutions in excess of  $90^\circ$  are avoided as they would result in damage to the physical properties of the sheet. In Figure 2 it is observed that the web cannot be separated from the press roll at a speed of 1350 m/min at the prescribed tension. Referring to Figure 3, it is observed that by reducing the work of adhesion,  $W$ , between the web and the roll from 1.8 to 0.18 J/m<sup>2</sup> the web can be peeled at a speed of 1350 m/min at a peel angle of  $20^\circ$ . Alternately, the web tension could be increased, but this would have increased the web strain and could have resulted in a loss of physical properties or in an increase in the probability of a web break. Hence, there is a very good reason to try to find ways to reduce the work of adhesion between the web and the roll surface. In addition to its role in increasing machine speeds, the work of adhesion is also important in controlling web picking. As is shown in the appendix, web picking occurs when the cohesion of the web is of the same order of magnitude as the forces of adhesion between the web and the roll surface. By reducing these adhesion forces, the potential for picking is reduced.

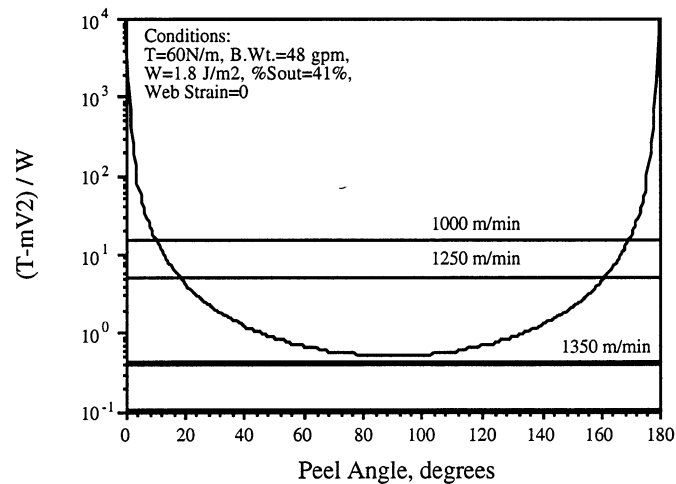
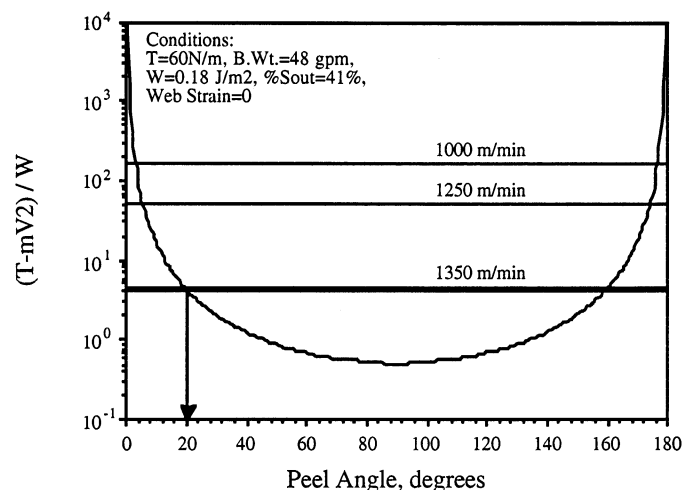


Figure 2. Theoretical Prediction of Peel Angle at Speeds of 1000, 1250, and 1350 m/min Assuming Negligible Web Strain at a Web Tension of 60 N/m, and Work of Adhesion Between the Web and Roll Surface of 1.8 J/m<sup>2</sup>.



**Figure 3.** Theoretical Prediction of Peel Angle at Speeds of 1000, 1250 and 1350 m/min, Assuming Negligible Web Strain at a Web Tension of 60 N/m, and Work of Adhesion Between the Web and Roll Surface of  $0.18\text{ J/m}^2$ .

The research challenge is to develop an in-depth understanding of the mechanisms responsible for these adhesion forces and develop new innovative methods of transferring webs at higher speeds. Recognizing the importance of this area of research, the Institute's Papermaking Project Advisory Committee has recently given the go ahead to initiate a research program to develop a mechanistic understanding of press roll adhesion and picking. Funding in the range of about \$100,000 a year for the next three years is anticipated.

As part of its impulse drying research, the Institute has developed a database on press roll sticking and picking for board grade furnishes over a range of press roll surfaces and press surface temperatures. The Institute has developed and patented specific roll surfaces that have advantages for impulse drying, The Institute, in cooperation with Beloit Corporation, has also recently developed a press roll treatment technology that significantly reduces picking resulting from impulse drying and which may have application to dryer cylinders.

#### *Objectives:*

The objectives of the proposed work are to develop an in-depth understanding of the mechanisms responsible for the adhesion forces between web and roll surfaces that will lead to new innovative methods of transferring webs at ultra-high speeds.

The following is a list of fundamental questions that are addressed in the proposed research

- The performance of roll surfaces depends on the composition of materials that deposit on roll surfaces during use as well as the materials and finishing techniques used in the roll surfaces' manufacture. It is important to understand what materials deposit on roll surfaces and the conditions that influence that deposition. Hence, the chemical composition and concentration of debris and

deposits that accumulate on roll surfaces in both controlled laboratory experiments and in the field will need to be measured.

- According to currently held theories, the work of adhesion is dominated by the work required to fracture the thin film of water between the wet web and the roll surface. Yet very little is known about how these films fracture and how roll surface chemistry and topology influence that mechanism. Hence, it is proposed to develop an experimental model system that can be used to study the dynamics and microstructure of the film splitting process. This would include the development of high-speed imaging systems to visualize the film splitting phenomena occurring as webs separate from the roll surfaces.
- It is important to be able to design web transfer systems that will function at the ultra-high speeds that will be commonplace in the coming decades. The Mardon equation will need to be tested to see if it properly predicts web transfer at these speeds. As part of that objective, mathematical models to predict the work of adhesion from first principles such as surface topology and surface chemical composition will need to be developed. It will also be important to develop mathematical models to relate web strain to web tension as a function of papermaking variables. These models should be verified in laboratory studies and finally in pilot paper machine evaluations.
- Picking is believed to start, or at least become a major problem, when fiber debris is allowed to build up on a roll. In such cases, fiber debris or contaminants may act as "nucleation sites" for sticking and picking. Hence, methods of improving on existing doctoring, wiping, and roll cleaning technologies will need to be developed. In this regard the Institute and Beloit have found that high pressure wiping with PTFE prevents picking on heated roll surfaces. There are, undoubtedly other surface treatment techniques that could play a role. The mechanisms responsible for this phenomena will be explored so that the wiping materials can be optimized and the technique can be applied in a wide range of pressing and drying applications.

#### *General Experimental Approach:*

#### Roles Of Participants:

The Institute of Paper Science and Technology will have responsibility for overall management of the project, as well as having the responsibility for the fundamental aspects of the research, including mathematical modeling, laboratory-scale simulations, and materials characterizations. Beloit Corporation will be responsible for preparation of material coatings, implementing evaluation procedures and techniques, pilot machine studies, and demonstration and commercialization of technology developed as a result of the project.

#### Capabilities and Facilities Available To The Project:

Table 1 lists the major facilities and capabilities of the Institute and of Beloit Corporation that will be utilized in the project. Also shown are the individuals who will be responsible for tasks which utilize these capabilities.

Table 1. R&D Facilities and Capabilities of IPST and Beloit Corporation

Facility or Capability ----->	IPST			BELOIT R&D		
	Math Model	High Speed Heated Roll Press	Analytical Capabilities & Facilities	Roll Cover Manufacture (Beloit-Manhattan)	MTS Pressing Simulator	Pilot Paper Machines
(Investigator)	see text (Orloff)	see text (Orloff)	DAC 120 Surf. Energy (Deng)	Materials Sourcing (Crouse)	Qualitative Screening (Crouse)	Evaluation (Crouse)
Description (Investigator)			X-Ray Diffraction (Deng)	Plasma Spraying (Crouse)		
Description (Investigator)			Laser Microscope (Nanko)			

*Benefits to the Industry Should the Research Yield Promising Results:*

The benefits to the industry will include:

- Improved paper-machine runnability that will be seen by the paper producer as less breaks per day. This will increase machine uptime and favorably impact capital effectiveness.
- Improved utilization of the first dryer section that will improve machine efficiency and energy usage.
- Increased machine operating speeds.
- Improved paper sheet surface properties, less damage to the sheet.

*Schedule:*Project Tasks:

Table 2 lists the tasks that will be undertaken in the project and the research schedule.

Table 2. Project Tasks And Research Schedule

Tasks	Year 1				Year 2				Year 3			
	1	2	3	4	1	2	3	4	1	2	3	4
1. Measure chemical composition and concentration of debris on press roll and dryer cylinder rolls. a.) In laboratory simulations (IPST). b.) In mills (IPST & Beloit).	-	-	-	-	-	-	-	-	-	-	-	-
2. Develop experimental models and investigate details of film splitting during peeling. a.) Design & build apparatus (IPST). b.) Develop film visualization technique (IPST). c.) Investigate effects of surface chemistry and topology on film splitting during peeling (IPST).	-	-	-	-	-	-	-	-	-	-	-	-
3. Develop a portable imaging system that can visualize the film splitting and peel angle on a roll surface. a.) Evaluate potential equipment (IPST). b.) Design & build measurement system (IPST). c.) Evaluate as diagnostic tool in mills (Beloit).			-	-	-	-	-					
4. Develop and verify a mathematical model that can predict web transfer peel angle using portable imaging system. a.) Mathematical model development (IPST). b.) Verification on pilot paper machines (Beloit) c.) Verification at mills (Beloit)					-	-	-	-	-	-	-	-
5. Proof of principle demonstration of PTFE Roll Wiping technology for use on dryer cylinder rolls. a.) Laboratory investigation of mechanism (IPST). b.) Pilot PM demonstration (Beloit).					-	-	-	-	-	-	-	-
6. Final Report											-	X

*Budget and Sources of Funding:*

Table 3 shows the estimated budget for this three-year research project.

Table 3. Estimate Budget

	Year 1	Year 2	Year 3
Salaries & Fringe Benefits	\$139,289	\$283,783	\$149,178
Out-of-Pocket Expenses	\$112,500	\$50,000	\$37,500
Indirect Costs	\$123,931	\$164,288	\$91,883
Total Project Budget	\$375,720	\$498,071	\$278,562

### *Appendix I. Review of the Pulp and Paper Journal Literature*

Prior to the twentieth century, wet press rolls were made of wood. By the first decade of the twentieth century, wood suitable for the manufacture of press rolls was very hard to obtain. Efforts to discover a stone of suitable characteristics led to the discovery of such a material in a quarry in Germany [1]. This stone had a fine crystalline character composed of quartz and a flinty material, both having the same hardness. Since that time and because of its unique release characteristics, granite has become the preferred material for the fabrication of single-felted press rolls.

With continued increases in paper-machine speeds as well as higher and higher press loads, naturally occurring granite has become undesirable due to the fact that it generally has flaws which can lead to catastrophic failure. Starting in the late 1980's, various paper-machine manufacturers have developed synthetic materials that can be used to fabricate press rolls. As a basis for this development, research was undertaken starting in the early 1980's to determine why granite was such a good material and to identify the preferred characteristics of a synthetic replacement.

In 1979, Mardon [2] studied the peeling of paper webs from common press roll cover materials. The results of peeling typical paper furnishes from 12 different press roll materials were presented for a range of take off angles and dryness levels typical of second press operation. The author concluded that there was a relationship between the ease of stripping and surface roughness. He found that wet webs were more easily stripped from rougher materials and that the work of separation decreased with the decreasing dryness.

Around the same time, various investigators tried to understand the mechanisms involved in peeling a web from a roll surface. They noted that there were two interrelated issues, i.e., web separation and web picking. In 1975, Shallhorn and Karnis [3] found that adhesion increased as surface microroughness increased. They attributed this to the web conforming to the surface and thereby increasing the area of contact. They cut MD and CD grooves in surfaces to explore the influence of macroroughness on adhesion. They found that the directionality was not important and that adhesion decreased when the fraction of uncut surface decreased. They concluded that the web was unable to conform to these macrorough surfaces and hence adhesion dropped as the contact area also dropped. In conclusion they suggested that it may be possible to machine a press roll surface in such a way that adhesion and therefore picking would be reduced without affecting the performance of the press section. In the phenomena of picking, they speculated that a variation in the contact angle rather than an average value may be important. They further speculated that variations in microscopic surface roughness of the press roll may result in local minima of the contact angle, with corresponding maxima in the picking tendency.

Also in 1975, Shallhorn et al. [4] published a paper describing the mechanism of press section picking. They found that the picking propensity of a wet-web was a function of fiber-to-fiber and fiber-to-press surface attractive forces. Picking was defined as the transfer of fiber from the web to the press roll as the web is separated from the roll surface. The physical origin of both adhesion and cohesion forces for wet-webs in the range of solids up to at least 30% was believed to be due to surface tension effects. Hence, in the case of adhesion, the authors envision a wet-web in contact with a

surface as two parallel plates separated by a thin film of liquid where the wetted surface fibers and the contacted surface form the two plates. The force of adhesion per unit area,  $F_a$ , between the two plates was then,

$$F_a = (\gamma/d_a)\{1+\cos(\delta)\}$$

where  $\gamma$  = surface tension of the liquid phase,  $\delta$  = contact angle between the liquid and the press roll surface, and  $d_a$  = distance of separation of the plates.

This assumed that the liquid completely wetted the surface fibers and partially wetted the press roll surface with a contact angle  $\delta$ .

The cohesion force arises from a similar type of surface tension effect, the capillary force between fibers in the web where the space (filled with water) between the fibers forms the capillary. The cohesion force per unit area,  $F_c$ , is,

$$F_c = 2\gamma/d_c$$

where  $d_c$  = the mean distance between fibers.

The authors propose that the amount of picking,  $P$  (as measured in grams per square meter attached to the press roll), increases as the difference between the adhesion force and the cohesion force,  $F_a - F_c$ , increases. Hence,

$$P = P(F_a - F_c)$$

Using an experimental apparatus previously used by Mardon [5], the authors measured the amount of picking,  $P$ , as well as cohesion,  $S_c$ , and adhesion,  $S_a$ , forces. A limitation of the experiments was that the measurements were made under almost static conditions from a flat press surface without a felt on the other side of the web. With these limitations in mind, the authors made the following observations:

1. The relationship of adhesion and cohesion to picking: The material picked,  $P$ , generally increased with increasing adhesion force,  $S_a$ , and decreasing cohesion force,  $S_c$ . Picking was greatest when  $S_a$  approached  $S_c$ , and was minimal when  $S_c$  was much greater than  $S_a$ .
2. The effects of moisture: The cohesion force,  $S_c$ , increases with percent solids for both hardwood and softwood furnishes. This is consistent with the idea that as moisture is removed, the fibers are drawn closer together. The adhesion force,  $S_a$ , decreases with increasing solids content.
  - a.) At a given solids level,  $S_c$  increases with refining.
  - b.) At the same freeness,  $S_a$  of hardwoods and softwoods were similar.
  - c.)  $S_a$  was not significantly influenced by refining or solids levels.
  - d.) Since picking decreases with increasing difference between the measured cohesion and adhesion, softwood Kraft picks less than hardwood Kraft. From the difference between cohesion and adhesion, picking must decrease with refining; in addition, picking decreases with increasing solids independent of the type of pulp and level of refining.

The effects of paper-machine speed on web peeling forces were characterized by Oliver [6] by adding a kinetic energy term to the peeling force equation. For peeling speeds greater than 300 m/min, the applied peel force,  $T$ , could be predicted by:

$$T = \{W/(1 - \cos \phi)\} + mV^2$$

where  $W$  is the effective work of peel and  $\phi$  is the peel angle.

The most significant findings of Oliver's quasi-static peel studies were:

a.) over a wide range of peel angles, i.e., 25° to 115°, a maximum in peel force occurred at about 25% dryness, b.) there is an increasing contribution of the web bending moment to the peel force at higher peel angles, and c.) the nature and physical properties of the adhesive film appear to be critical factors in web adhesion and release.

In another paper, Oliver [7] postulated several mechanisms that relate the surface topology of Granite to web adhesion and web release in the press section. These mechanisms were liquid film adhesion, liquid cavitation, and crack propagation. Oliver attributes to Decew [1] the theory that granite, which is composed of quartz, feldspar, and mica, functions well as a release surface because its nonuniform hardness results in small pits during wear. The theory is that air is trapped when a wet web covers the roll; as the web is compressed in the nip, the air is compressed; and in the outgoing part of the nip, the air exerts a pressure helping to force the web away from the surface. Oliver notes that up until 1982, there were no experiments to confirm this theory and he doubted its validity.

While Oliver felt that his data was not conclusive, he did postulate several mechanisms for granite's release properties; these were a.) liquid film thickness: the work of adhesion necessary to separate the web from the press roll surface originates from the surface tension and thickness of the adhesive water film between the roll surface and the web. In regions of the roll surface where there are cavities, the film thickness will increase. As the work of adhesion is reduced with increased film thickness, the cavities will help reduce adhesion and hence promote web release; b.) liquid cavitation: microscopic sharp features of granite are expected to exhibit an excess surface free energy, and may serve as nucleation sites. Oliver suggested that air bubbles could become attached to these sites, and in the exit region of the nip they may weaken the adhesive properties of the water film between the web and the press roll; and c.) crack propagation: the presence of cavities in the granite surface may initiate stress concentrations at the interface between the web and the roll. As such these microscopic sharp jagged roll surface features may act as a trigger for interfacial debonding by creating a plane of weakness along the web peel line.

In 1985, Pye et al. [8] studied the open draw of a newsprint machine. In that work they utilized a modified version of the peel equation, attributed to Mardon, that took wet web strain as well as machine speed into effect;

$$T = \{(W)/(1 - \cos \phi + \epsilon)\} + \{(mV^2)((1 - \cos \phi - \epsilon \cos \phi)/(1 - \cos \phi + \epsilon))\}$$

where  $T$  is the tension in the web,  $W$  is the work required to overcome adhesion,  $\phi$  is the angle of release,  $m$  is the wet web basis weight,  $V$  is the machine speed, and  $\epsilon$  is the web strain.

In a 1989 paper, Wahren [9] discussed the stability of webs in open draws. He confirmed that the necessary minimum web tension due to adhesion of the web to the roll increases in proportion to the speed and in proportion to the square root of the work of separation of the web from the roll. He further found that the most critical web parameters governing runnability are specific web stiffness, web dryness, and stretch. A characteristic parameter governing much of the behavior of the web was the dimensionless group  $Wd/m_{od}V^2$ , where  $W$  is the work of separation,  $d$  is the web dryness,  $m_{od}$  is the bone dry basis weight, and  $V$  is the machine speed.

In more recent work, Alastalo et al. [10] reviewed various sheet release mechanisms that were previously proposed to explain the release properties of granite rolls; these included:

- Liquid film thickness between the web and the roll. The work of adhesion increases with decreasing film thickness.
- Liquid cavitation. Microscopic sharp features in the roll exhibit an excess surface energy and may serve as nucleation sites for condensation, particle separation, and air-bubble formation, all of which can reduce adhesion and facilitate web release.
- Surface energy. Surface energies of roll cover and sheet materials are important factors in evaluation of wettability and release mechanisms.
- Other factors known to effect web release are furnish, fillers, fines, temperature, pH, machine speed, roll surface roughness, and whitewater composition.

The authors measured the surface energies of ceramic and rubber-based roll covers and compared them to that of granite. Static sheet release experiments were also performed in which furnish composition, pH, and chemicals were varied.

Also in a recent paper, Pikulik et al. [11] extended the work on web adhesion into the area of impulse drying. Paper adhesion was expected to be particularly troublesome during impulse drying. In the study fine paper, specialty groundwood, and newsprint were investigated. Using a chromium-plated press roll and an undisclosed furnish, the work of separation increased to a maximum when the roll press surface temperature was increased from 20°C to 100°C. From 100°C to 140°C the work of separation decreased and then increased slightly again at 180°C. These observations agree with Back's conjecture that the greatest adhesion occurs at a critical resin viscosity which is temperature sensitive. Hence, for this study the critical temperature was 100°C. The authors further speculated that wet web separation at high roll temperatures may also be assisted by the pressure of steam which forms on the roll surface. Note that this mechanism is similar in concept to that inferred from DeCew [1] and discarded by Oliver [7].

*Appendix II. Review of the Patent Literature***Valmet Technology***Roll Surface Materials*

In 1989, Miihkinen [12] patented a press roll surface coating formed either of a metallic component or of a mixture of metallic and ceramic components. Where the coating material includes only a metallic component, such a metallic component is chosen so that a separate ceramic component precipitates during the alloying of the materials. The coating material was formulated to obtain a surface energy and polarity component to provide the roll with suitable web release properties for particular pulps. Surface energy within the range of between 35 to 50 mJ/m<sup>2</sup> were claimed. When the pulp contains hydrophilic substances, the coating should be more hydrophobic than granite with a polarity component lower than about 7.1 mJ/m<sup>2</sup>. Likewise, when the pulp contains hydrophobic substances, the coating should be more hydrophilic than granite and have a polarity component greater than 7.1 mJ/m<sup>2</sup>.

In the following year, Miihkinen [13] included PTFE in a press roll surface structure. The surface was composed of metallic and inorganic materials that could be formed by thermal spraying or be bound by a binder such as PTFE. Inorganic particle were specified to have a size range between 5 to 500 microns and be between 10 to 90 parts by volume of the overall volume of the metal - inorganic mixture. The roll surface was so constructed as to have a surface energy of about 41 to 50 mJ/m<sup>2</sup>.

In 1991, Salo [14] patented a resilient roll coating. A metallic press roll is coated with a resilient polymer coating, and onto this is coated a thinner coating of metal, ceramic, cermet, or plastic. The thinner, outer coating is noncontinuous such that resilient yielding of the resilient polymer coating can occur. Also in that year, Leino [15] developed a roll in which the outer face is formed of carbide-rich areas and of metal matrix areas placed between the carbide-rich areas. In the following year, Leino [16] patented a method for manufacturing such a roll.

In 1992, Telma [17] patented a press roll surface made of a porous material in which the pores were sealed by an electrolyte to achieve optimal paper web dewatering capacity, lessen adherence of a paper web to the roll surface, and improve corrosion resistance and mechanical strength. The resulting coating had a porosity of 4 to 50% and a pore size of 5 to 50 microns. In that same year, Leino [18] patented a composite press roll surface described as consisting of metal and ceramic phases, where carbides were included in the ceramic phase. The surface had a micro-hardness greater than about 900 HIV 0.3.

In 1996, Snelling [19] patented a method for coating a press roll composed of ceramic or metal-ceramic with a polymer in order to obtain desired adhesion properties. The polymer was a fluoro-plastic, such as PTFE, and was sprayed on in a pattern such that there were regions of the roll where the polymer coating was applied and there were regions where it was not applied. Also in 1996, Snellman [20] patented a center roll in the paper machine made of a ceramic or metal-ceramic basic material. At least one portion of the center roll was coated or soaked with a polymer coating in order to obtain the desired adhesion properties of the face of the center roll. That coating agent was also polytetrafluoroethelene (PTFE).

### *Roll Heating to Reduce Adhesion*

In 1989, Niskanen [21] patented a method of detaching a web from a surface of a roll with inductive heating. In this technology, a momentary and local heating effect is directed at the web from outside the roll within the area or vicinity of a detaching point. The outer coating of the smooth roll face is at least somewhat magnetically conductive. High-frequency induction heating is used to insure that the heat is local and momentary in nature. Water present between the roll face and the web vaporizes thereby assisting in detaching the web from the roll face.

In 1990, Ilmarinen [22] expanded on the earlier work of Niskanen and patented a method for detaching a moist web from a roll, whereby the roll surface temperature was adjusted to affect adhesion between the web and the roll.

Also in that year, Jaakkola [23] developed a method for heating a cylinder or roll with an electrically conductive ceramic outer layer. A relatively thin outer layer of an electrically conductive ceramic material is used as the cylinder or roll face, in which the resistive heating effect is concentrated. The face of the roll was heated to approximately 140 to 500°C. The application of heat intensifies pressing or promotes detaching of the paper or paperboard web from the heated cylinder or roll.

In 1997, Niskanen [24] patented a method and device in a press section of a paper machine for detaching a web from a face of a press roll. In the method, negative pressure is applied to the transfer zone while the face of the smooth roll, at the transfer point, is heated to between 50 and 100°C. Vaporization occurs at or near the roll surface-wet web interface which facilitates web transfer.

### *Roll Separation Devices*

In 1994, Paloviita [25] patented a method of preventing air from entering between a web and a backing roll. In 1997, Vestola and Harinen [26] patented a method and device for conditioning a ceramic or metal-ceramic coating on a press roll while it is in place on a paper machine. The grinding member, with particles in the size range of 15-200 mm, assures an optimum roll surface roughness.

### **Beloit Technology**

In 1992, Bonander [27] obtained a patent on an electrically conductive synthetic roll cover. The electrically conductive material is applied to the external boundary of at least some fibers which are randomly dispersed within the synthetic roll cover. When slippage occurs between a web and the cover, an electrostatic charge generated by the slippage is discharged by the conductive material from the outer face of the cover to the electrically conductive roll so that scorching of the web by electric discharge through the web is eliminated.

Also in 1992, Jaget [28] patented a material for a roll surface that incorporated an elastomeric material with hollow particles randomly dispersed within. When the surface was machined, a portion of these particles are ruptured, generating a porous surface intended to control adhesion of the web to the roll surface. The polymer material was epoxy resin, while the hollow particles were of glass or graphite.

In 1995, Crouse [29] patented a coating for a backing roll of a high temperature press which reduces web sticking. The backing roll surface coating included 15 to 55 weight percent chromium and 45 to 85 weight percent polytetrafluorocarbon and could be heated to between 82 and 343°C. The coating could also include a mixture of chromium and zirconium. Prior to use, the coating was abraded so that a high percentage of chromium nodules were exposed with the balance of the mixture between the chromium nodules being PTFE.

### **Albany International Technology**

In 1994, Eklund [30] patented a transfer belt that could be used to eliminate an open draw between a press and a transfer point. The belt provided good release by utilizing a surface that has a pressure-responsive recoverable degree of roughness. Leaving the press nip, the paper sheet is held to the transfer belt by the thin, almost continuous water film. Following the exit of the nip, the surface of the transfer belt recovers its uncompressed roughness, breaking up the water film, thereby facilitating release. The uncompressed roughness ranges from  $R_z = 0$  to 20 microns. The air permeability of the belt was less than 20 cubic feet per square foot per minute.

### **Yamauchi Technology**

In 1987, Watanabe [31] patented a press roll with a ceramic outer layer having a porosity of 1 to 30% and having a surface roughness of 0.1 to 3s ( $R_{max}$ ). The porosity was small at the surface and greater in the interior of the ceramic layer. The thickness of the ceramic layer was from 1 to 30 mm. A release agent was impregnated in the pores of the ceramic layer in an amount such that the pores were not closed. The release agent was a silicone plastic, a silicone oil, or a fluoroplastic.

In 1993, Watanabe [32] patented a press roll that was made of a metal core, a metal ground layer having a small coefficient of expansion, a mixture layer composed of ceramic and a water retentivity impacting particulate such as mica. In a surface layer of the mixture layer, an organic high polymer such as synthetic resin or wax was filled in the interstices between particles of the ceramic and particles of mica. The roughness of the outer surface was between 0.2 and 2.0 micrometers ( $R_a$ ), except where the mica was present.

### **Ishikawajima - Harima Heavy Industries Technology**

In 1994, Nasu [33] patented a press roll having a metal base and a sprayed coating on the outer surface of the metal base. The outer layer of the sprayed coating was a mixture of a plastic and a ceramics or a cermet. The outer surface of the plastic portion of the sprayed coating had a lapped, depressed surface relative to the outer surface of the ceramic or cermet portion. The amount of the depression was not specified in the claims.

### **Mitsubishi Heavy Industries Technology**

In 1992, Aoki [34] patented a roll in which a checkerboard or striped pattern was formed on the surface of a roll, with part of the pattern being composed of a fluoro resin and another part being formed of stainless steel. It is claimed that differentiation of wettability improves pressing of a wet web of paper.

### **Paprican Technology**

In 1993, Daunais [35] patented a transfer system in which an air jet was used to assist in separating a moist web from a press roll.

#### *Appendix III. References*

1. DeCew, J. A., "Stone as a Material for Press Rolls," Pulp and Paper Magazine Canada, 11(13):453 (1913).
2. Mardon, J., "A Comparative Study of Peeling of Paper Webs from Common Press Roll Cover Materials," Paperi ja Puu-Papper Och Tra, 61(5):402 (1979).
3. Shallhorn, P. M., and Karnis, A., "The Mechanism of Picking at the Presses of a Paper Machine," 61st Annual Meeting, TS/CPPA, Montreal, January 1975, Preprint B127-B132.
4. Shallhorn, P. M., Karnis, A., Senneville, P. Q., "The Mechanism of Picking at the Presses of a Paper Machine," Transactions, 1(4):102(1975).
5. Mardon, J., Truman, A., O'Blenes, G., and Meadley, K., "A Consideration of the Factors Involved at the Open Draws of Couch and Presses of Fourdrinier Paper Machines," Pulp and Paper Magazine Canada 59(9):135(1958).
6. Oliver, J. F., "Adhesive Film Properties Affecting Web Adhesion and Release from Press Rolls," TAPPI Journal, 65(3): 119 (1982).
7. Oliver, J. F., "The Surface Character of Granite Press Rolls," Journal Of Pulp And Paper Science, 8(1):TR1 (1982).
8. Pye, I. T., Daunaius, R., and Batty, R. C., "A Study of a Newsprint Web in an Open Draw after the Press Section," J. Pulp Paper Sci., Vol. 11, no.5, J145-149, 1985.
9. Wahren, D., "Stability of Webs in Open Draws," Annual Meeting of the CPPA, B19, (1989).
10. Alastalo, A., Neimo, L., and Paulapuro, H., "Sheet Adhesion on Press Roll Materials," TAPPI Papermakers Conference, 411 (1996).
11. Pikulik, I. I., McDonald, J. D., and Aitcin, P.-C., "The Release of Wet Paper from Novel Press Roll Materials," 78th Annual Meeting of the CPPA, A15 (1996).
12. Miihkinen, V., "Press Roll for Paper Making Machines," U.S. Patent No. 4,796,342, Assigned to Valmet Oy, Issued January 10, 1989.
13. Miihkinen, V., "Synthetic Press Roll for Paper Machines and Method for Manufacturing the Same," U.S. Patent No. 4,951,392, Assigned to Valmet Paper Machinery Inc., Issued August 28, 1990.
14. Salo, J., et al., "Coating Roll for a Paper Making Machine," U.S. Patent No. 5023985, Assigned to Valmet Paper Machinery Inc., Issued June 18, 1991.

15. Leino, J., et al. "Roll for Directly Contacting a Web," U.S. Patent No. 4,989,306, Assigned to Valmet Paper Machinery Inc., Issued February 5, 1991.
16. Leino, J., et al., "Method for Manufacturing a Roll Directly Contacting a Web," U.S. Patent No. 5,167,068, Assigned to Valmet Paper Machinery Inc., Issued December 1, 1992.
17. Telma, A., "Paper Machine Roll," U.S. Patent No. 5,111,568, Assigned to Valmet Paper Machinery Inc., Issued May 12, 1992.
18. Leino, J., et al., "Roll for Use in Paper Production and Method of Manufacture Thereof," U.S. Patent No. 5,111,567, Assigned to Valmet Paper Machinery Inc., Issued May 12, 1992.
19. Snelling, J., "Method for the Coatings of the Center Roll in the Press of a Paper Machine and a Center Roll in the Press of a Paper Machine," U.S. Patent No. 5,456,946, Assigned to Valmet Paper Machinery Inc., Issued October 10, 1995.
20. Snellman, J., "Center Roll in the Press of a Paper Machine," U.S. Patent No. 5,569,142, Assigned to Valmet Corporation, Issued October 29, 1996.
21. Niskanen, J., "Method of Detaching a Web from a Surface of a Roll with Inductive Heating," U.S. Patent No. 4,889,598, Assigned to Valmet Paper Machinery Inc., Issued December 26, 1989.
22. Ilmarinen, A., et al., "Control of Detachment of a Paper Web from a Roll Using Heat," U.S. Patent No. 4,919,759, Assigned to Valmet Paper Machinery Inc., Issued April 24, 1990.
23. Jaakkola, J., "Method for Heating a Cylinder or Roll with an Electrically Conductive Ceramic Outer Layer," U.S. Patent No. 4,948,466, Assigned to Valmet Paper Machinery Inc., Issued August 14, 1990.
24. Niskanen, J., "Method and Device in a Press Section of a Paper Machine for Detaching a Web from a Face of a Press Roll," U.S. Patent No. 5,665,206, Assigned to Valmet Corporation, Issued September 9, 1997.
25. Paloviita, P., "Method and Assembly for Preventing Air Entry Between a Moving Material Web and a Roll," Canadian Patent No. 2,113,134. Assigned to Valmet Paper Machinery Inc. Issued July 14, 1994.
26. Vestola, J., and Harinen, P., "Method and Device for Conditioning the Coating of a Paper Machine Roll," U.S. Patent No. 5,597,449, Assigned to Valmet Corporation, Issued January 28, 1997.
27. Bonander, J., "Roll Cover Apparatus," U.S. Patent No. 5,142,759, Assigned to Beloit Corporation, Issued September 1, 1992.
28. Jaget, C.W., "Composition of Matter for Covering a Roll," Canadian Patent No. 2,069,046, Assigned to Beloit Technologies Inc., Published December 21, 1992.
29. Crouse, J.W., "Heated Backing Roll Apparatus," Canadian Patent No. 2,065,166, Assigned to Beloit Technologies, Issued July 18, 1995.

30. Eklund, N., et al., "Transfer Belt in a Press Nip Closed Draw Transfer," U.S. Patent No. 5,298,124, Assigned to Albany International Corp., Issued March 29, 1994.

31. Watanabe, A., et al., "Press Roll for Paper Machine," U.S. Patent No. 4,704,776, Assigned to Yamauchi Rubber Industry Co., Issued November 10, 1987.

32. Watanabe, A., et al., "Press Roll for Paper Machines," U.S. Patent No. 5,257,966, Assigned to Yamauchi Corporation, Issued November 2, 1993.

33. Nasu, T., et al., "Press Roll in a Paper Machine," U.S. Patent No. 5,334,288, Assigned to Ishikawajima-Harima Heavy Industries Co., Issued August 2, 1994.

34. Aoki, S., "Roll," Japanese Patent Kokai 82,989/92, Assigned to Mitsubishi Heavy Industries Ltd., Publication Date March 16, 1992.

35. Daunais, R., et al., "Wet Cellulosic Web Transfer Method Using Air Doctor Blade," U.S. Patent 5,232,555, Assigned to Pulp and Paper Research Institute of Canada, Issued August 3, 1993.

**Delamination Buckling and Spalling  
of  
Plasma Sprayed Thermal Barrier Coating  
for Impulse Drying Rolls**

by

Tim Patterson and David I. Orloff  
Engineering Division  
Institute for Paper Science and Technology  
500 10th St., N.W.  
Atlanta, Ga. 30318

and

Frederick Bloom  
Department of Mathematical Sciences  
Northern Illinois University  
DeKalb, IL 60115



# TABLE OF CONTENTS

Executive Summary

1. Introduction .....

2. Linear Elastic Fracture Mechanics .....

3. Cracking in Coating-Substrate Systems .....

4. Delamination Buckling and Spalling .....

5. Experimental Determination of Coating Toughness .....

References .....

Figures .....



## Executive Summary

The intent of this report is to highlight the theoretical background and the practical problems associated with determining the failure characteristics of coating substrate systems. The emphasis is on impulse dryer rolls coatings and a model of delamination buckling and spalling is presented which can be used to compute critical coating thicknesses under a variety of conditions including thermal cycling. The important points to note are that the in service (but not fatigue) failure of a coating is a function of the critical strain energy release rate which is referred to as the fracture toughness. The strain energy release rate is directly related to the stress intensity factor at the crack tip. The stress intensity factor is a function of the relative proportion of tensile and shear loading. These factors are affected by the coating-substrate system geometry, by the manner in which the coating was applied, by the thickness of the coating, by the presence and composition of a bond coat, by residual stress, and by thermal cycling. A valid laboratory test of such a system requires that the stress field that exists in service applications be duplicated in the laboratory tests. Current testing methods may not provide the means to make this possible. A fracture mechanics examination of the system is the primary way of determining the viability of reliable laboratory testing. When presented with a large range of choices for a coating substrate system, a simplified approach is to make a relative ranking of the coating systems using a basic test method such as the ASTM C633 or similar method. However, care must be taken to distinguish between adhesion and cohesion failure modes. The testing to determine the in service fracture toughness of a coating-substrate system is only a portion of the process of characterizing the system. Other aspects include all the steps up to and including the application of the coating and life modeling of the system.

## 1 Introduction

Impulse drying is most efficiently implemented using a shoe press. In an impulse dryer the shoe portion of the press is unchanged from a standard wet pressing configuration. The roll portion is modified by adding a heating device which is used to maintain the roll pressing surface at temperatures of between 175 and 250 °C. Impulse drying requires a roll surface with thermal properties considerably different from those of plain steel or iron, which are typical press roll structural materials. Steel and iron are good thermal conductors, while the desired roll surface should act as a thermal insulator. A thermal insulating surface provides some control over how the heat energy of the roll is transferred to the sheet and by modifying how the energy is transferred to sheet, sheet delamination can be minimized. An additional reason for using a modified roll surface is sheet sticking. Sticking of the sheet to the roll surface can be a problem depending on the furnish, the roll temperature, and roll surface properties. The currently accepted method of dealing with these problems is to “design” a roll coating composed of one or more materials and to apply it to the surface of a standard steel or iron roll using plasma spraying techniques. This is similar to what is done for many granite replacement rolls. The most important and critical difference between the coating on a granite replacement roll and the coating on a impulse drying roll is that the latter is thermally cycled while in use.

The process of plasma spraying does not produce a microscopically homogeneous material, i.e., Berndt, et. al., [1]. During plasma spraying solid particles are melted and propelled towards the surface that is being coated, i.e., the substrate. When a particle impacts the surface it rapidly deforms the way a rain drop does when hitting a rigid surface. Unlike a raindrop, the plasma sprayed particle freezes in “mid splat” forming a flattened roughly round shape. In freezing it bonds with the previously existing surface, be it the substrate or previously deposited coating splats. The freezing processes results in a coating with residual

stresses induced by the different thermal coefficients of the coating and the substrate and the manner in which the coating is applied, (McPherson [2], Howard [3]). There are also small void spaces and/or weakly bonded areas created by contamination or variations in the spraying process. These areas are where future cracks initiate. The propagation of cracks from these areas is caused by a combination of existing residual stresses, applied external loads, and loads caused by thermal cycling of the coating/substrate system.

Plasma sprayed coatings can fail. These coatings are used in many applications outside the paper industry including jet engine turbine blades and as coatings for diesel engine cylinders. Generally, the coatings are used as thermal barriers and experience thermal cycling to some extent. In all applications there have been failures, although with the current state of knowledge a significant portion could have been avoided. There are three different time frames for coating failure which can be addressed:

1. Formation of the initial void or weak spot from which a crack grows.
2. The “in use” crack growth and failure process.
3. The long term or fatigue failure modes.

The work presented here is primarily concerned with the second process. The first point is not addressed at all in this report except to cite sources which state that initial formation of the coating is important to the overall properties of the coating. The third point, fatigue, is an extremely difficult problem even for microscopically homogeneous materials. It is not addressed except to note the work of one investigator.

Given that plasma sprayed coatings are currently used in pilot scale impulse dryers, will be used in commercial scale impulse dryers, and that these coatings could fail in use, there are several questions which must be answered:

1. What are the “in use” crack growth modes by which plasma sprayed coatings fail?

2. What is the predominant failure mode for an impulse dryer roll coating?
3. What parameter is best used to quantify the failure resistance of an impulse dryer roll coating?
4. What testing method is best used to obtain the parameter which quantifies the failure resistance of impulse dryer roll coatings?
5. What additional factors are important in determining the durability of plasma sprayed coatings?

Plasma sprayed coatings are generally brittle materials and fail by cracking. The cracking process can take many forms depending on the applied loads, the residual stresses, and the relative material properties of the coating and substrate. The failure mode of a brittle coating on a ductile substrate is different from the failure mode of a brittle coating on a brittle substrate. In plasma sprayed coatings the failure can begin in one of three locations: the coating, the substrate, or the interface between the coating and the substrate. Once the crack initiates the crack can propagate to one of the other regions of the coating-substrate system. In the case of an impulse dryer roll a brittle coating is applied to a relatively ductile substrate. Failure in the substrate or propagation of a crack into the substrate is an unlikely occurrence with this type of system (Evans [4]).

The plasma spraying techniques and the thermal insulating coating materials used with impulse dryer rolls result in a coating which is subjected to in-plane biaxial compressive stresses. The plasma spraying process deposits a hot liquid insulating material with a low thermal expansion coefficient on a cooler metal substrate with a high thermal expansion coefficient. The cooling from liquid to solid, and the thermal expansion mismatch, results in a compressive stress state. The most likely, and also previously observed, failure mode is buckling followed by spalling and coating failure. If the initial crack is in the coating,

spalling can result in crack propagation to the bi-material interface. If the initial crack is at the interface, crack propagation is generally along the interface. Whether crack initiation occurs in the coating or at the material interface is dependent on which has the lower fracture toughness (fracture toughness is defined in §2).

The following sections of this report present the fracture mechanics approach to crack propagation, describe a number of testing techniques, discuss the applicability of those techniques to impulse dryer roll coatings, and present a brief discussion of other factors affecting coating durability. We also present, in §4, a model of delamination buckling and spalling of thermal barrier coatings which can be used to predict a critical coating thickness below which delamination should not occur even under thermal cycling of the roll.

## 2 Linear Elastic Fracture Mechanics

The crack growth process can be modeled using fracture mechanics. Prior to delving into the primary subject of this report it is useful to review some principles and terminology from fracture mechanics. Current literature on coating-substrate failure assumes a considerable background knowledge and occasionally employs inconsistent terminology. In this section we discuss fracture mechanics for elastic homogeneous materials. It is possible to apply the concepts developed in this section to the analysis of some specimens used in the testing of coating-substrate systems; this is possible when an in depth analysis of the crack tip is not required.

The first treatment of crack propagation was the *Energy Balance Approach*. It was first introduced by Griffith in the late 1940s and then modified by Irwin. This approach relates the change in the elastic energy of the plate  $U_a$ , caused by the creation of the crack, to the change in elastic surface energy,  $U_\gamma$ , produced by the formation of the crack surface. In this

formulation an infinite plate of unit thickness is subjected to a uniform tensile stress,  $\sigma$ , applied at infinity. The plate contains a crack as shown in Figure 1.1.

The energy balance for the configuration in Figure 1 is

$$\mathcal{U} = \mathcal{U}_0 + \mathcal{U}_a + \mathcal{U}_\gamma - W_f \quad (2.1)$$

where  $\mathcal{U}_0$ , is the elastic energy in the uncracked plate and  $W_f$  is the work performed by external forces. Under the condition of no displacement at the point of loading  $W_f = 0$ . Using stress analysis Griffith showed that for unit thickness

$$\mathcal{U}_a = (\pi\sigma^2 a^2)/E. \quad (2.2)$$

where  $E$  is Young's Modulus for the material. Also, the elastic surface energy is proportional to the product of the surface energy of the material,  $\gamma_e$ , and the new surface area of the crack

$$\mathcal{U}_\gamma = 2(2a\gamma_e). \quad (2.3)$$

The total energy, with  $W_f = 0$ , is thus

$$\mathcal{U} = \mathcal{U}_0 + \mathcal{U}_a + \mathcal{U}_\gamma. \quad (2.4)$$

Taking the derivative, noting that  $\mathcal{U}_0$  is constant, and that the equilibrium condition for crack extension requires  $d\mathcal{U}/da = 0$ , gives

$$\frac{d}{da} [(-\pi\sigma^2 a^2)/E + 4a\gamma_e] = 0. \quad (2.5)$$

The equilibrium condition is obtained by setting the quantity in brackets in (2.5) equal to zero, i.e.,

$$\frac{\pi\sigma^2 a}{E} = 2\gamma_e. \quad (2.6)$$

An unstable situation results “when the elastic energy release due to a potential increment in crack growth,  $da$ , outweighs the demand for surface energy for the same crack growth.” This version of the energy balance approach is only valid for an ideally sharp crack with a fixed grip and only indicates the criterion for instability of the crack.

The energy balance approach introduces two concepts which are used in most treatments of crack growth. The left hand side of (2.6) is the energy per unit crack length that is available for infinitesimal crack growth and is referred to as the *strain energy release rate*. This term is fairly general throughout the literature although it is sometimes shortened to energy release rate; in this report the symbol,  $\mathcal{G}$ , is used to represent this quantity. The quantity on the right hand side of (2.6) is the surface energy increase that would occur due to an infinitesimal crack extension (true only for brittle materials). Although not shown in the equation, this parameter is a function of the relative magnitudes of the shear ( $\sigma_{12}$ ) and tension ( $\sigma_{22}$ ) stresses near the crack tip. In this report it is referred to as the *fracture toughness*  $\Omega$ ; in the literature it is also referred to as the fracture resistance or crack resistance, and is denoted by various symbols some of which are also used for different parameters. One can avoid confusion by noting that the units for both quantities  $\mathcal{G}$ , and  $\Omega$ , are *(force/area)(distance)*. Assuming that  $\Omega$  is a constant, (i.e., the relative magnitudes of  $\sigma_{12}$  and  $\sigma_{22}$  remain constant) when  $\mathcal{G}$  exceeds a critical value,  $\mathcal{G}_c$ , unstable crack growth occurs, i.e., when

$$(\pi\sigma^2 a/E) \geq (\pi\sigma_c^2 a/E) = \mathcal{G}_c = \Omega. \quad (2.7)$$

A second approach to describing the crack propagation process is the *Stress Intensity Approach*, developed by Irwin in the 1950s.

The stress intensity approach introduces a third important concept. Figure 2.1 shows a representative crack. From linear elastic theory the stresses in the vicinity of the crack tip are given by the representation

$$\sigma_{ij} = \frac{K}{(2\pi r)^{1/2}} f_{ij}(\theta) + \dots \quad (2.8)$$

where  $r, \theta$  are cylindrical polar coordinates of a point with respect to the crack tip and  $K$  is the *Complex Stress Intensity Factor*; it has units of  $(\text{force/area})(\text{distance})^{1/2}$  and in the literature this parameter is also referred to as the fracture toughness and fracture resistance. Some confusion can be avoided by noting the difference in units between this parameter and the strain energy release rate. The general form of the equation for  $K$  is

$$K = \sigma(\pi a)^{1/2} f(a/w) \quad (2.9)$$

where  $f(a/w)$  is a dimensionless parameter that depends on the geometries of the specimen and the crack. The parameter “a” is used as a characteristic length in the relationship. In some formulations  $r$  is used as the characteristic length. The concept that  $K$  is linearly related to the applied stress and directly related to the square root of a characteristic length is the primary result.

In the one dimensional case discussed here (elastic homogeneous material), there is no imaginary component; however, in the case where tensile and shear stresses exist,  $K$  is given by

$$K = K_I + iK_{II} \quad (2.10)$$

or

$$[K]^2 = K K = K_I^2 + iK_{II}^2 \quad (2.11)$$

where

$$K_I = \sigma_{22}(2\pi r)^{1/2}, \quad K_{II} = \sigma_{12}(2\pi r)^{1/2}.$$

In (2.10),  $K_I$  is the stress intensity factor for tensile loading only (mode I) and  $K_{II}$  is the stress intensity factor for shear loading only (mode II).

The complex stress intensity factor gives the magnitude of the elastic stress field and is therefore directly related to the strain energy release rate. In fact, it has been demonstrated that if a crack is extended by an amount  $da$ , the work done by the stress field ahead of the crack when moving through displacements corresponding to a crack length  $(a + da)$  is formally equivalent to the change in the strain energy given by  $\mathcal{G}da$ . Thus the achievement of a critical complex stress intensity factor,  $K_c$ , is exactly equivalent to the Griffith-Irwin energy approach, which requires the achievement of a stored elastic strain energy equal to  $\mathcal{G}_c$ .

The equivalence of  $K$  and  $\mathcal{G}$  can be stated mathematically. In the case of tensile loading ( $K_{II} = 0$ ), the relationship between  $\mathcal{G}$  and  $K$  is given by rewriting (2.9) as  $K^2 = (\sigma^2\pi a)$  and substituting into (2.7) so as to obtain

$$\mathcal{G} = K_{Ic}^2/E \quad \text{plane stress} \quad (2.12)$$

$$\mathcal{G} = (K_{Ic}^2/E)(1 - \nu^2) \quad \text{plane strain}$$

where  $\nu$  is Poisson's ratio and  $E$  is Young's modulus. The mixed mode case is described by

$$\mathcal{G} = (K_I^2 + K_{II}^2)/E \quad \text{plane stress}$$

$$\mathcal{G} = [(K_I^2 + K_{II}^2)/E](1 - \nu^2) \quad \text{plane strain.} \quad (2.13)$$

and the failure criterion in terms of  $K$  is given by

$$\sigma(\pi a)^{1/2} \geq \sigma_c(\pi a)^{1/2} = K_{ic}. \quad (2.14)$$

The basic form of the equations, above, is retained in the case of coating-substrate systems. What makes the stress intensity approach important is the fact that if one knows the state of stress in a specimen during crack growth then the complex stress intensity factor can easily be determined, from that the strain energy release rate can be calculated. Also,  $K$  is applicable to stable crack growth. In the case of a homogeneous specimen, with a through crack, the calculations for determining the stress field are relatively straight forward, if not brief. In the case of a plasma sprayed coating on a substrate, the calculations are not straight forward and finite element techniques are usually the only recourse.

Returning to the energy balance approach, the energy content of a remotely loaded cracked elastic plate is

$$\mathcal{U} = \mathcal{U}_0 + \mathcal{U}_a + \mathcal{U}_\gamma - W_f \quad (2.15)$$

where the parameters are the same as previously defined. Since stable crack growth requires that an increase in  $\mathcal{U}$  is balanced by an increase in crack length,  $a$ , instability occurs when

$$d\mathcal{U}/da \leq 0. \quad (2.16)$$

Taking into account that  $\mathcal{U}_0$  is constant, gives

$$\frac{d}{da}(\mathcal{U}_a + \mathcal{U}_\gamma - W_f) \leq 0 \quad (2.17)$$

or

$$d(W_f - \mathcal{U}_a)/da \geq d\mathcal{U}_\gamma/da. \quad (2.18)$$

On the left hand side of equation (2.18),  $dW_f/da$  is the external work and  $d\mathcal{U}_a/da$  is the increase in elastic energy due to the crack length increase caused by the external work; thus, the left hand side of this equation is the energy for expansion of the crack and this provides an alternative expression for the strain energy release rate of the form

$$\mathcal{G} = \frac{d}{da}(W_f F - \mathcal{U}_a) \quad (2.19)$$

while the fracture toughness,  $\Omega$ , is given by

$$\Omega = d(\mathcal{U}_\gamma)/da. \quad (2.20)$$

In the case of fixed grips (equivalent to a fracture test using displacement control) there is no motion at the point where the external load is applied ( $v = 0$ ). When the crack forms there is no displacement associated with the external loads, therefore  $dW_f/da = 0$  and (2.19) becomes

$$\mathcal{G}_c = -d\mathcal{U}_a/da. \quad (2.21)$$

The elastic strain energy decreases because the increased crack size reduces the stiffness of the plate and because there is no increase in energy provided by the external forces.

In the constant load case (equivalent to a fracture test using force control) the position associated with the external load changes as the crack grows to compensate for the reduction in plate stiffness. The elastic energies in an initial configuration before and after crack growth are given by  $\mathcal{U}_{a1}$  and  $\mathcal{U}_{a2}$ , respectively and the elastic energy for the new configuration is

$$W_f - \mathcal{U}_{a1} = \mathcal{U}_{a2}. \quad (2.22)$$

Then (2.19) becomes

$$\mathcal{G} = d(W_f - \mathcal{U}_a)/da = d\mathcal{U}_a/da. \quad (2.23)$$

For the constant load case the external forces provide the energy for both the increase in the elastic energy and the crack extension. We note that under both types of loading conditions the strain energy release rate is the same, although the signs are opposite. These results show that an investigator desiring to study controlled crack growth should select a position controlled means of applying loads to the test specimen. Given the above relationships, crack growth is directly related to the position of the ends of the sample for the position controlled case. This results in the more stable case where there is decreasing available elastic energy for crack growth. In the force controlled case, crack growth is related to the applied load and to changes in sample stiffness; this is more difficult to control in an experimental setup.

The parameters  $K$  and  $\mathcal{G}$  are not easily obtained. To determine critical crack growth conditions the energy balance approach requires a priori knowledge of the stress field in the sample and the surface energy which is related to crack growth. The stress intensity approach requires knowledge of the stress field and some knowledge of the crack geometry. An alternative approach, the compliance approach, is made possible by the relationship between strain energy and compliance (the inverse of stiffness); the ideas here are as follows:

A cracked body is shown in Fig 2.2. Recalling the equation for the strain energy release rate, i.e., (2.19) and referring to Fig. 3, (2.22) can be rewritten as

$$\mathcal{G} = (1/B)[P(dv/da) - (d\mathcal{U}_a/da)]$$

or

$$\mathcal{G} = (1/B)[P(dv/da) - (1/2)(d(Pv)/da)] \quad (2.24)$$

where for an elastic material the strain energy  $\mathcal{U}_a$  is equal to the area under the load displacement graph, i.e.,  $\frac{1}{2}Pv$ .

Noting that the compliance,  $C = v/P$ , is the inverse of stiffness, and substituting into (2.24) yields, after some algebraic manipulations

$$\mathcal{G} = (1/2B)P^2(dC/da) \quad (2.25)$$

Thus the strain energy release rate can be found by applying a known load condition and determining the compliance of the specimen under the load condition.

The equivalence of the strain energy release rate for the constant load and fixed grip (constant position) cases is obtained by considering the elastic strain energy  $\mathcal{U}_a$  for both cases. The general expression for the change due to  $\mathcal{U}_a$  is given by

$$(1/B)(d\mathcal{U}_a/da) = (1/2B)[P(dv/da) + v(dP/da)] \quad (2.26)$$

Using the relationship between  $C$ ,  $v$ , and  $P$ , then yields

$$(1/B)(d\mathcal{U}_a/da) = (P^2/2B)(dC/da) + (v/B)(dP/da). \quad (2.27)$$

In the constant load case,  $P = \text{const}$  and, therefore,  $dP/da = 0$ ; substituting this result into (2.27) produces

$$(1/B)(d\mathcal{U}_a/da) = (P^2/2B)(dC/da) \quad (2.28)$$

For the fixed grip (constant position) condition, (2.26) may be rewritten as

$$(1/B)(d\mathcal{U}_a/da) = (P^2/2B)(dC/da) + (v/B)(d(v/C)/da) \quad (2.29)$$

which simplifies, after some algebraic manipulations, to

$$(1/B)(d\mathcal{U}_a/da) = -(P^2/2B)(dC/da). \quad (2.30)$$

Equations (2.28) and (2.30) show that if the load drops (with the position constant) upon crack extension,  $dU_a/da$  decreases; also, if the position changes (load constant)  $dU_a/da$  increases. This again indicates that for controlled crack growth experiments the constant position approach is preferred.

The strain energy release rate can be used to determine the stress intensity factor using the relations

$$K_1^2 \approx \bar{E}\mathcal{G} = (\bar{E}P^2/2B)(dC/da) \quad (2.31)$$

where

$$\begin{cases} \bar{E} = E, & \text{for plane stress} \\ \bar{E} = E(1 - \nu^2), & \text{for plane strain} \end{cases}$$

and this can be generalized to

$$K^2 = \bar{E}\mathcal{G} = (\bar{E}P^2/2B)(dC/da) \quad (2.32)$$

with  $K$  as given in (2.10).

### 3 Cracking in Coating-Substrate Systems

A coating-substrate system exhibits an interface between the coating (or film) and the substrate. The properties of the coating, the properties of the substrate, and the existence of the interface can affect how a crack will propagate through the bi-material. A bi-material can develop a crack in the coating, in the substrate, or at the interface between the two. Once a crack begins to propagate it can extend from the coating or the substrate to the interface. The crack can also propagate from the interface into either the coating or substrate. In this section we briefly summarize the theoretical treatment of bi-materials. As noted previously, crack propagation in the substrate is unlikely for impulse dryer rolls. Thus, substrate crack

propagation is not addressed here. The approach presented in this section is primarily due to Hutchinson and Suo [5].

In a brittle, homogeneous, isotropic material a crack will propagate in a manner which maintains pure mode I conditions (out-of-plane tensile loading) at the crack tip. Typical impulse dryer plasma sprayed roll coatings, which do not have property gradients, can be considered to have those characteristics on a macroscopic scale. Given a mixed loading condition, consisting of both mode I (tensile) and mode II (shear), the crack will change direction, or kink, in order to eliminate the shear loading. The relative magnitude of tensile and shear loading is described by the phase angle  $\Psi$ , where

$$\psi = \tan^{-1}(K_{II}/K_I) \quad (3.1)$$

or

$$\psi = \tan^{-1}(\sigma_{12}/\sigma_{22}). \quad (3.2)$$

and, at the interface, this behavior can be modified. If the mechanical properties of the coating and the substrate are significantly different, or if the bond between the coating and the substrate has a low toughness, the crack may propagate in a manner which maintains mixed loading conditions or the crack propagation can be oscillatory in nature, i.e., mode I  $\rightarrow$  mixed mode  $\rightarrow$  mode I.

In order to delineate, in §4, the conditions governing the formation of a one-dimensional blister (buckle) in the film (and the subsequent spallation which can occur) some definitions, notations, and relations are needed. For a wide class of plane problems of elasticity for bi-materials there are two critical nondimensional combinations of the elastic parameters,

the Dunder's parameters, which figure prominently in the analysis; these are given by

$$\left\{ \begin{array}{l} \hat{\alpha} = \frac{\Gamma(k_s + 1) - (k_f + 1)}{\Gamma(k_s + 1) + (k_f + 1)} \\ \hat{\beta} = \frac{\Gamma(k_s - 1) - (k_f - 1)}{\Gamma(k_s + 1) + (k_f + 1)} \end{array} \right. \begin{array}{l} \left[ \begin{array}{l} \text{measures the mismatch in} \\ \text{the plane tensile modulus} \\ \text{across the crack interface} \end{array} \right] \\ \left[ \begin{array}{l} \text{measures the mismatch in} \\ \text{the in-plane bulk moduli} \end{array} \right] \end{array} \quad (3.3)$$

where

$$k_f = \begin{cases} 3 - 4\nu_f & \text{(plane strain)} \\ (3 - \nu_f)/(1 + \nu_f) & \text{(plane stress)} \end{cases} \quad (3.4)$$

$$k_s = \begin{cases} 3 - 4\nu_s & \text{plane strain)} \\ (3 - \nu_s)/(1 + \nu_s) & \text{(plane stress)} \end{cases} \quad (3.5)$$

while

$$\Gamma = G_f/G_s \quad (3.6)$$

The subscripts  $f$  and  $s$  refer, respectively, to the film (i.e., coating) and substrate.

The complex stress vector at distance  $r$  ahead of a crack tip is given by

$$\sigma_{12} + i\sigma_{22} = \frac{K r^{i\epsilon}}{\sqrt{2\pi r}} \quad (3.7)$$

where

$$\epsilon = \frac{1}{2\pi} \ln \left( \frac{1 - \hat{\beta}}{1 + \hat{\beta}} \right) \quad (3.8)$$

while  $K$  is the complex stress intensity factor as given by (2.10) with  $K_I$ , and  $K_{II}$ , respectively, the mode I and mode II stress intensity factors; also, as in (3.2),

$$\psi = \tan^{-1} \left( \frac{\sigma_{12}}{\sigma_{22}} \right)$$

With respect to the conditions at an 'interface' crack, which involve a combination of opening (mode I) and shearing (mode II), it may be shown that

$$|K| = K\bar{K} = K_I^2 + K_{II}^2 = E_f \cdot \mathcal{G}/(1 - \nu_f^2) \quad (3.9)$$

In service, failure of bimetals can and often does occur under mixed mode conditions. A number of investigators have attempted to develop mixed mode fracture specimens for failure at the bimaterial interface; in all cases fracture toughness  $\Omega$  is a function of the relative amount of mode I and mode II loading acting on the interface. Thus, the relationship for critical energy release rate has the form

$$\mathcal{G}_c = \Omega(\psi). \quad (3.10)$$

The fracture toughness at the interface,  $\Omega(\psi)$ , is a measure of effective surface energy that depends on the method of loading and the resultant stress field at the crack tip. The interface fracture toughness cannot be determined analytically; it must be found experimentally.

## 4 Delamination Buckling and Spalling

We consider a model for the problem of buckling and spalling of a thin film or coating which is bonded to a metallic ‘substrate’; for the case at hand, the ‘substrate’ should be thought of as being the metallic bond coat which is intermediate to a ceramic (or FGM) coating and the actual roll (substrate). The bond coat has thickness  $H$  while the film (coating) has thickness  $h$ . It will be assumed that both the bond coat and film are linearly elastic with (respectively) Young’s modulus, Poisson’s ratio and thermal expansion coefficients  $(E_s, \nu_s, \alpha_s)$  and  $(E_f, \nu_f, \alpha_f)$ . If the film is actually a functionally gradient medium then  $E_f, \nu_f, \alpha_f$  will vary with position (depth) in the film in a manner that will be indicated below. Finally, we denote by  $G_s, G_f$  (respectively) the shear modulus in the bond coat and film.

A system, such as the one described above, consisting of strongly bonded dissimilar materials with mismatches in both material constitutive constants and thermal expansion coefficients is stress-free only at the temperature  $T_0$  at which the layers were joined. Cooling

of the system to 'room' temperature then leads to compressive stresses, specifically, to a biaxial residual stress state in the surface layer (film). If  $T_c$  denotes the current temperature<sup>1</sup> at a depth of  $z$  units into the film (*measured* from the film/bond coat interface) then, as a general rule of thumb,

$$T_c(z, t) = T_0 + (T_R - T_0) \operatorname{erf} (z/2\sqrt{t\kappa_f}) \quad (4.1)$$

where  $T_R$  is 'room' temperature and  $\kappa_f$  is the thermal diffusivity coefficient of the film. Also, the biaxial residual stress state is given by

$$\sigma(z, t) = \sigma_0 \operatorname{erf} (z/2\sqrt{t\kappa_f}) \quad (4.2)$$

where

$$\sigma_0 = E_f \Delta\alpha \cdot \Delta T / (1 - \nu_f) \quad (4.3)$$

with

$$\Delta\alpha = \alpha_f - \alpha_s, \quad \Delta T = T_0 - T_R. \quad (4.4)$$

The analysis of precompressed films shows that such films are only susceptible to delamination and eventual spalling once film buckling has been initiated. After buckling a stress intensification develops at the perimeter of the delamination. The stress intensity depends on the magnitude of the prestress ( $\sigma_0$  for a steady-state situation) and the film thickness  $h$ . A critical value of  $\sigma\sqrt{h}$  at depth  $z$ , at time  $t$ , must be exceeded before a delamination originating in the film, at that depth, can propagate and cause spallation. To summarize, films which are subject to residual compression decohere by first buckling above an initial crack (separation) and then spalling as the crack subsequently propagates through the film. Spalling is characterized by the comparative values of the fracture resistance of the film and the residual crack driving force (as measured, e.g., by the energy release rate). If there exist

---

<sup>1</sup>i.e., the temperature  $t$  units of time after the removal of the heat source.

many small cracks parallel to the free surface of the film the overall stress needed to induce a surface buckling mode is lowered.

Whenever there exists a small separation (crack) at the film/bond coat interface, or within the film just above that interface, the film is susceptible to buckling; such a crack parallel to the free surface of the film does not, itself, disturb a stress field since that field also acts parallel to the film's free surface. Therefore, a stress concentration along the edge of the crack is not induced; but, if the film buckles away from the bond coat layer the resulting separation generates large tensile stresses at the perimeter of the interface crack which induces crack extension into the film. Thus, the failure mechanism for such systems couples buckling with crack propagation; it will be made clear, below, that the propagation of the crack, subsequent to the development of a straight-sided blister (buckle) on the film is a 'mixed-mode' event. However, the fact that the crack tip becomes *mostly* mode II as a one-dimensional buckle spreads has been used to explain why such blisters have a characteristic width, i.e., do not keep spreading along their edges under constant overall load.

In the work of Chai, et. al. [6], Whitcomb [7], Evans and Hutchinson [8], and Hutchinson and Suo [5] one finds analyses geared towards the derivation of formulas relating the energy release rate  $\mathcal{G}$  of the crack to the parameters which also govern formation of a blister (buckle); some of these relations have been described in §2. Because of the availability of relationships between interface stress intensity factors and moments/resultant force changes at the edge of a blister (buckle), which has a pre-existing crack or separation at its base, the requisite one-dimensional analysis may be carried out in closed form.

We depict, in Fig. 4.1, a segment of a straight-sided (one-dimensional) blister above a crack, at its base, of length  $2a$  and width  $b$ .

The unbuckled film is subject to uniform, equi-biaxial compressive in-plane stresses  $\sigma = -\sigma_{xx} = -\sigma_{yy}$ . It is assumed that the film thickness  $h$  is sufficiently small so that the film segment in question can be represented as a clamped Euler column of width  $2a$ . The

critical (classical) buckling stress,  $\sigma_c$ , for such a situation is known to be given by

$$\sigma_c = \frac{\pi^2}{12} \cdot \frac{E_f}{(1 - \nu_f^2)} \cdot \left(\frac{h}{a}\right)^2 \quad (4.5)$$

For stress levels  $\sigma > \sigma_c$ , the ‘normalized’ amplitude of the buckling deflection,  $\xi = w(0)/h$ , is given by

$$\xi = \left[ \frac{4}{3} \left( \frac{\sigma}{\sigma_c} - 1 \right) \right]^{1/2} \quad (4.6)$$

As has been indicated in §2, in order to determine the energy release rate  $\mathcal{G}$  associated with this process, it is necessary to examine the change in the stored energy of the buckle as the perimeter of the rectangular base of the blister is loaded under increasing stress; if the elastic energy lost in that process is greater than or equal to the critical energy release rate  $\mathcal{G}_c$ , required to create a unit of new delamination, then growth of the crack (spallation) will take place.

Using the fact that the elastic strain energy stored in a unit area of the film is

$$\mathcal{U} = (1 - \nu_f)\sigma^2 h / E_f, \quad (4.7)$$

an elementary (but non-trivial) calculation shows that the energy release rate is given by

$$\mathcal{G} = (1 - \nu_f)(1 - \hat{\alpha})h(\sigma^2 - \sigma_c^2) / E_f \quad (4.8)$$

where  $\hat{\alpha}$  is the first Dundurs’ parameter as given by (3.3). Combining (4.8) with (3.9) we find for the magnitude of the effective stress intensity factor

$$|K| / (\sigma\sqrt{h}) = \left[ \frac{1 - \hat{\alpha}}{1 + \nu_f} \right]^{1/2} \left[ 1 - \left( \frac{\sigma_c}{\sigma} \right)^2 \right]^{1/2} \quad (4.9)$$

Furthermore, for residual stresses  $\sigma \geq 3\sigma_c$ ,  $|K|$  is well-approximated by the relation

$$|K| / (\sigma\sqrt{h}) \simeq \left( \frac{1 - \hat{\alpha}}{1 + \nu_f} \right)^{1/2} \quad (4.10)$$

By approximating the radical  $\sqrt{1 - \left(\frac{\sigma_c}{\sigma}\right)^2}$ , and substituting for the critical buckling stress  $\sigma_c$  from (4.5), we find that

$$|K|/(\sigma\sqrt{h}) \simeq \left(\frac{1 - \hat{\alpha}}{1 + \nu_f}\right)^{1/2} \left[ 1 - \frac{\pi^2}{12} \cdot \frac{E_f}{1 - \nu_f^2} \frac{1}{\sigma} \left(\frac{h}{a}\right)^2 \right] \quad (4.11)$$

For a steady-state situation, the residual stress  $\sigma$  may be approximated by  $\sigma_0$  as given by (4.3), i.e.;

$$\sigma_0 = E_f \Delta\alpha \cdot \Delta T / (1 - \nu_f)$$

in which case

$$|K| \simeq \left(\frac{1 - \hat{\alpha}}{1 + \nu_f}\right)^{1/2} \sigma_0 \left[ 1 - \frac{\pi^2}{12} \cdot \frac{E_f}{1 - \nu_f^2} \frac{1}{\sigma_0} \left(\frac{h}{a}\right)^2 \right] \sqrt{h} \quad (4.12)$$

while, by virtue of (4.8), with  $\sigma \rightarrow \sigma_0$ ,

$$\mathcal{G} \simeq \frac{(1 - \nu_f)}{E_f} \cdot (1 - \hat{\alpha})(\sigma_0^2 - \sigma_c^2)h \quad (4.13)$$

approximates the energy release rate. On the other hand, if we combine the approximation (4.10) with the relation (3.9) and employ:  $\sigma \rightarrow \sigma_0$  we obtain

$$\begin{aligned} \mathcal{G} &\simeq \left(\frac{1 - \hat{\alpha}}{1 + \nu_f}\right)^{1/2} \frac{1 - \nu_f^2}{E_f} \cdot \sigma_0 \sqrt{h} \\ &= \left(\frac{1 - \hat{\alpha}}{1 + \nu_f}\right)^{1/2} \frac{1 - \nu_f^2}{E_f} \left\{ \frac{E_f \Delta\alpha \cdot \Delta T}{1 - \nu_f} \right\} \sqrt{h} \\ &\simeq \sqrt{(1 - \hat{\alpha})(1 + \nu_f)} \Delta\alpha \cdot \Delta T \cdot \sqrt{h} \end{aligned} \quad (4.14)$$

If we *do not* replace  $\sigma \rightarrow \sigma_0$ , then

$$\mathcal{G} \simeq \left(\frac{1 - \hat{\alpha}}{1 + \nu_f}\right)^{1/2} \frac{1 - \nu_f^2}{E_f} \cdot \sigma \sqrt{h} \quad (4.15)$$

with  $\sigma$  given by (4.2). Thus

$$\mathcal{G} \simeq \sqrt{(1 - \hat{\alpha})(1 + \nu_f)} \Delta\alpha \cdot \Delta T \cdot \sqrt{h} \cdot \operatorname{erf} \left( \frac{z}{2\sqrt{t\kappa_f}} \right) \quad (4.16)$$

where

$$\operatorname{erf}\left(\frac{z}{2\sqrt{t\kappa_f}}\right) = \frac{1}{\sqrt{2\pi}} \int_0^{\frac{z}{2\sqrt{t\kappa_f}}} e^{-1/2\lambda^2} d\lambda \quad (4.17)$$

**Remarks:** Cyclic processes are barely touched in the literature; however, (4.16) has already been set up so as to encompass such a situation, i.e., we note that while

$$\sigma_0 = E_f \Delta\alpha \cdot \Delta T / (1 - \nu_f),$$

with  $\Delta T = T_0 - T_R$ ,

$$\sigma(z, t) = E_f \Delta\alpha \widetilde{\Delta T}(z, t) / (1 - \nu_f) \quad (4.18)$$

with

$$\widetilde{\Delta T}(z, t) = T_0 - T_c(z, t) \quad (4.19)$$

Indeed, by virtue of (4.1) and (4.18),

$$\begin{aligned} \widetilde{\Delta T}(z, t) &= (T_0 - T_R) \operatorname{erf}\left(\frac{z}{2\sqrt{t\kappa_f}}\right) \\ &\equiv \Delta T \operatorname{erf}\left(\frac{z}{2\sqrt{t\kappa_f}}\right) \end{aligned} \quad (4.20)$$

substitution of which in (4.18) produces the result in (4.2).

In order to handle a cyclic heating/cooling process we begin by replacing the bonding temperature  $T_0$  at the interface by  $\tilde{T}_0(t)$  [boundary condition]. For a sequence of heating/cooling over time intervals  $[0, t_1]$ ,  $[t_1, t_2]$ , ...,  $[t_i, t_{i+1}]$ , ..., we would then have, for  $t_i < t \leq t_{i+1}$ ,

$$T_c(z, t) = \tilde{T}_0^i + (T_c(z, t_i) - \tilde{T}_0^i) \operatorname{erf}\left(\frac{z}{2\sqrt{t\kappa_f}}\right) \quad (4.21)$$

where  $\tilde{T}_0^i = \tilde{T}_0(t_i)$  and, for  $i = 0$ ,  $\tilde{T}_0(0) = T_0$ . In this case we replace (4.20) by

$$(\widetilde{\Delta T})_i(z, t) = (\tilde{T}_0^i - T_c(z, t_i)) \operatorname{erf}\left(\frac{z}{2\sqrt{t\kappa_f}}\right) \quad (4.22)$$

for  $t_i \leq t \leq t_{i+1}$ , and for the same time interval easily compute that  $\sigma(z, t)$  is modified to

$$\sigma^i(z, t) = E_f \Delta\alpha (\widetilde{\Delta T})_i(z, t) / (1 - \nu_f) \quad (4.23)$$

Also, in lieu of (4.16), we have for the associated energy release rate in the interval  $[t_i, t_{i+1}]$

$$\mathcal{G}_i \simeq \sqrt{(1 - \hat{\alpha})(1 + \nu_f)} \Delta\alpha \cdot (\widetilde{\Delta T})_i(z, t) \cdot \sqrt{h} \quad (t_i \leq t \leq t_{i+1}) \quad (4.24)$$

We observe that

$$T_c(z, t_i) = \tilde{T}_o^i + (T_c(z, t_{i-1}) - \tilde{T}_o^i) \operatorname{erf} \left( \frac{z}{2\sqrt{t_i \kappa_f}} \right) \quad (4.25)$$

Substituting for  $(\widetilde{\Delta T})_i$ , from (4.22) into (4.24), yields, for the interval  $t_i \leq t \leq t_{i+1}$ ,

$$\mathcal{G}_i \simeq \sqrt{(1 - \hat{\alpha})(1 + \nu_f)} \Delta\alpha (\tilde{T}_o^i - T_c(z, t_i)) \sqrt{h} \operatorname{erf} \left( \frac{z}{2\sqrt{t \kappa_f}} \right) \quad (4.26)$$

in which  $T_c(z, t_i)$  is given by the iterative procedure defined in (4.25) so that

$$\tilde{T}_o^i - T_c(z, t_i) = (\tilde{T}_o^i - T_c(z, t_{i-1})) \operatorname{erf} \left( \frac{z}{2\sqrt{t_i \kappa_f}} \right) \quad (4.27)$$

Iterating on (4.27) we easily obtain

$$\begin{aligned} \tilde{T}_o^i - T_c(z, t_i) &= (\tilde{T}_o^i - T_R) \times \\ &\quad \left\{ \operatorname{erf} \left( \frac{z}{2\sqrt{t_i \kappa_f}} \right) \operatorname{erf} \left( \frac{z}{2\sqrt{t_{i-1} \kappa_f}} \right) \dots \right. \\ &\quad \left. \dots \operatorname{erf} \left( \frac{z}{2\sqrt{t_1 \kappa_f}} \right) \right\} \end{aligned} \quad (4.28)$$

and substitution of (4.28) into (4.26) yields, as the final expression for the energy release rate at  $z$ ,  $0 \leq z \leq h$ , and  $t$ ,  $t_i \leq t \leq t_{i+1}$ ,

$$\begin{aligned} \mathcal{G}_i &= \sqrt{(1 - \hat{\alpha})(1 + \nu_f)} \Delta\alpha \cdot (\delta T)_i \cdot \sqrt{h} \\ &\quad \times \left\{ \operatorname{erf} \left( \frac{z}{2\sqrt{t_i \kappa_f}} \right) \operatorname{erf} \left( \frac{z}{2\sqrt{t_{i-1} \kappa_f}} \right) \right. \\ &\quad \left. \dots \operatorname{erf} \left( \frac{z}{2\sqrt{t_1 \kappa_f}} \right) \operatorname{erf} \left( \frac{z}{2\sqrt{t \kappa_f}} \right) \right\} \end{aligned} \quad (4.29)$$

where  $(\delta T)_i = \tilde{T}_o^i - T_R$ ,  $i = 1, \dots, n$ , and  $(\delta T)_0 = T_0 - T_R$ .

Using (4.29) we now employ a suitable fracture toughness function  $\Omega(\psi)$  and deduce that, once a blister has formed, the crack at the base of the blister will propagate upward through

the film at a time  $t_p$ ,  $t_i \leq t_p \leq t_{i+1}$ , provided<sup>2</sup>

$$\mathcal{G}_i(\delta, t_p) > \Omega(\psi) = \mathcal{G}_c \quad (4.30)$$

We now set

$$G_i(z, t) = \mathcal{G}_i(z, t) / \sqrt{h}$$

Then, for an initial crack in the film parallel to the film/bond coat interface, and at a depth of  $\delta$  units into the film (measured from the film's free surface) spallation will not occur if

$$\sqrt{h} \leq \Omega(\psi) / G_i(\delta, t) \quad (4.31)$$

for each  $i = 1, 2, \dots$ , and each  $t$ ,  $t_i \leq t \leq t_{i+1}$ . In order to make quantitative predictions of a critical film thickness  $h_c$ , based on (4.31), the  $\Omega$  vs.  $\psi$  relationship must be known, i.e., determined by experiment. In almost all the cases discussed in the literature,  $\Omega(\psi)$  has the form

$$\Omega(\psi) = \Omega_c \tilde{f}(\psi) \quad (4.32)$$

where  $\Omega_c$  is the pure mode I fracture toughness associated with an ideally brittle 'interface'. Some experimentally determined forms for  $\tilde{f}(\psi)$  which have been noted in the literature include

$$\tilde{f}(\psi) = 1 + \tan^2[(1 - \lambda)\psi], \quad \lambda \geq 1 \quad (4.33a)$$

$$\tilde{f}(\psi) = 1 + (1 - \lambda) \tan^2 \psi, \quad \lambda \geq 1 \quad (4.33b)$$

and

$$\tilde{f}(\psi) = \{1 + (\lambda - 1) \sin^2 \psi\}^{-1}, \quad \lambda \geq 1 \quad (4.33c)$$

For all three of these cases,  $\lambda = 1$  corresponds to an ideally brittle interface and crack propagation will initiate when

$$\mathcal{G}_i(\delta, t_q) = \Omega_c$$

---

<sup>2</sup>We assume that the crack over which the blister initiated is at a depth  $z = \delta$  in the film, as measured from the film/bond coat interface.

for some  $t_q$ ,  $t_i \leq t_q \leq t_{i+1}$ , for all mode combinations; thus,  $\lambda$  in (4.33a,b,c) is a parameter whose function it is to adjust the mode II contribution to the criteria.

**Remarks:** If  $\tilde{f}(\psi) \geq 1$  then, by virtue of (4.32),  $\Omega(\psi) \geq \Omega_c$  and (4.31) will hold provided that for each  $i = 1, 2, 3, \dots$ , and all  $t$ ,  $t_i \leq t \leq t_{i+1}$ ,

$$\sqrt{h} \leq \Omega_c / G_i(\delta, t) \quad (4.34)$$

We may express (4.34) in the alternative form

$$\sqrt{h} \leq \frac{\Omega_c}{\max_{1 \leq i \leq n} \left( \max_{t_i \leq t \leq t_{i+1}} G_i(\delta, t) \right)} \quad (4.35)$$

for  $n$  cycles of heating/cooling over the intervals  $[0, t_1], [t_1, t_2], \dots, [t_{n-1}, t_n]$  where, for  $t_i \leq t \leq t_{i+1}$ ,

$$G_i(\delta, t) = \sqrt{(1 - \hat{\alpha})(1 + \nu_f)(\alpha_f - \alpha_s)}(\tilde{T}_0^i - T_R) \times \left\{ \operatorname{erf} \left( \frac{\delta}{2\sqrt{t_i \kappa_f}} \right) \dots \operatorname{erf} \left( \frac{\delta}{2\sqrt{t_1 \kappa_f}} \right) \operatorname{erf} \left( \frac{\delta}{2\sqrt{t \kappa_f}} \right) \right\} \quad (4.36)$$

with  $\hat{\alpha}$  the first Dundurs' parameter.

**Remarks:** For  $0 \leq z < h$  and  $t_i \leq t \leq t_{i+1}$  the temperature is given by

$$T_c(z, t) = \tilde{T}_0^i + (T_R - \tilde{T}_0^i) \left\{ \operatorname{erf} \left( \frac{z}{2\sqrt{t_i \kappa_f}} \right) \times \dots \dots \operatorname{erf} \left( \frac{z}{2\sqrt{t_1 \kappa_f}} \right) \operatorname{erf} \left( \frac{z}{2\sqrt{t \kappa_f}} \right) \right\} \quad (4.37)$$

We now note that the function  $\operatorname{erf} \left( \frac{z}{2\sqrt{t \kappa_f}} \right)$  increases monotonically both as  $z$  increases and as  $t$  decreases; thus, in as much as  $\delta \leq h$  (the initial crack is in the film or, at worst, at the interface between the film and the bond coat) we obtain from (4.36)

$$G_i(\delta, t) \leq \sqrt{(1 - \hat{\alpha})(1 + \nu_f)(\alpha_f - \alpha_s)}(\tilde{T}_0^i - T_R) \times \left\{ \operatorname{erf} \left( \frac{h}{2\sqrt{t_i \kappa_f}} \right) \dots \operatorname{erf} \left( \frac{h}{2\sqrt{t_1 \kappa_f}} \right) \operatorname{erf} \left( \frac{h}{2\sqrt{t \kappa_f}} \right) \right\} \quad (4.38)$$

for  $t_i \leq t \leq t_{i+1}$ . From this last result we infer that

$$\begin{aligned} \max_{t_i \leq t \leq t_{i+1}} G_i(\delta, t) &\leq \sqrt{(1 - \hat{\alpha})(1 + \nu_f)}(\alpha_f - \alpha_s)(\tilde{T}_0^i - T_R) \\ &\times \left\{ \operatorname{erf} \left( \frac{h}{2\sqrt{t_1 \kappa_f}} \right) \dots \operatorname{erf} \left( \frac{h}{2\sqrt{t_{i-1} \kappa_f}} \right) \right\} \end{aligned} \quad (4.39)$$

Finally, as we assume that the ‘cyclic’ heating-cooling process is periodic, we have  $t_{i+1} - t_i = t_1 - 0 \equiv \Delta t$  for all  $i = 1, \dots, n$ ; thus,

$$\begin{aligned} \max_{1 \leq i \leq n} \left( \max_{t_i \leq t \leq t_{i+1}} G_i(\delta, t) \right) \\ \leq \sqrt{(1 - \hat{\alpha})(1 + \nu_f)}(\alpha_f - \alpha_s)(\tilde{T}_0^i - T_R) \left[ \operatorname{erf} \left( \frac{h}{2\sqrt{\Delta t \cdot \kappa_f}} \right) \right]^{n+1} \end{aligned} \quad (4.40)$$

For such a cyclic (periodic) process of heating and cooling (4.35) will be satisfied provided

$$\sqrt{h} \leq \Omega_c / F(f; s)(\tilde{T}_0^i - T_R) \left[ \operatorname{erf} \left( \frac{h}{2\sqrt{\Delta t \kappa_f}} \right) \right]^{n+1} \quad (4.41)$$

where  $F(f; s)$  depends solely on the elastic and thermal properties of the film and substrate (bond coating) and is defined by

$$F(f; s) = \sqrt{(1 - \hat{\alpha})(1 + \nu_f)}(\alpha_f - \alpha_s) \quad (4.42)$$

We note that the error function  $\operatorname{erf}$ , as given by (4.17), is a monotonically increasing function of its argument  $\zeta = z/2\sqrt{t\kappa_f}$  and that  $\operatorname{erf}(\zeta) \rightarrow 1$  as  $\zeta \rightarrow \infty$ . Thus, for all finite values of  $z/2\sqrt{t\kappa_f}$ ,  $\operatorname{erf}(z/2\sqrt{t\kappa_f}) < 1$ . By shifting all terms in (4.41) that involve  $h$  to the left-hand side of the inequality, we find for the critical film thickness the largest value  $h_c$  such that

$$\frac{\sqrt{h_c}}{\left\{ \operatorname{erf} \left( \frac{h_c}{2\sqrt{\Delta t \cdot \kappa_f}} \right) \right\}^{n+1}} \leq \frac{\Omega_c}{F(f; s)(\tilde{T}_0^i - T_R)} \quad (4.43)$$

The problem of dealing with the transcendental function on the left-hand side of (4.43) may be avoided if the crack depth  $\delta$  in (4.35), (4.36) can be accurately estimated (in terms of its distance from the film/bond coat interface). Then from (4.35), (4.36), and the assumption

that  $t_{i+1} - t_i = t_1 - 0 \equiv \Delta t$ , for all  $i = 1, \dots, n$ , the criteria assumes the form

$$\sqrt{h} \leq \Omega_c / F(f; s) (\tilde{T}_0^i - T_R) \left[ \operatorname{erf} \left( \frac{\delta}{2\sqrt{\Delta t \cdot \kappa_f}} \right) \right]^{n+1} \quad (4.44)$$

with  $F(f; s)$  defined by (4.42).

**Remarks:** A *better* result than that afforded by (4.44) would consist of using (4.35) coupled with (4.36) where, in (4.36), in lieu of using  $\tilde{T}_0^i - T_R$ , we employ, instead, the function  $\tilde{T}_0(t) - T_R$  for  $t_i \leq t \leq t_{i+1}$ .

**Remarks:** In lieu of taking  $\tilde{T}_0^i = T_0(t_i) \equiv T_0(\Delta t)$  we might consider using

$$\tilde{T}_0^i = \frac{1}{\Delta t} \int_0^{\Delta t} T_0(t) dt \equiv \frac{1}{t_{i+1} - t_i} \int_{t_i}^{t_{i+1}} T_0(t) dt \quad (4.45)$$

for all  $i = 1, 2, \dots, n$ .

### Remarks: FGM Coatings

If the thin film (coating) is not a pure ceramic but is a FGM, i.e., a composite (of either inclusion matrix type or multilayer type) with the local volume fraction of metal varying through the coating thickness, terms in our formulas which involve  $E_f, \nu_f, G_f$ , and  $\alpha_f$  must be modified accordingly.

We assume that the FGM coating is ceramic rich near the coating surface and metal rich near the interface with the metallic bond coat; to deal with this situation we modify the work of Bao and Wang [9], taking into account the fact that in the local coordinate system we have chosen  $z = 0$  corresponds to the coating/bond coat interface while  $z = h$  corresponds to the coating surface. Thus, let  $g(z)$  denote the local volume fraction of metal in the film for  $0 \leq z \leq h$ ;  $g(z)$  characterizes the gradation of the coating. We take, specifically,

$$g(z) = g_0 + (1 - g_0) \left( \frac{h - z}{h} \right)^n \quad (4.46)$$

so that at the coating surface at  $z = h$ ,  $g(h) = g_0 \equiv$  volume fraction of metal at the coating surface. If we have pure ceramic near the coating surface then  $g_0 = 0$ , as will be assumed

here. Also,  $g(0) = 1$  so that near the interface we have 100% metal in the coating. As  $g_0 = 0$ ,

$$g(z) = \left( \frac{h-z}{h} \right)^n \quad (4.47)$$

The *total volume fraction* of metal in the coating is

$$\begin{aligned} f_\nu &= \frac{1}{h} \int_0^h g(z) dz \\ &= \frac{1}{h^{n+1}} \int_0^h (h-z)^n dz \\ &= \frac{1}{n+1} \end{aligned} \quad (4.48)$$

Thus,  $n = \frac{1}{f_\nu} - 1$  and

$$g(z) = \left( \frac{h-z}{h} \right)^{\frac{1-f_\nu}{f_\nu}} \quad (4.49)$$

If the FGM coating is of inclusion/matrix type the microgeometry of each phase can be expected to be irregular so that the spatial distribution of the phases is not uniform in the  $z$ -direction. As a first approximation for the effective properties of a FGM inclusion-matrix type coating we may employ the rule of mixtures so as to obtain the following results:

$$\begin{cases} E_c^{eff}(z) = g(z)E_s + (1-g(z))E_f \text{ (upper bound)} \\ E_{eff}^c(z) = \frac{g(z)}{E_s} + \frac{(1-g(z))}{E_f} \text{ (lower bound)} \end{cases} \quad (4.50a)$$

$$\nu_c^{eff}(z) = g(z)\nu_s + (1-g(z))\nu_f \quad (4.50b)$$

$$\alpha_c^{eff}(z) = g(z)\alpha_s + (1-g(z))\alpha_f \quad (4.50c)$$

$$\begin{cases} k_c^{eff}(z) = k_8 + \frac{(1-g(z))(k_f - k_s)}{1 + g(z)[(k_f - k_s)/(k_s + \frac{4}{3}G_s)]} \\ \text{(effective coating bulk modulus)} \end{cases} \quad (4.50d)$$

and the effective shear modulus  $G_c^{eff}(z)$  is determined by solving

$$A \left( \frac{G_c^{eff}(z)}{G_s} \right)^2 + B \left( \frac{G_c^{eff}(z)}{G_s} \right) + C = 0 \quad (4.50e)$$

where  $A, B, C$  are functions of  $g(z)$ ,  $\frac{G_f}{G_s}$ ,  $\nu_f$  and  $\nu_s$  as given in [10].

We now take the effective Young's modulus for the coating to be an average of the upper and lower bounds in (4.50a) and employ (4.50b)-(4.50e) for the effective coating Poisson's ratio, thermal expansion coefficient, bulk modulus, and shear modulus, in place of  $E_f, \nu_f, \alpha_f, k_f$ , and  $G_f$ , in (4.35), (4.36).

## 5 Experimental Determination of Coating Toughness

In sections 2 and 3 the concepts of strain energy release rate, critical strain energy release rate, and fracture toughness were introduced. A material under loading with an incipient or growing crack has a strain energy release rate,  $\mathcal{G}$ . This strain energy release rate is equal to the fracture toughness  $\Omega(\psi)$  which is related to the surface energy for crack propagation. Fracture toughness is a function of the relative amount of tensile and shear loading as given by the phase angle,  $\psi$ . Thus, under a given loading condition,  $\Omega(\psi)$  is a useful parameter for comparing the relative strengths of coatings. These concepts hold regardless of the exact failure mode.

The generic means for determining  $\Omega(\psi)$  can be explained in a few sentences, although more than a few are used here:

### 1. Determine the most likely failure mode.

One can examine the exact in service failure mode and develop an analytical relationship describing the mechanical conditions at failure. In the case of plasma sprayed coatings for impulse dryer rolls, failure is most likely caused by buckling, followed by spalling, as we have indicated in §4. Buckling initiates either in the coating or at the bi-material interface. While buckling in either location is essentially the same process, a complete testing of the bi-material requires that crack propagation at both locations be induced and that  $\Omega(\psi)$  be determined for both types of failure; this is the only

means of determining where is the most likely location for crack initiation. In §4 we have given a detailed description of the buckling failure process and how it is influenced by thermal cycling. Hutchinson and Suo [5] give an overview of various other failure modes.

**2. Determine the most likely range of  $\psi$  for the failure mode.**

In the case of interfacial fracture this range can be large, and the entire range needs to be tested if the interface properties are to be fully characterized.

**3. Subject a representative sample to loading conditions which give the desired  $\psi$  and load until crack propagation occurs.**

A number of testing techniques can be used to produce different loading and failure conditions.

**4. Determine the stress field at crack propagation, and/or compliance characteristics and loading condition at the point of crack propagation, and the sample mechanical properties.**

Determination of the actual sample stress field usually requires numerical methods in some form. In the case of a bi-material this invariably requires the use of finite element methods. As an example, Hutchinson and Suo [5] state that for buckling of a thin film coating at the *interface*,  $\psi$  is given by

$$\begin{aligned} \tan \psi &= \operatorname{Im}[Kh^{i\epsilon}]/\operatorname{Re}[Kh^{i\epsilon}] \\ &= [(12)^{1/2}M \cos \omega + h\Delta N \sin \omega]/[-(12)^{1/2}M \cos \omega + h\Delta N \sin \omega] \end{aligned} \quad (5.1)$$

where  $M$  is the moment applied to the crack tip,  $N$  is the in-plane force applied to the crack tip,  $h$  is the thickness of the coating, and  $\omega$  is a function of  $\hat{\alpha}$  and  $\hat{\beta}$  (for  $\hat{\beta} = \hat{\alpha} = 0, \omega = 53^\circ$ ). While this formulation is apparently simple, one still needs to determine  $M$  and  $N$ ; this is not a trivial task, particularly in a sample subjected to

residual stresses. Determination of the specimen compliance requires exact knowledge of when the crack is propagating and when it is not propagating and the loading conditions at those times.

5. Calculate  $\mathcal{G}_c$  (or  $K$ ) and  $\Omega(\psi)$  with the appropriate relationships for the given failure mode.  $\Omega(\psi)$  is simply the energy release rate  $\mathcal{G}$  at which crack propagation occurred.

The last step, calculation of  $\mathcal{G}$  and  $K$  is relatively simple given completion of the previous steps. However, the prerequisites for the final step are not trivial.

If the goal is to make a ranking of the relative fracture toughness of coatings, then much of the analytical work can be avoided. One simply subjects samples of the same geometry to identical test conditions. The samples that fail at the highest load condition have the greatest fracture toughness, for the given loading. Without the analytical/numerical information on the stress fields, etc., no absolute magnitudes can be assigned to the fracture toughness.

There are two problems involved with predicting the in service failure of a coating. The first is describing the loading conditions which exist during the in-service application, i.e., stresses, strains, strain energy release, etc. The second is selecting a test specimen which results in similar loading conditions. The test need only duplicate the in service combination of tensile and shear stresses as given by the phase angle and need only take into account whether plane strain or stress exists; this approach is usually the only reasonable one as there are an infinite variety of in service conditions, many of which are extremely difficult to duplicate in the laboratory. We offer, below, a summary of the theory behind various types of test samples which are used to determine fracture toughness.

The simplest case is that of a homogeneous isotropic specimen as depicted in

Figure 5.1. A general elasticity solution was developed for this case by Suo [11] and is summarized here. Far from the crack the strain distributions are described using elementary beam theory. (We note that in the analysis of test specimens, most investigators resort to a simple beam analysis if at all possible; this approach provides considerable simplification).

The strain energy release rate is then the difference between the strain energy stored in the edges far behind the crack and the strain energy stored in the edges far ahead of the crack tip and is given by

$$\mathcal{G} = (1/2\bar{E})[(P_1^2/h) + 12(M_1^2/h^3) + (P_2^2/H^3) - (P_3^2/(h+H)) - 12(M_3^2/(h+H)^3)] \quad (5.2)$$

Using the relationship (for homogeneous fracture) given by (2.13), i.e.,

$$\mathcal{G} = (K_I^2 + K_{II}^2)/\bar{E}$$

the stress intensity factors are

$$K_I = P \cos \Omega / (2hU)^{\frac{1}{2}} + M \sin(\Omega + \gamma) / (2h^3V)^{\frac{1}{2}} \quad (5.3)$$

$$K_{II} = P \sin \Omega / (2hU)^{\frac{1}{2}} - M \cos(\Omega + \gamma) / (2h^3V)^{\frac{1}{2}} \quad (5.4)$$

where

$$\begin{aligned} P &= P_1 - C_1 P_3 - C_2 M_3 / h \\ M &= M_1 - C_3 M_3 \\ C_1 &= 1 / [(1/\eta) + 1] \\ C_2 &= (6/\eta) / [(1/\eta) + 1]^3 \\ C_3 &= 1 / [(1/\eta) + 1]^3 \\ \eta &= h / H \\ 1/V &= 12(1 + \eta^3) \\ 1/U &= 1 + 4\eta + 6\eta^2 + 3\eta^3 \\ \sin \gamma &= (UV)^{\frac{1}{2}} (6\eta^2(1 + \eta)). \end{aligned}$$

The parameter  $\omega$  is determined by numerical solution of an integral equation and is given by

$$\omega = 52.1^\circ - 3^\circ\eta.$$

This type of solution is used to calibrate specific fracture specimen geometries.

For the homogeneous isotropic sample, there are no material property differences, yet recourse to numerical techniques is still required. A modification of this approach could be used to treat “in coating” failures. However, the interaction between the coating and substrate would have to be taken into account and this is not a trivial endeavor.

The homogeneous isotropic case can be simplified by assuming that  $h = H$ ; this yields three illustrative examples upon which many testing techniques for both homogeneous and bi-materials are based. Figure 5.2 presents such examples as background information for the reader.

Hutchinson and Suo [5] studied a problem more applicable to the testing of bimetals, including plasma sprayed coatings. Figure 5.3 presents a schematic of the bi-material specimen in which each layer is homogeneous, isotropic, and linearly elastic. A long distance in front of the crack tip the specimen can be treated as a composite beam. The energy release rate in closed form is

$$\mathcal{G} = (1/2\bar{E}_1)[(P_1^2/h) + 12(M_1^2/h^3)] + (1/2\bar{E}_1)[P_2^2/H + 12(M_2^2/H^3) - (P_3^2/Ah) - (M_3^2/Ih^3)] \quad (5.5)$$

Using the relationship for interface fracture, the stress intensity factor is

$$K = h^{-i\epsilon}[(1 - \alpha)/(1 - \beta)^{1/2}][P/(2hU)^{1/2} - ie^{i\gamma}M/(2h^3V)^{1/2}] \quad (5.6)$$

where  $P, M, U, V$ , and  $\gamma$  are the same as in (5.3),  $\epsilon$  is given in (3.8) and

$$C_1 = \Sigma/A$$

$$C_2 = \Sigma/I(1/\eta + \frac{1}{2} - \Delta)$$

$$C_3 = \Sigma/12I$$

$$A = 1/\eta + \Sigma$$

$$I = \Sigma[(\Delta - 1/\eta)^2 - (\Delta - 1/\eta + 1/3) + \Delta/\eta(\Delta - 1/\eta) + \frac{1}{3}\eta^3]$$

The parameter  $\Omega$  is a function of the Dundur's parameters and must be determined numerically.

Figure 5.4 shows a particular implementation of the four point bend specimen that has been used by a number of researchers to test bi-material interface fracture toughness. When the crack length 'a' exceeds  $3h$  the crack can be considered semi-infinite and both the driving force and mode mixity become independent of the crack length. The possible range of mode mixity for this type of sample is

$$\begin{aligned} 42^\circ < \psi < 62^\circ, & \quad h/H = 0.1 \\ 34^\circ < \psi < 47^\circ, & \quad h/H = 1.0 \end{aligned}$$

This type of specimen is not generally used to evaluate "in-coating" toughness.

Another mixed mode fracture mechanics specimen is the Rigid Grips specimen. This is shown in Figure 5.5. An interface crack is driven by the relative translations  $U$  and  $V$  of the grips. The mode mixity is controlled by the relative proportions of  $U$  and  $V$  translations; this is similar to the ASTM C633 test standard for plasma sprayed ceramic coatings and the ASTM F1044 test for porous metals. In ASTM C633 only  $V$  translations occur and in ASTM 1044 only  $U$  translations occur. Care should be taken in assuming that the phase angle is always directly related to the proportion of relative vertical and horizontal translation, particularly for interfacial fracture. Differences in material elastic constants can alter the relationship, i.e., Evans, et. al. [4].

Under test conditions with the Rigid Grip specimen "the bonded layers far behind the crack tip are stress free, while the bonded layer far ahead of the crack tip is in a uniform

strain state". Using energy methods the strain energy release rate is found to be

$$\mathcal{G} = (V^2/2)[h/\bar{E}_1 + H/\bar{E}_2]^{-1} + (U^2/2)[h/\mu_1 + H/\mu_2]^{-1} \quad (5.7)$$

where

$$\bar{E}_i = 2\mu(1 - \nu)/(1 - 2\nu), \text{ for plane strain}$$

$$\bar{E}_i = 2\mu/(1 - \nu), \text{ for plane stress}$$

while the stress intensity factor is

$$K = h^{-i\epsilon} e^{i\omega} [E^*/(1 - \beta^2)]^{1/2} [V/2^{1/2}(h\bar{E}_1 + H\bar{E}_2)^{-1/2} + iU/2^{1/2}(h/\mu_1 + H/\mu_2)^{-1/2}] \quad (5.8)$$

where  $U$  and  $V$  are the same as in (5.4) and  $\omega$  is a function of  $\mu_1/\mu_2$ ,  $\nu_1$ ,  $\nu_2$ , and  $h/H$ .

It should be noted that a complete evaluation of a plasma sprayed coating for an impulse dryer requires determination of the fracture toughness at the coating-substrate interface and in the coating itself. This determination should be made over a wide range of phase angles. None of the general methods outlined in this section addresses both tasks.

Since bi-materials first came into widespread use a number of testing techniques have been proposed and used. Some of these tests, such as the peel test in which the force required to peel the coating off the substrate is measured are not applicable to brittle plasma sprayed coatings, i.e., Evans, et. al., [4]. Other methods involve two part test specimens. In these specimens the two pieces are held in close proximity during the coating spraying process resulting in a single piece held together by the coating. The specimen is then subjected to either a tensile or a shear loading. The loading at failure is related to the fracture toughness of the coating. Depending on the sample type, failure is either at the coating-substrate interface (referred to as an adhesion failure) or in the coating (referred to as a cohesion failure). Occasionally, a combined adhesion and cohesion failure occurs; this is not desired as it is then not possible to distinguish the fracture toughness of either the interface or the coating. Another problem with these types of specimens is the two part nature of the

specimen. Insuring that the coating forms on each piece in the same manner can be a concern, i.e., Berndt, et. al., [1]. The implementation of three test methods which can be used with plasma sprayed coatings will now be examined; these methods are:

1. Four Point Bend
2. Double Cantilever Beam (DCB) and modifications
3. ASTM C633 Tensile Test

### Four Point Bend Test

The literature contains work by several researchers using the four point bend specimen, e.g., Evans, et. al., [4], Charalambides [12], Howard and Clyne [3], Babu and Kumar [13] and Hu and Evans [14]. The Four Point Bend test is generally an adhesion or interface fracture test. It is used to determine the fracture toughness of the bond between the coating and the substrate.

Evans, et. al. [4] evaluated a number of coating/bond/substrate systems. Table 5.1 shows the systems. The important aspects and conclusions of the work are described below.

Table 5.1

Coating	Substrate	Bond Material
PMMA	Al	Epoxy
Glass	Steel	Epoxy
Glass	Glass	Thermoplastic
$Al_2O_3$	$Al_2O_3$	Glass
Al	Glass	Thermoplastic

### *Steady State Strain Energy Release Rate Zone*

When  $h \ll H$  the interface crack has a steady state strain energy release rate between the inner loading points. In this region the strain energy release rate is a function of  $h/H$ . Given a dimension of  $0.05 < h/H < 0.5$ , steady state behavior occurs in the crack length range of  $0.2h < a < 0.9c$ , where  $c$  is the inner span.

### *Friction and Residual Stress*

In performing this test with a bi-material sample two factors must be taken into account, friction at the loading point and residual stresses in the tests specimen. The amount of friction at the loading points can be determined by measuring compliance hysteresis; this is done by loading and unloading the specimen below the load required for crack growth and measuring the displacement at the sample center point. Residual stresses can have a significant effect on  $\mathcal{G}$  and on  $\psi$ . The effect can be compensated for by calculating the magnitude of the stresses and determining a correction factor to  $\mathcal{G}$ .

We note that there are relatively few unqualified measurements of the fracture energy of bi-material interfaces, wherein effects on  $\mathcal{G}$  ( $\psi$  of residual stresses, friction, etc. have been rigorously analyzed. Consequently, a general picture of the trends in  $\Omega$  with the structure of 'microstructure' of the interface does not yet exist.

Charalambides [12] continued the work presented in Evans, et. al., [4]; the primary concern in this work were the frictional effects at the points of loading. However, a number of other points were addressed.

### *Effects of a Thin Bonding Layer*

Several researchers have examined the effect of a thin bonding layer between the substrate and the primary coating. This is similar to the type of arrangement used with plasma sprayed coatings for impulse dryer rolls. In such a case the  $\mathcal{G}$  and  $K$  far from the crack tip can be expected to be different from  $\mathcal{G}_{tip}$  and  $K_{tip}$ . The quantities are related by the thickness of the bond layer. However, several authors have stated that calculations have shown that over a broad range of bi-material properties  $\mathcal{G} = \mathcal{G}_{tip}$  and that the following relationship holds

$$\frac{K_{tip}}{K} = \frac{((1 - \nu_1)/\mu_1) + (1 - \nu_2)/\mu_2 \cos h^2(\pi\epsilon_{13})}{((1 - \nu_1)/\mu_1) + (1 - \nu_3)/\mu_3 \cos h^2(\pi\epsilon_{12})} \quad (5.9)$$

### *Frictional Effects and Strain Energy Release Rate*

Friction is treated by superimposing the frictional loads on the applied loads. This

requires the assumption of linear elastic behavior. When the crack is in a *steady state* with the strain energy release rate region as defined by Evans, et. al., [4], the strain energy release rate  $\mathcal{G}_{ss}$  can be calculated either analytically or numerically. The analytical relationship may be stated as

$$\mathcal{G}_{ss}(E_2 b^2 h^3)/[(1 - \nu_2^2)P^2 l^2] = (3/2)[1/\eta_2^3 - \lambda/Q](1 - fh/l)^2 = k_1(1 - fh/l)^2 \quad (5.10)$$

where

$$Q = \eta_1^3 + \lambda\eta_2^3 + 3\lambda\eta_1\eta_2/(\eta_1 + \lambda\eta_2)$$

$$\eta_i = h_i/h \quad i = 1, 2$$

$$\lambda = (1 - \nu_1^2)E_2/(1 - \nu_2^2)E_1 \quad (\text{plane strain})$$

$f$  is the coulomb friction coefficient at the loading points,  $b$  is the width of the sample,  $l$  is the distance between the inner and outer loading points,  $P/2b$  is the load applied at the outer loading points (the loads at the inner loading points are the reaction forces),  $k = 3 - 4\nu$  (plane strain), and  $h$  is the total thickness of the sample. By (5.10) the strain energy release rate decreases with increasing friction and increasing  $h/l$ . Thus, it is recommended that  $0.25 \leq (h/l) \leq 0.5$  so as to minimize the uncertainties associated with unknown friction effects. Ignoring the effect of friction can result in an over estimate of  $\mathcal{G}$ . With this implementation the fracture toughness of the interface is determined by comparing the load at which crack propagation occurred with the analytically or numerically determined strain energy release rate.

### *Phase Angle*

The phase angle is found using numerical procedures. It has been shown that the four point bend specimen is inherently mixed mode with a phase angle of approximately  $\pi/4$  and that in the steady state strain energy release rate zone (between the inner loading points) friction has no effect on phase angle; however, this effect is important for crack growth between the inner and outer loading points.

### *Beam Compliance*

The beam compliance is determined, numerically, by assuming linear elastic behavior and superimposing the frictional effects on the applied load effects. It is shown as in Evans, et. al., [4] that beam compliance hysteresis can be used to determine the friction effects.

#### *Experimental Procedure*

The following procedures were used in the four point bend test reported in [12]:

1. The sample was precracked by loading the specimen in three point flexure. This precracking serves as the starting point for crack growth during the actual test.
2. The specimen is positioned in the four point loading fixture. First the loading and unloading compliances are measured with no crack growth; this is done to evaluate the effects of friction at the loading points. Excessive friction requires modification to the experimental setup such as reduction of roughness at the loading points, use of a solid lubricant at the loading points, etc.
3. A load is applied until the onset of crack growth and crack growth is indicated by an increase in the specimen compliance, i.e., by the amount of bending for the loading used. Testing was done under load control.
4. The compliance hysteresis is calculated from the loading-unloading data.
5. Using numerical methods the phase angle is calculated.
6. Using the relationship (5.10) the critical strain energy release rate, i.e., the fracture toughness is calculated. It is assumed that, as long as the crack is between the inner loading points, residual stress has a minimal effect. Only one measurement of fracture toughness is possible with a given sample. Repeat measurements require additional samples.

Howard and Clyne [3] used vacuum plasma sprayed coatings of various thickness with a four point point bend specimen. The coating used was commercial purity titanium deposited

on a titanium alloy (Ti-6Al-4V). The primary difference between this work and that of Charalambides [12], is that Charalambides assumed that the loaded specimen had a linear stress distribution, whereas Howard assumed a non-linear distribution; this work utilized position control, allowing the changes in compliance to be seen on a load vs time chart. The same theoretical development of expressions for  $G$  and  $\Omega$  were used by both investigators. Other noteworthy points made by Howard and Clyne [3] are stated below.

#### *Residual Stresses*

It is stated in [3] that residual stresses may change the relative proportions of tensile and shear loading at the crack tip; this in turn affects the stress intensity factor at the crack tip.

#### *Phase Angle*

The phase angle was calculated to vary between  $40^\circ$  and  $60^\circ$  depending on the Dundur's parameters for the particular sample and the thickness ratio of the coating and the substrate.

#### *Material Properties*

The authors state that the material properties must be measured directly and that bulk properties can not be relied on. A difference of roughly 50% was found between the bulk property of the coating material and the coating as used.

#### *Experimental Procedures*

The following procedures were used in the research reported in [3].

1. The specimen is precracked; this is done by masking the central portion of the specimen prior to grit blasting. After grit blasting the mask is removed and the coating is applied to the specimen; this results in a weak bond in the previously masked area. Prior to beginning the test a wire saw was used to make a cut through the coating to the underlying substrate at the center of the masked area.
2. The specimen is placed in the four point bend set up and loaded at a constant displacement. The loads are applied through rollers.

3. The applied load is recorded with time. As the load is increased the specimen bends.
4. Upon crack advance the load drops suddenly and the compliance increases almost instantaneously. It is assumed the rollers do not move during crack advance.
5. The free ends of the precrack are observed using a traveling microscope to determine if one or both crack fronts advance at a given load drop.
6. Crack propagation extended to just short of the inner loading points.
7. The critical strain energy release rate is calculated by comparing the total strain energy in the beam before and after crack propagation and dividing by the area of the crack created. The total strain energy was calculated using finite element techniques. Residual and applied loads were summed algebraically. In this implementation multiple determinations of fracture toughness can be made with the same sample.

Comparisons of the work of Charalambides [12] and Howard and Cline [3] demonstrates the advantage of position control in applying a load to the specimen. Using force control only one measurement of fracture toughness per sample was possible in Charalambides [12]. Using position control, in Howard and Clyne [3], multiple measurements were possible; this advantage was pointed out from a theoretical viewpoint in §2.

Babu and Kumar [13] used a four point bend specimen but do not provide an in depth theoretical development; the experimental procedures are similar to those of Howard and Clyne [3] and the work concentrated on determining the effect of coating thickness on interfacial fracture toughness. The coating used was commercial purity molybdenum with a mild steel substrate. A number of worthwhile points are made in [13] which may not have been clearly brought out in other works; these include:

1. Evaluation of  $K$  at the crack tip requires knowledge of the stresses at the crack tip.

2. The system used, a four point bend specimen with a thin coating, can be considered to be in plane strain.
3. The fracture toughness and the phase angle decreases ( $60^\circ$  to  $26^\circ$ ) as the coating thickness increases.

It is worth noting that in all the above mentioned work the issue of testing the coatings at different phase angles while keeping all other coating parameters constant is not addressed. While it is shown that the phase angle changes with coating thickness, this not a practical means of testing different phase angles because the coating thickness for a particular application is often fixed. The theoretical development implies that by changing the properties of the substrate one can alter the phase angle tested; however, this is of limited utility as the most valid test is one in which the test substrate material is the same as that used in the actual application.

### **Double Cantilever Bean (DCB) Test and Modifications**

A review of the literature shows that another type of test that is often used to test plasma sprayed coatings is the Double Cantilevered Beam test. One of the primary advantages of the DCB test is that multiple measurements of toughness can be made with the same test sample. A similar test to the DCB is the Short Bar (SB) test. While the specimens for the two tests appear similar there are important differences and these differences are addressed below. A third test is the Single Edge Notched or Double Torsion test. Again the specimens used appear similar to those used for the DCB test but in this case the applied loads are quite different. The Double Torsion test in at least one study produced considerably greater data spread than the DCB test; this is also addressed in the discussion which follows. All three tests can be used to test either adhesion (coating-substrate bond), fracture toughness, or cohesion (in coating) fracture toughness. One failure mode or the other is induced by preparing the specimen with a specific geometry for the coating or at the interface.

Berndt and Lin [1] provide one of the more recent examinations of the DCB test using alumina plasma sprayed on a metal substrate. The theoretical development is essentially the same as was presented by Hutchinson and Suo [5] and summarized in §2 of this paper. The strain energy release rate is given by (2.19), i.e.

$$G = \frac{d}{da}(W_f - U_a)$$

where  $W_f$  is the work done by the external forces,  $U_a$  is elastic energy of the system, and  $a$  is the area of the crack. Experimentally, the objective is to establish a condition where the elastic energy provided by an external force is balanced by the propagation of a stable crack. The elastic energy supplied by the external force is controlled by the specimen geometry, specimen material properties, and the applied load.

The DCB test measures changes in compliance in order to determine the strain energy release rate. This is done using (2.25), i.e.,

$$\mathcal{G} = (1/2B)P^2(dC/da).$$

where  $B$  is the specimen thickness,  $P$  is the load required to extend the crack,  $a$  is the crack length, and  $C$  is the specimen compliance. The stress intensity factor is found using (2.13), i.e.,

$$[(K_I^2 + K_{II}^2) = \mathcal{G}_c E / (1 - \nu^2)].$$

The following important observation may be made with regard to these equations: the physical representation of the equations is such that the change in compliance of the specimen controls the energy input into the creation of new fracture surfaces. Thus, the corollary of this theory is the the crack path and rate of crack growth can be controlled very precisely by appropriate design of the specimen.

Figure 4.6 illustrates the testing process in terms of applied force and displacement of the specimen ends. “Force” corresponds to the load which is applied to the end of a rigid

moment arm which in turn applies a torque to the end of the specimen. The ideal implementation results in a pure torque being applied to the beam at the crack tip. Although a full explanation is not given, it is assumed that for this arrangement a knowledge of the exact crack length is not required. In addition, the displacements of the free ends of the beams are measured and the elastic energy of the specimen arms controls how much energy is available for crack propagation. The load is increased and some beam displacement then occurs with no crack growth. The specimen compliance in this phase is described by line A in Fig. 5.6. At the critical load, point  $(\mu, F)$  on line A, the crack propagates; this is shown by the line - "crack growth". The new compliance is given by line  $A + \delta A$ , with the crack length indicated by the displacement corresponding to point  $(\mu + \delta\mu, F + \delta F)$ . The specimen is then unloaded. The area enclosed by the three lines represents the energy transferred for crack growth. Since the slope of lines A and  $A + \delta A$  are dependent on both the crack length and elastic modulus and geometry of the beams, the energy input into the coating can be controlled by altering the geometry or material of the beams. The entire process is repeated until the specimen fails. After failure the specimen is examined to determine where the crack propagation occurred: in the coating, along the interface or a combination of the two. Using (2.25), and an experimentally determined calibration for  $dC/da$ , the strain energy release rate may be determined.

The specimen used in this type of tests consists of two beams. The coating is applied to one of the beams. The beam without the coating is then bonded with the exposed surface of the coating using an epoxy. By altering the specimen geometry in proximity to the coating it is possible to promote either cohesive or adhesive failure (See Figure 5.7). An advantage of the DCB specimen test is that the epoxy need only have a fracture toughness greater than the coating or the coating-substrate interface.

No mention is made in this research of using a finite element model of the sample. The loading is specified, i.e., a pure torque at the crack tip, to conform with a previously

developed model. In this particular case this limits the need for a finite element model. However, there is no explicit determination of the stresses and therefore there can be no exact determination of the stress intensity factor or the relative proportion of mode I and mode II stresses. Given this lack of specification, it is not surprising that the phase angle is left unspecified. Specification of the phase angle or the stress intensity factor would be required in order to compare the predictions with an in service application; this can be accomplished by employing a finite element model in the same way as was done in Charalambides [12], Howard and Clyne [3], or Babu and Kumar [13] for the four point bend specimens.

Guo and Wang [15] compare three test specimens: the Single Edge Notched (SEN), the Short Bar (SB), and the Double Cantilever Bar (DCB). The coatings used were  $ZrO_2$  with several different stabilizers added. In all cases the method used to determine  $\mathcal{G}$  is the compliance method and this requires an experimental calibration of  $dC/da$ . The reported work does not specify the phase angle for these tests. A not fully explained experimental calibration is used to obtain  $\mathcal{G}_{Ic}$  and from that  $K_{Ic}$  is obtained using (2.13). It was assumed that  $\psi = 0$ .

The SEN specimen is shown in Figure 5.8. The reported results show that the SEN sample produced a much higher variation in the data than in either of the other two test types. Only one test can be performed with each sample.

The SB has the same basic shape as the DCB specimen except that the bars are shorter and are intended to be rigid. In addition, a chevron shaped notch, with the point of the chevron directed towards the point of load application, is made in the coating. This has the same purpose as precracking did with the four point bend specimen. The SB specimen is shown to be sensitive to fracture mode and to have a relatively narrow calibration range in comparison with the DCB specimen. Only one test can be performed with each sample. Filiaggi and Pilliar [16] provide an in depth description of a SB specimen implementation.

The DCB specimen test has an advantage over the four point bend specimen test in that

it can be used to determine fracture toughness for adhesive and cohesive failures. As stated previously, one specimen can also be used to obtain multiple measurements. The literature examined did not contain a theoretical treatment of the test similar to that which was given for the four point point bend specimen test. There was also a lack of discussion of phase angle and finite element techniques which might be used to obtain it.

### ASTM C633 Tensile Test

Perhaps one of the simplest tests described in the literature is the ASTM C633 Standard Test Method. In Berndt and Lin [1] it is stated that “the tensile adhesion method as detailed in ASTM C633 is simple and often used in industry for ranking different coatings.” When used as a ranking tool this test type does not invoke the methods of fracture mechanics. In an attempt to make this simple test more informative, on a fundamental level, several researchers have applied fracture mechanics concepts to this test.

The intent of Babu and Kumar [13] was to take the ASTM C633 test specimen and convert it in to a fracture mechanics test specimen, i.e., one where crack growth is controlled to some extent and where a fracture mechanics analysis of that growth can be made. A molybdenum coating was used with a mild steel substrate.

The standard test specimen is modified by protecting the outer annular region from the grit blasting used to prepare the specimen surface (See Figure 5.9); this results in a circumferential crack between the coating and the substrate and serves the same purpose as precracking in the four point bend specimen test, i.e., it promotes adhesive failure of the specimen. The authors [13] state that the specimen could be further modified to promote cohesive failure, that a crack at the coating substrate interface in this type of sample has mixed mode behavior (mode I tensile and mode II shear loading), and that the fracture toughness is given by the following empirical expression

$$\Omega_{Ic} = P[-1.27 + 1.47(D/d)]D^{-3/2}.$$

where  $\Omega_{I_c}$  is the fracture toughness ( $Nm^{-3/2}$ ),  $P$  is the load at fracture ( $N$ ),  $D(m)$  and  $d(m)$  are as shown in Figure 5.9. A finite element model of the test specimen was used to obtain the stress field at the precrack and through the test specimen. No attempt was made to correlate the model with the empirical relationship used to determine the fracture toughness; in a more extensive study this would be a logical step, equivalent to what was done in Charalambides [12] and Howard and Clyne [3] with the four point bend specimen test. It is stated in [13] that such a process could successfully be used to develop new test specimens of any configuration having complex stress conditions.

A closing statement is made in [13] which is applicable to all specimen types:

“the fracture resistance of the interface is not unique for a particular combination of coating-substrate system. The lack of uniqueness is related to mode mixity (shear/opening) effects experienced by interface cracks, as characterized by the phase angle of loading. The phase angle is, in turn, influenced by the choice of test specimen.”

A related test is given in ASTM F1044-87 Shear testing of Porous Metal Coatings. This is a lap shear test intended for testing porous metal coatings adhering to dense metal substrates. The method was originally developed for shear testing of porous coatings applied to medical implants. Although, the literature cited in this area does not mention this test it seems reasonable to believe that this test could prove to be a compliment to the ASTM C633 tensile test, particularly in the modified form suggested in [13]. Ideally, because of the different specimen structure and loading, the shear test could yield fracture toughness data for significantly different phase angles than those in the tensile test, verification requires an in depth fracture analysis of the specimen.

The methods described in this section all employ the concepts of fracture mechanics. This level of analysis is required in order to develop a fundamental understanding of the

crack propagation process. However, the methods presented are lacking in utility for reasons we now indicate below.

The four point bend specimen tests provide a description of the stress field in the specimen and consequently a thorough knowledge of the strain energy release rate, fracture toughness, stress intensity factors and phase angle, however, the test allows for a determination of only the adhesive or bond fracture toughness and it is not possible to determine the coating fracture toughness. It also does not appear possible to alter the phase angle, although this is to some extent due the nature of interfacial cracks.

The Double Cantilever Beam, Short Bar, Single Edge Notched, and ASTM C633 tests appear to allow determination of both adhesive and cohesive fracture toughness; however, there is little information presented regarding the phase angle for these tests.

The determination of the in-service fracture toughness of a particular bi-material is a non-trivial task. Regardless of the test type, knowledge of the stress field at the crack is required to fully understand the crack propagation and to select a test which will duplicate the in-service conditions experienced by the bi-material. If the in service bi-material has the potential to experience multiple phase angles, then multiple test specimens may be required to determine the fracture toughness at each phase angle. The phase angle corresponding to the lowest fracture toughness is the one most likely to exist when crack propagation occurs. These problems require extensive empirical testing or the use of finite element techniques. Any finite element model would have to be verified. (A biaxial loading device is proposed in Liechti and Chai [17] which can apply loads resulting in a broad range mode mixity. However, the device is relatively complicated, requiring the use of a microscope for observation of crack propagation, crack opening interferometry, and finite element modelling to determine the stress intensity factors.)

An additional problem is determination of the coating and substrate material properties. A substrate such as steel is easily characterized. However, a plasma sprayed coating can

have different properties depending on the coating thickness; thus, obtaining a sample large enough to determine representative properties is difficult.

### **Scratch Test**

The scratch test has been proposed as an alternative means of determining fracture toughness, i.e., Beltzung, et. al., [18]. In this test a cross section of the bi-material is used. Beginning at a point on the substrate an indenter type probe is pushed into the substrate. The probe is then moved along the cross section perpendicular to the plane of the coating-substrate system. The direction of travel is towards the free surface of the coating and at a critical distance  $L_c$  from the free surface, scratching leads to a half-cone shaped cracking. The cone is oriented with the wide end towards the free surface of the coating, with  $L_c$  denoting the height of the cone. The normal and tangential loads on the indenter are recorded during the process. The critical length is directly related to the penetration depth and the normal force and a relationship is developed between the stress intensity factor and both the normal load and  $L_c$ . The relationship is partly empirical. The work was performed using alumina plasma sprayed onto a steel substrate.

### **Contact Testing**

This method is described in Pajares et. al, [19]. It utilizes Hertzian indentation testing to evaluate indentation stresses, yield stresses, and the elastic modulus of two ceramic-metal coating-substrate systems: alumina on steel and zirconia on superalloy. Indentation stress-strain curves are used to determine the roles of the coatings and substrates in the net deformation of the system. A coating controlled and a substrate controlled response are defined. No correlation with strain energy release rate or stress intensity factors are given. It is stated that the method may be useful in fatigue testing.

### **Other Factors Influencing Coating Failure**

The issues raised, below, have been studied to a much lesser extent, but still remain important with regard to failure of the bi-material system.

## In Use Temperature

Residual stresses can be induced in a plasma sprayed coating during the spraying and cooling process. These residual stresses affect the fracture toughness of the coating-substrate system (Charalambides [12], Howard and Clyne [3], Berndt and Lin [1], Greving et.al, [19], and Thouless and Jensen [20]). Another temperature effect which needs to be considered is the in use temperature of the system.

As reported by Bennett [21] high in use temperatures can promote oxidation of the thin bond coat between the coating and the substrate. At temperatures below  $950^{\circ}\text{C}$  it is stated that a basic NiCr bond coat provides sufficient oxidation resistance. However, as little as 150 hr at  $1050^{\circ}\text{C}$  results in complete oxidation of the bond coat. Under thermal cycling the bond coat is progressively oxidized, leading to a gradual decline in plasticity and mechanical strength which contributes to the spallation of the ceramic layer. A more resistant bond coat is MCrA—Y where M can be nickel, cobalt, or mixtures of both. Similar results using a stabilized zirconia coating and a similar bond coat are reported in Strangman and Schienle [22] and Wortman, et.al., [23].

In Lin and Bernt [24] a study is made of specimen hardness after aging at various temperatures. The bi-material system studied was a  $1400\mu\text{m}$  cerium-stablize zirconia with a  $200\mu\text{m}$  NiCoCrA—Y bond coat thermally sprayed onto a metallic substrate. The coating-substrate was aged at 400 and  $800^{\circ}\text{C}$  for 100, 500, and 1000hr. Aging at  $400^{\circ}\text{C}$  for any of the studied times did not adversely affect the hardness of the bond coat or the ceramic coating. Aging at  $800^{\circ}\text{C}$  did result in some changes. The aging time at the higher temperature was also a factor, but was not a factor at the lower temperature.

Zarzour and Onesto [25] examined the effect of thermal cycling on coating failure. Specifically an alumina coating on a high purity nickel substrate was cycled between ambient temperature and temperatures between  $800^{\circ}\text{C}$  and  $1100^{\circ}\text{C}$  where the time duration at the elevated temperature in a cycle was approximately 1500 sec. Specimens with a coating thick-

ness greater than 1 mm (0.039 in) failed by cracking; specimens with coating thickness less than 1 mm (0.039 in) did not fail.

Impulse dryer rolls are currently limited to roll temperatures of  $\sim 250^{\circ}\text{C}$  by non-coating considerations. This is significantly below the temperatures which contributed to coating failure in the above cases. However, different coating/substrate combinations may react differently.

### **Feed Stock/Spray Variations**

As stated previously, a plasma sprayed coating is not a microscopically homogeneous material. The irregularities on the microscopic level can effect the properties of the coating. These irregularities come about for various reasons.

McPherson [2] states that the factors controlling the microstructure of any given coating material will be particle velocity, temperature, and diameter. Although coatings are assumed to form from the impact of molten droplets, partly melted particles may be incorporated into the coating and these will have an effect on the microstructure.”

In the work reported in Filiaggi and Pilliar [16] there were some problems attributed to variability in the specimens. The studies for which semi-automated control was available, and the need for reproducibility, emphasized that unanticipated though seemingly insignificant alterations in equipment design resulted in measurable changes in coating adhesion.

In Khor and Cheang [26] the effect of feedstock particle shape was examined. Two feedstock of the same chemical composition were prepared in two different ways. The result was one feedstock with more rounded particle shapes and the other feedstock with more angular particle shapes. The difference in shape resulted in different coating structures and properties.

### **Fatigue or Life Modeling**

There has been relatively little work done in the area of fatigue or life modeling for coating-substrate systems although an effort at providing a simple model which is directly

applicable to the problem of immediate interest has been made in §4. Fatigue is relatively difficult to quantify even for homogeneous non-ferrous materials. A bi-material presents a difficult problem. This problem is addressed to some extent in Miller [27], [28]. Despite the extensive nature of the reported work there are still many unanswered questions. It is stated in [28] that “creep and inelasticity in both the ceramic coating and the bond coat are aspects of the problem that are poorly understood.”

## References

- [1] Berndt, C.C. and C.K. Lin, "Measurement of Adhesion for Thermally Sprayed Materials, Journal Adhesion Science Technology," 7, (1993), 1235-1264.
- [2] McPherson, R. "The relationship Between the Mechanism of Formation, Microstructure and Properties of Plasma Sprayed Coatings," Thin Solid Films, 83, (1981), 297-310.
- [3] Howard, S.J. and T.W. Clyne, "Interfacial Fracture Toughness of Vacuum-plasma-sprayed Coatings," Surface and Coating Technology, 45, (1991), 33-342.
- [4] Evans, A.G., Ruhle, M. and B.J. Dalgeish, Charalambides, P.G., "The Fracture Energy of Bimaterial Interfaces," Metallurgical Transactions A (Physical Metallurgy and Materials Science), 21A, (1990), 2419-2429.
- [5] Hutchinson, J. W. and Z. Suo, "Mixed Mode Cracking in Layered Materials," Advances in Applied Mechanics, 29 (1992), 63-191.
- [6] Chai, H., Babcock, C., and W. Knauss, "One Dimensional Modelling of Failure in Laminated Plates by Delamination Buckling", *Int. J. Solids Structures*, 17, (1981), 1069-1083.
- [7] Whitcomb, J.D., "Parametric Analytical Study of Instability-Related Delamination Growth", *Comp. Sci. and Technology*, 25, (1986), 19-48.
- [8] Evans, A. and J. Hutchinson, "On the Mechanics of Delamination and Spalling in Compressed Films", *Int. J. Solids Structures*, 20, (1984), 455-466.
- [9] Bao, G. and L. Wang, "Multiple Cracking in Functionally Graded Ceramic/Metal Coatings", *Int. J. Solids Structures*, 32, (1995), 2853-2871.
- [10] Christensen, R. and K. Lo, "Solutions for Effective Shear Properties in Three Phase Sphere and Cylinder Models", *J. Mech. Phys. Solids*, 27, (1979), 315-330.
- [11] Suo, Z., "Singulartics, Interfaces, and Cracks in Dissimilar Anisotropic Media," Proc. Roy. Soc. London, A427, (1990), 331-358.
- [12] Charalambides, P.G., "A Mixed Mode Fracture Specimen: Analysis and Experiments,"
- [13] Babu, M.V. and R.K., "Fracture Mechanics Approaches to Coating Strength Evaluation," Engineering Fracture Mechanics, 55, (1996), 235-248.
- [14] Hu, M.S. and A.G. Evans, "The cracking and Decohesion of thin Films on Ductile Substrates," Acta Metallica, 37, (1989), 917-925.
- [15] Guo, D.Z. and L.J. Wang, "Measurement of the Critical Strain Energy Release Rate of Plasma-Sprayed Coatings," Surface and Coatings Technology, 56 (1992), 19-25.
- [16] Filiaggi, M.J. and R.M. Pilliar, "Mechanical Testing of Plasma-Sprayed Ceramic Coatings on Metal Surfaces: Interfacial Fracture Toughness and Tensile Bond Strength," Journal of Material Science, 26, (1991), 5383-5395.

- [17] Liechti, K.M., Chai, Y.Ss., "*Biaxial Loading Experiments for Determining Interfacial Fracture Toughness*," *Journal of Applied Mechanics*, 58, (1991), 680-687.
- [18] Beltzung, F., Zambelli, G., Lopez, E., Nicoll, A.R., "*Fracture Toughness Measurement of Plasma Sprayed Ceramic Coatings*," *Thin Solid Films*, 181, (1989), 407-415.
- [19] Greving, D.J., Shadley, J.R., Rybicki, E.F., "*Effects of Coating Thickness and Residual Stresses on the Bond Strength of ASTM C633-79 Thermal Spray Coating Test Specimens*," *Journal of Thermal Spray Technology*, 3, (1994), 371-378.
- [20] Thouless, M.D., Jensen, H.M., "*The Effect of Residual Stresses on Adhesion Measurements*," *Journal of Adhesion Science and Technology*, 8, (1994), 579-586.
- [21] Bennet, A. "*Properties of Thermal Barrier Coatings*," *Materials Science and Technology*, 2 (1986), 257-261.
- [22] Strangman, T.E., Schienle, J.L., "*Tailoring Zirconia Coatings for Performance in a Marine Gas Turbine Environment*," *Journal of Engineering for Gas Turbines and Power*, 112, (1990), 531-535.
- [23] Wortman, D.J., Duderstadt, E.C., Nelson, W.A., "*Bond Coat Development for Thermal Barrier Coatings*," *Journal of Engineering for Gas Turbines and Power*, 112, (1990), 527-530.
- [24] Lin, C.K., Berndt, C.C., "*Statistical Analysis of Microhardness Variations in Thermal Spray Coatings*," *Journal of Material Science*, 30, (1995), 111-117.
- [25] Zarzour, J.F., Onesto, E.J., "*Failure Mechanisms of a Ceramic-Metal Interface under the Application of High Temperature Loading*," *Recent Advances in Solids/Structures and Application of Metallic Materials*, ASME PVP-vol 342/MD-vol 72, (1996), 67-74.
- [26] Khor, K.A., Cheang, P., "*Effects of Feedstock and Laser Post-spray Treatment on Plasma Sprayed Bioceramic Coatings*," *Materials and Manufacturing Processes*, 11, (1996), 869-882.
- [27] Miller, R.A., "*Progress Toward Life Modeling of Thermal Barrier Coatings for Aircraft Gas Turbine Engines*," *Journal of Engineering for Gas turbines and Power*, 109, (1987), 448-451.

## Figures



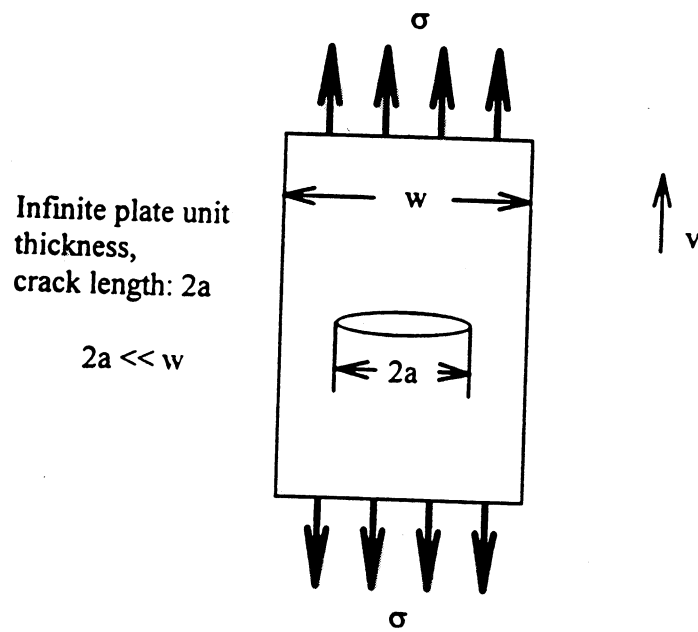
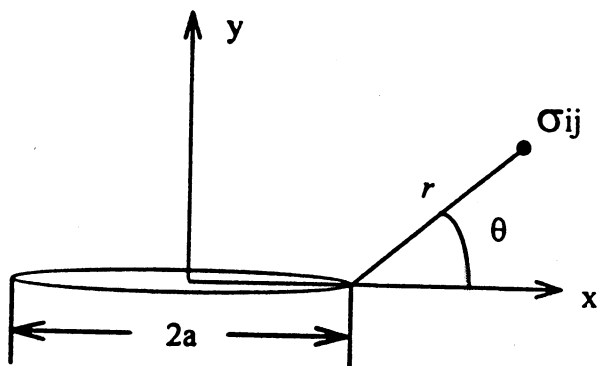


Figure 1.1 Infinite Plate with a Crack



**Figure 2.1** Stress at a Point a Distance  $r$  from the Crack

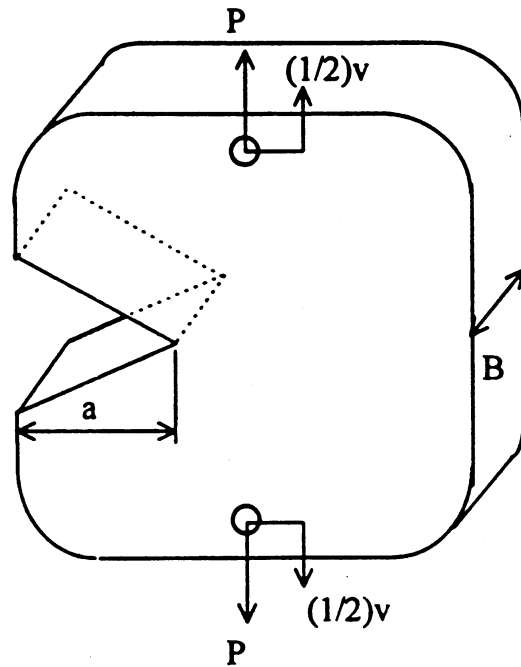


Figure 2.2 The Loaded Crack Specimen

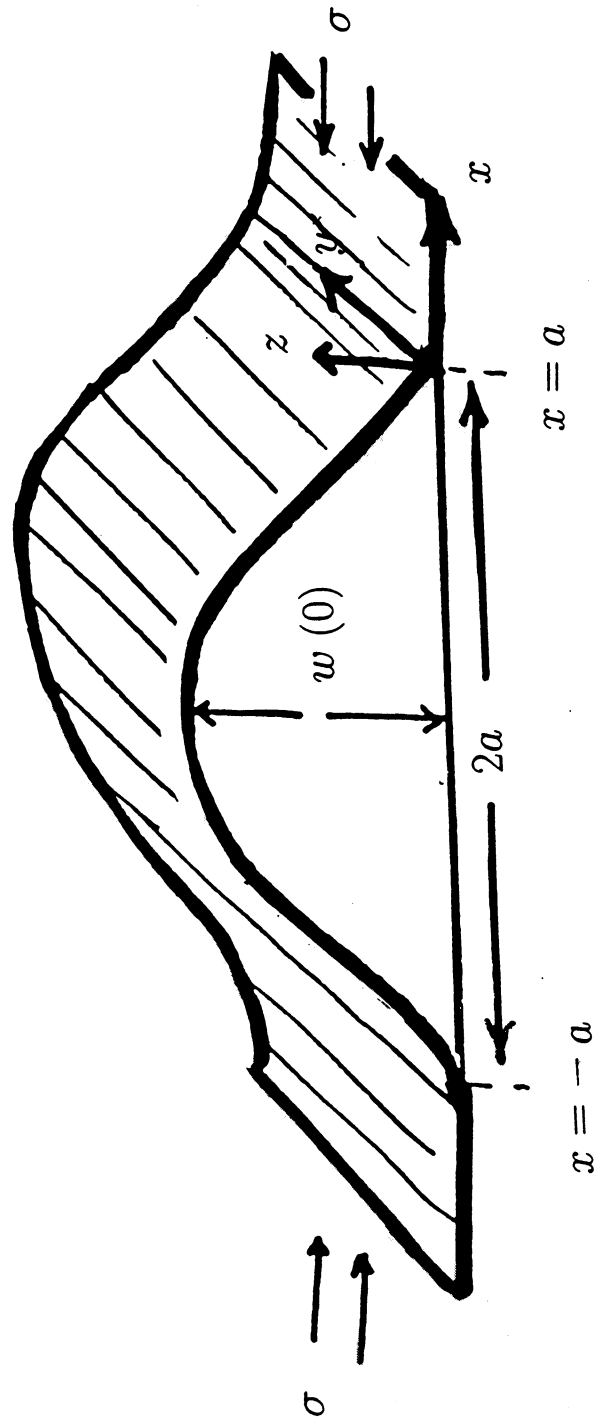


Figure 4.1 Delamination Buckling

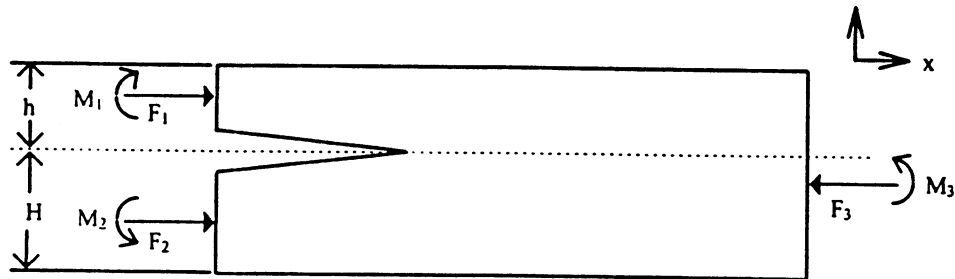
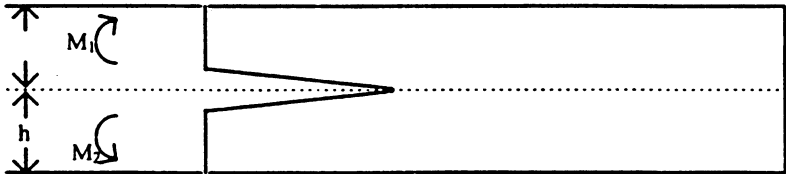


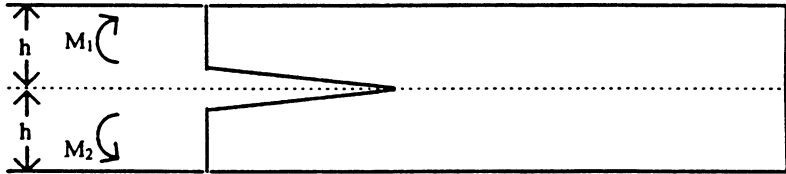
Figure 5.1 A Homogeneous Isotropic Sample

A. Double Cantilever Beam (DCB)



$\mathcal{G}_I$	$\mathcal{G}_{II}$
$\frac{12M^2}{Eh^3}$	0
0	$\frac{9M^2}{Eh^3}$
$\frac{3M^2}{Eh^3}$	$\frac{9M^2}{Eh^3}$

B. End Loaded Split (ELS)



C. Four Point Bend

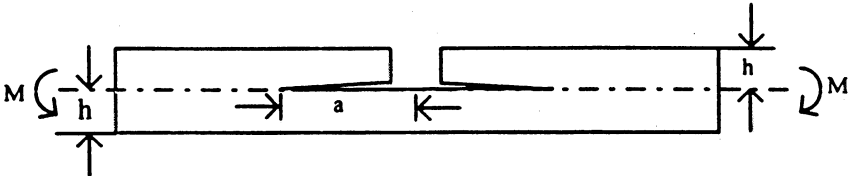


Figure 5.2 Simplifications of Fig. 5.1

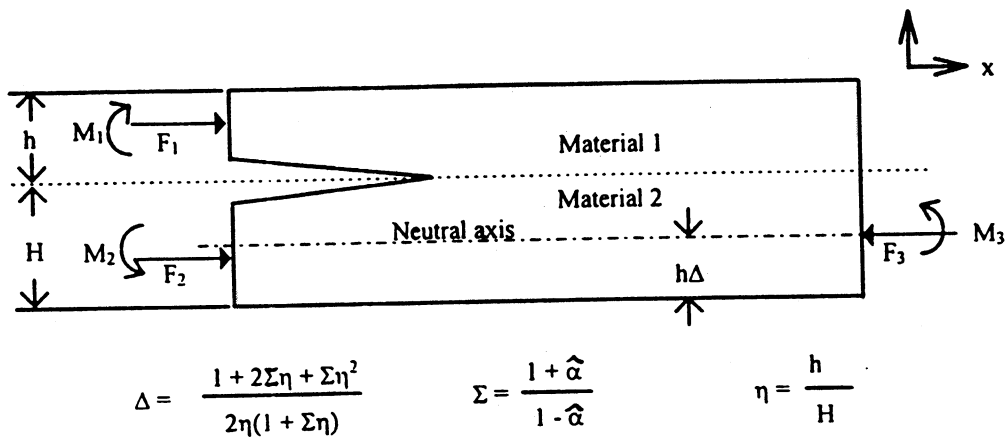


Figure 5.3 A Bi-Material Specimen

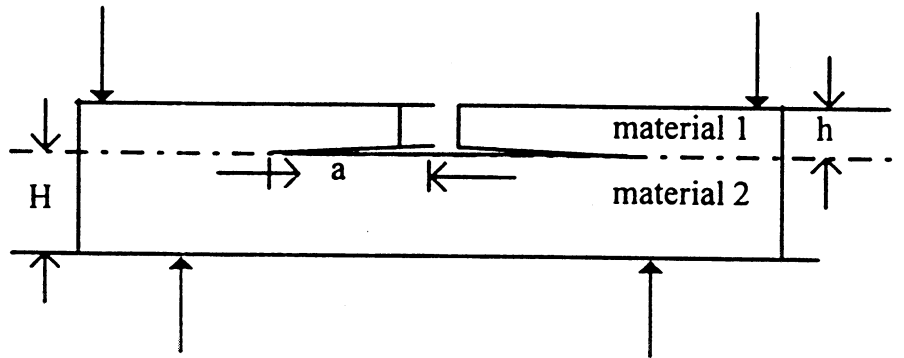


Figure 5.4 The Bi-Material Four Point Bend Specimen

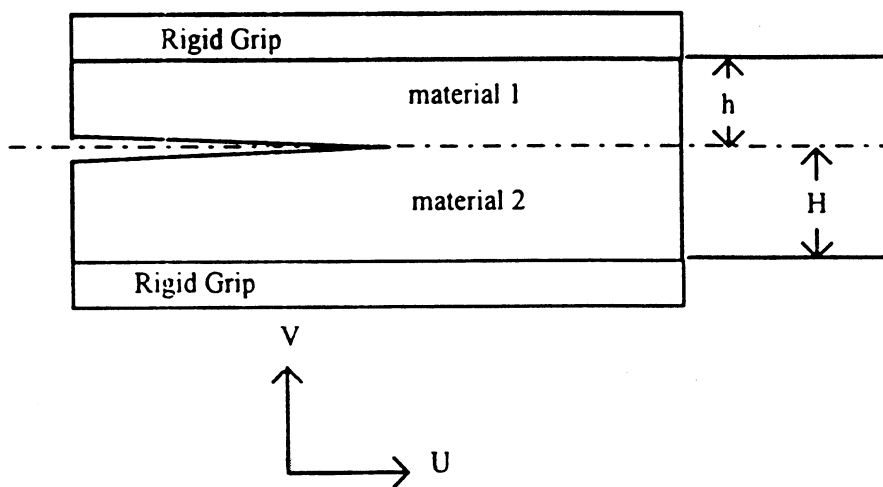


Figure 5.5 The Bi-Material Rigid Grips Specimen

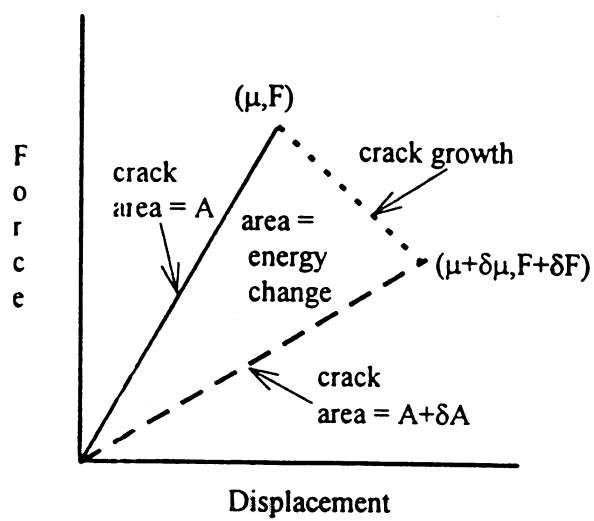


Figure 5.6 Force Displacement for the DCB Test Specimen

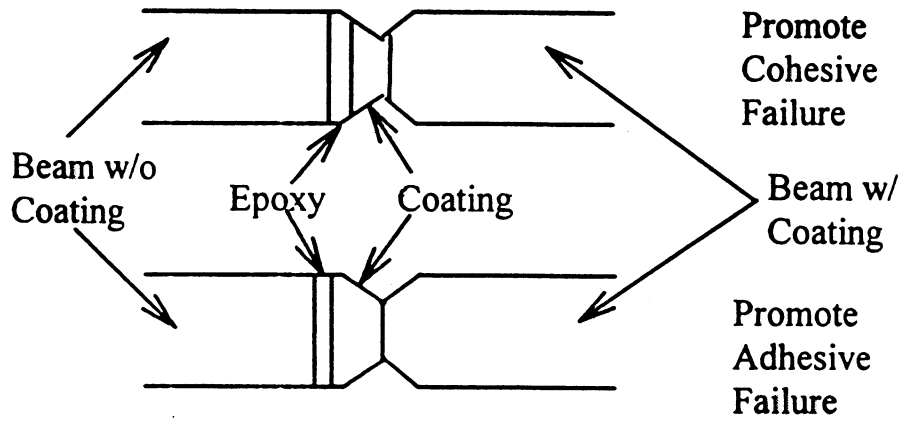


Figure 5.7 Specimen Geometry to Control Failure Location

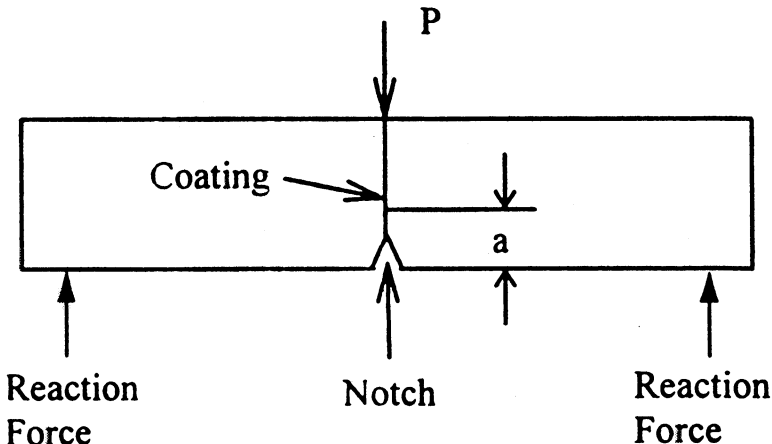


Figure 5.8 The Single Edge Notched Specimen

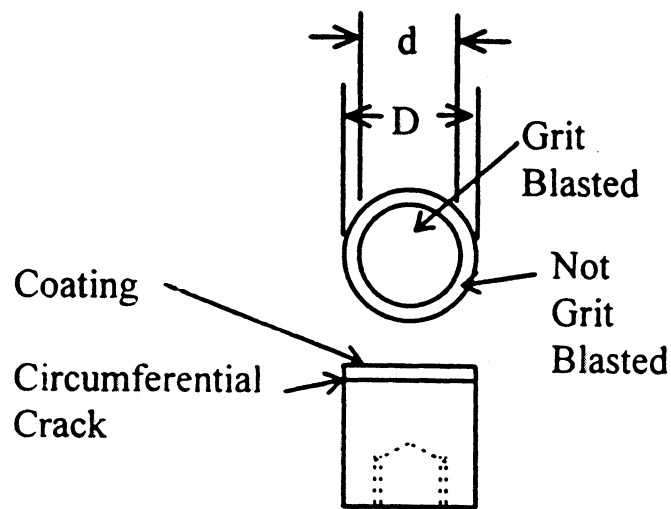


Figure 5.9 The Modified ASTM C633 Test Specimen

Coating	Substrate	Bond Material
PMMA	Al	Epoxy
Glass	Steel	Epoxy
Glass	Glass	Thermoplastic
Al <sub>2</sub> O <sub>3</sub>	Al <sub>2</sub> O <sub>3</sub>	Glass
Al	Glass	Thermoplastic

Table 5.1

FUNDAMENTALS OF WEB HEATING

STATUS REPORT

FOR

PROJECT F002

Timothy F. Patterson (PI)

Isaak Rudman

Zhigang Feng

Andre Dowdell

March 23-24, 1998

Institute of Paper Science and Technology

500 10th Street, N.W.

Atlanta, Georgia 30318



## DUES-FUNDED PROJECT SUMMARY

**Project Title:** Fundamentals of Web Heating  
**Project Code:** STMBOX  
**Project Number:** F002  
**PAC:** Papermaking  
**Division:** Engineering  
**Project Staff**  
**Faculty/Senior Staff:** Timothy Patterson (PI), Isaak Rudman, Zhigang Feng  
**Staff:** Andre Dowdell  
**FY 98-99 Budget:**  
**Allocated as Matching Funds:** \$152,184  
**Time Allocation**  
**Faculty/Senior Staff:** Timothy Patterson (40%), Isaak Rudman (40%)  
**Support:** Andre Dowdell (70%)  
**Supporting Research**  
**M.S. Students:** 0  
**Ph.D. Students:** 0  
**External:** Georgia Tech/IPST Seed Grant - Infrared (\$40,000)

### RESEARCH LINE/ROADMAP:

Increase machine efficiency by 30%. Reduce net energy consumption per ton by 30%.

### PROJECT OBJECTIVE:

To develop a quantitative understanding of the processes occurring during web preheating and during pressing of heated webs. Such an understanding will make possible the optimum use of web preheating for both production increases and product quality increases.

### PROJECT BACKGROUND:

The initial work on this project was performed as part of Project F001 Fundamentals of Drying. The work performed included the design, construction, and shakedown of the Steambox Comparator (4/94 - 9/94). The first PAC report on this project was presented at the Fall 95 Papermaking PAC. Initially David Orloff and Timothy Patterson were co-PIs on this project. The current PI is Timothy Patterson.

### SUMMARY OF RESULTS:

#### 4/94 - 7/95

- Design, construction, and shakedown of the Steambox Comparator (4/94 - 9/94). A paper documenting the results of the shakedown testing was published in TAPPI Journal, March 1996.
- Two Master's student projects and two proprietary projects were conducted using the Steambox Comparator between 9/94 and 7/95.

#### 8/95 - 3/96

- The Fall PAC meeting of 1995 was the first meeting at which a report on F002 was presented. At that time a summary of the shakedown tests and the previous student work was presented as well as a proposed plan for the project. This plan included
  - a literature search on web preheating
  - a literature search of possible means for modeling the steaming process

- a literature search on modeling of pressing of heated webs
  - development of an experimental test plan
- The literature searches on modeling were completed. A potential model for the steaming process was identified. A number of models of the pressing process were found, none were considered adequate.

3/96 - 9/96

- An experimental plan was developed and executed using the Steambox Comparator. The work is referred to as the First Steambox Comparator Experiment. The results are documented in Member Report 2 (August 1997) for this project. The work validated the experimental setup and examined the effects of vacuum and sheet solids content.
- An experimental plan to investigate the effects of web preheating on pressing results was developed and executed using the MTS Press Simulator. The results are documented in Member Report 5, Appendix B, First MTS Experiments (February 1998) for this project. The work indicated that sheet moisture profile may play a role in water removal and mechanical property development. It also highlighted the importance of pressing impulse selection with respect to solids content and heating condition.
- Work on implementing a model of the steaming process was initiated.

9/96 - 3/97

- A half factorial, five parameter experimental plan was developed for determining the factors controlling steam heating. Execution of the test plan on the Steambox Comparator was initiated (2<sup>nd</sup> Steambox Comparator Experiment).
- An experimental plan for extending/clarifying the results from the First MTS experiments was developed and execution of the plan was initiated.
- A thorough literature search on web preheating and pressing of preheated webs was completed. The results are documented in Member Report 1 (August 1997) for this project.
- Initiated Georgia Tech/IPST Seed Grant Project - Infrared Heating

3/96 - 9/97

- The half factorial, five level experimental plan for determining the factors controlling steam heating was completed. Analysis of the results was completed. The results are documented in Member Reports 3 and 4 (September 1997) for this project. The significant result was the finding that wet sheet air permeability is a primary controlling factor in the steaming process and that there is a relationship between wet sheet permeability, energy absorbed from the steam, and vacuum level. The work also confirmed that for heavy weight grades little energy is lost by convection from the top of the sheet and that significant temperature redistribution, by conduction, occurs in the sheet after leaving the steambox.
- The experimental plan for extending/clarifying the results from the First MTS experiments was completed. The results are documented in Member Report 5 (February 1998) for this project. The results confirmed that sheet moisture profile effects water removal and sheet property development, indicated that there is potentially a threshold pressure impulse required to obtain benefit from preheating, and estimated the potential maximum benefit from preheating for a linerboard furnish.

9/97 - 3/98

- A test plan for examining the effect of conduction temperature redistribution in the sheet after steaming was developed. The experimental apparatus to be used was the pilot paper machine at IPST. The steambox was installed on the machine, the felt run was modified, and provision were made for feeding Formette sheet through the press section instead of a continuous web. Trial runs were made. Testing to be completed by 3/98.

- An investigation of air permeability, water permeability, and the relationship between the two was initiated. A summary of current results is provided in this report.
- A literature search on jet impingement was performed with the intent of identifying concepts applicable to steamboxes. A summary of results is provided in this report.
- A test plan for an additional set of Steambox Comparator experiments (3<sup>rd</sup> Steambox Comparator Experiment) was developed. Execution of the plan is scheduled for spring/summer 1998.
- Formulated boiler plate for "Guidelines for the Use of Sheet Preheating."
- Work on implementing the steaming model continued.
- Completed Georgia Tech/IPST Seed Grant Project - Infrared Heating.

#### Publications/Reports

- Orloff, D. I.; Patterson, T.; Strand, M. A., Apparatus for the Evaluation of Web Heating Technologies-Development, Capabilities, Preliminary Results, and Potential Uses, Tappi Journal 79, no. 3: 269-278 (March 1996).
- Patterson, T. F., Iwamasa, J. M., Review of Web Heating and Wet Pressing Literature, IPST Member Report 1, Project F002. August 1997
- Patterson, T. F., Iwamasa, J. M., First Steambox Comparator Experiment: Initial Investigation of Steambox Performance, IPST Member Report 2, Project F002. August 1997
- Iwamasa, J. M., Patterson, T. F., Second Steambox Comparator Experiment: Statistical Analysis, IPST Member Report 3, Project F002. September 1997.
- Patterson, T. F., Iwamasa, J. M., Second Steambox Comparator Experiment: Wet Sheet air Permeability Analysis , IPST Member Report 4, Project F002. August 1997
- Patterson, T. F., Rudman, I., Preliminary Hot Pressing Investigation, IPST Member Report 5, Project F002. February 1998.

#### **GOALS FOR FY 98-99:**

1. Complete pilot paper machine experiment on internal sheet conduction.
2. Complete 3<sup>rd</sup> Steambox Comparator Experiment. Confirm earlier identified relationship with wet sheet air permeability; expand furnishes, basis weights considered, incorporate MTS pressing of sheets similar to those used in the steaming experiments.
3. Complete model of internal sheet steaming process.
4. Investigate heat transfer/flow processes occurring between exit of steambox and the sheet surface.
  - a. Model using ADINA software.
  - b. Experimental measurements.

#### **DELIVERABLES (FY 98-99):**

1. Member Report on Pilot Paper Machine Experiment
2. Member Report on 3<sup>rd</sup> Steambox Experiment.
3. Member Report on comparison of steaming model with experimental results.
4. PAC Report on ADINA modeling and associated experimental work.
5. Preliminary version of "Guidelines for the Use of Sheet Preheating."

**SCHEDULE**

Task	1998												1999						
	J	F	M	A	M	J	J	A	S	O	N	D	J	F	M	A	M	J	
Paper Machine Experiment																			
Experiment Report		X																	
3 <sup>rd</sup> Steambox Experiment																			
Experiment Steambox					X	X	X	X											
Report - Steambox									X										
Related MTS Pressing										X									
Report - Pressing											X		X	X					
Steaming Model																			
Modeling Report		X	X	X	X	X													
ADINA																			
Modeling Experimental			X	X	X	X	X	X	X	X	X	X	X	X	X	X	X	X	X
Preliminary Guidelines												X	X	X	X	X	X	X	X

## **F002 Fundamentals of Web Heating PAC Report - Spring 1998**

### **1. Summary**

### **2. Summary of MTS Hot Pressing MTS Experiments**

- 2.1 Background*
- 2.2 Layered Sheet Pressing*
- 2.3 Single Stage Pressing*
- 2.4 Three Stage Pressing*
- 2.5 MTS Pressing - Conclusions*

### **3. Georgia Tech/IPST Seed Grant - Infrared Heating**

- 3.1 Summary*
- 3.2 Purpose*
- 3.3 Basic Experimental Plan*
- 3.4 Conclusions*

### **4. Paper Machine Steambox Experiment**

- 4.1 Rationale*
- 4.2 Implementation*

### **5. Permeability of Wet Samples**

- 5.1 Introduction*
- 5.2 Air Permeability Measurements of Wet Sheets*
- 5.3 Interrelation Between Water and Air Permeability*
- 5.4 References*

### **6. Jet Impingement Literature Search**

- 6.1 Introduction*
- 6.2 Jet Flow*
- 6.3 Nozzle Geometry*
- 6.4 Nozzle-to-Plate Spacing*
- 6.5 Nozzle-to-Nozzle Spacing*
- 6.6 Surface Motion*
- 6.7 Permeable Surface with Through Flow*
- 6.8 Other Factors*
- 6.9 References*

### **7. Plan for Third Steambox Experiment**

- 7.1 Introduction*
- 7.2 Test Plan*
- 7.3 Related Pressing Study*

### **8. Steambox Implementation Guidelines**

## **F002 Fundamentals of Web Heating**

### **PAC Report - Spring 1998**

#### **1. Summary**

This report is in seven additional sections, which cover completed work, in progress work, and planned work. Sections Two and Three cover completed work. Sections Four, Five, and Six cover in-progress work, and Sections Seven and Eight cover work which is planned.

Section Two is a summary of MTS Press Simulator work which is reported on in detail in Member Report 5 for this project, Preliminary Hot Pressing Investigation. This work investigated the effects of temperature, web solids, web solids profile, and pressing pulse on water removal and outgoing sheet properties. Single and multi-ply sheets were used. One of the significant results was the finding that web solids profile can effect both water removal and sheet properties. This finding is a new one and has not been previously reported in the literature. The work using multi-ply sheets has not been previously reported to the PAC. Section Three covers work that was done as part of a Georgia Tech/IPST Seed Grant on infrared heating. The intent was to determine if infrared radiation in a narrow focused wavelength band can be used to produce uniform (zd) web heating. While the work was inconclusive on that subject, the results were useful from the standpoint of implementation/design of infrared heating devices.

Section Four reports on the current status of an investigation into steambox position relative to the nearest downstream press and the effect of that location on water removal efficiency. This work is in progress, but should be complete by the end of March 1998. Section Five reports on recent work on the validity of using air permeability as a measure of sheet openness to steaming. This work is also in progress, current results indicate that air permeability is a valid measure of sheet openness. Results also indicate that there may be a direct relationship between air permeability and water permeability for wet paper. This work was motivated by the finding, reported in Member Report 4 for this project, that wet sheet air permeability is an indicator of a sheet's ability to absorb steam energy. This work has value in that it may confirm relationship between a previously used, but difficult to implement method (water permeability) for characterizing wet sheets with a new implementation of an easier to use method. Section Six is a summary of a recent literature search into jet impingement. This is the first step in extending the work of this project to the processes which occur between the steambox nozzle exit and the surface of the sheet.

Section Seven is an outline of the experimental plan for a third Steambox Comparator experiment. The objective of this experiment is to confirm the previously identified relationship between wet sheet air permeability and steam energy absorbed by the sheet. It is anticipated that this will be the final large scale experiment using that apparatus. As part of this work, additional pressing work, similar to the earlier MTS pressing reported in Member Report 5 will be performed. The objective is to evaluate the response of sheets of different furnishes, but the same permeability, to heating prior to pressing. The work will include microscopic examination of the sheets to determine if heating produces structural changes to the sheet. Section Eight is a boiler plate for a set of guidelines for steambox implementation. This is intended to be the final product of this research.

## 2. Summary of MTS Hot Pressing MTS Experiments

### 2.1 Background

This work was initiated to investigate the interaction between web moisture profile and both water removal and final sheet mechanical properties. In an initial set of experiments (Pressing of Heated Sheets - 1<sup>st</sup> MTS Experiments (summer 1996)), the effect of ingoing consistency (solids) and ingoing temperature were investigated using a pressure pulse which was not varied with sample solids content. Ingoing sheet temperature was varied by steaming. Additionally, the effect of ingoing solids and temperature on the compression and permeability of the wet paper were measured. With no attempt to optimize the pressure profile, the results indicated that:

1. Increasing sheet temperature by steaming did not necessarily increase the water removal and mechanical strength;
2. The moisture profile of the steamed sheet may affect water removal and mechanical strength of the sheet.

Based on these observations, it was decided to examine how preheating methods, which change the sheet moisture profile, effect the pressing response of sheets at different ingoing solids and sheet temperatures. Two heating methods were used, steaming and plate heating. A secondary reason for this comparison was that a number of references used plate heating as a means of sheet heating for pressing studies. Specific areas of interest were water removal, final mechanical strength, and sheet compression. The pressing pulse was increased as the sheet solids was increased. The results of the research indicated that moisture profile and ingoing sheet temperature are significant factors governing water removal and development of mechanical strength.

The furnish used was an OCC furnish at a freeness of 616 ml CSF. All sheets were made using a Formette Dynamique. The work was conducted in two phases:

1. Single-stage pressing of sheets with ingoing solids of 25% and 45%. This entailed preheating the sheet by one of two means, pressing the sheet, drying the sheet under constraint, conditioning the sheet and then measuring soft platen caliper; specific elastic modulus, CD STFI, and MD STFI. Two types of sheets were used, one consisted of three layers of equal basis weight which had a combined basis weight of 205 gsm and the other was a single layer sheet with a total basis weight of 205 gsm. The multi-layer samples were only tested at 25% solids. This work provided information on temperature, moisture profile and the relative effect of those parameters.
2. Three stage pressing of sheets with an initial ingoing solids of 25%. This entailed measuring the sheet caliper, preheating the sheet, pressing the sheet, and measuring the sheet caliper. This was done three times, each successive pressing used a higher impulse. The samples were heated to approximately the same temperature prior to each pressing and except for the first pressing, no attempt was made to regulate ingoing solids. After the third pressing, the sheet was dried under constraint, and measurements were made of soft platen caliper,

specific elastic modulus, CD STFI, and MD STFI. This work provided information on the maximum attainable benefits of a particular means of heating.

The work performed with the layered sheets has not been reported on previously. The results from previous work was re-evaluated based on those results. All the work is presented in Member Report 5 for this project.

## **2.2 Layered Sheet Pressing**

### 2.2.1 Layered Sheet Pressing - Results

A number of interesting trends can be observed in Figure 2.1, Figure 2.2, and Figure 2.3. Figure 2.1 shows quite clearly that under all measured pressing conditions, water removal is greatest in the bottom layer and least in the top layer. The result suggests that if the bottom of the sheet could be heated, instead of the top of the sheet, than there should be an increase in water removal. In that case the heating and the corresponding decrease in viscosity would occur where a majority of the water is being moved.

There was not always a direct correlation between density and specific elastic modulus (SEM). For example, the unsteamed layered sheet showed a maximum SEM and conditioned density for the bottom layer, which is generally expected. The sheet steamed for 20-seconds showed a maximum SEM for the middle layer, while the minimum SEM was measured for bottom layer which had the maximum density. In contrast, steaming followed by the 200-second waiting time, produced a maximum SEM in the top layer which showed the minimum density.

The case of 20-second steaming tended to yield properties which were equal to or greater than those for the no steaming case. The 40-second steaming with 200-second waiting case tended to yield properties which were less than those for the case of no steaming. This result is intriguing because the total moisture gain and average temperature were the same for both steaming cases. Both cases had approximately the same total energy content at pressing. The 200-second waiting case also had a shallower moisture profile and an almost flat temperature profile as compared to the 20-second steaming case. This would seem to indicate that moisture profile as well as temperature plays a role in water removal and sheet property development.

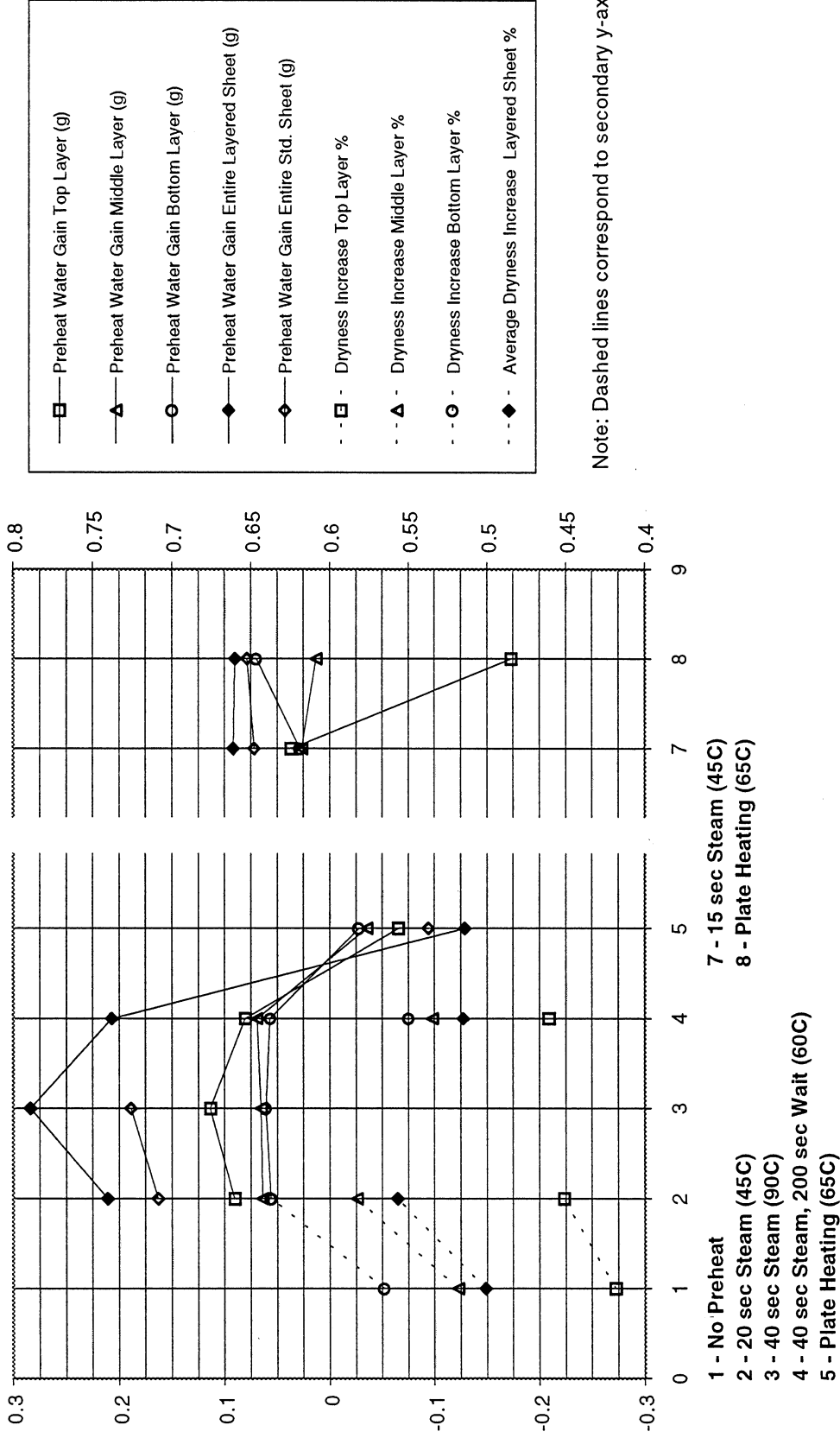
### 2.2.2 Layered Sheet Pressing - Conclusions

The work with preheating and pressing of layered sheets yielded a number of conclusions.

1. Preheating alters the moisture profile of the sheet. Steam heating yields a moisture profile which has the greatest moisture at the top of the sheet and the least at the bottom of the sheet. Plate heating yields the opposite profile.
2. A waiting period after preheating reduces the temperature and moisture gradients in the sheet.
3. The bottom portion of the sheet shows the greatest water loss during pressing and the top portion shows the least water loss. Water removal is a non-uniform process with respect to vertical position within the sheet.
4. There is not always a direct correlation between sheet conditioned density and sheet conditioned specific elastic modulus.

5. Steaming to  $\sim 60^{\circ}\text{C}$  and pressing immediately tended to yield greater water removal and more enhanced sheet properties than either steaming to  $90^{\circ}\text{C}$  and waiting 200-seconds until the average sheet temperature reached  $60^{\circ}\text{C}$  or no preheating at all. The result suggests that moisture profile as well as temperature profile play a role in water removal and sheet property development.

Summary of Layered Heating & Pressing Results

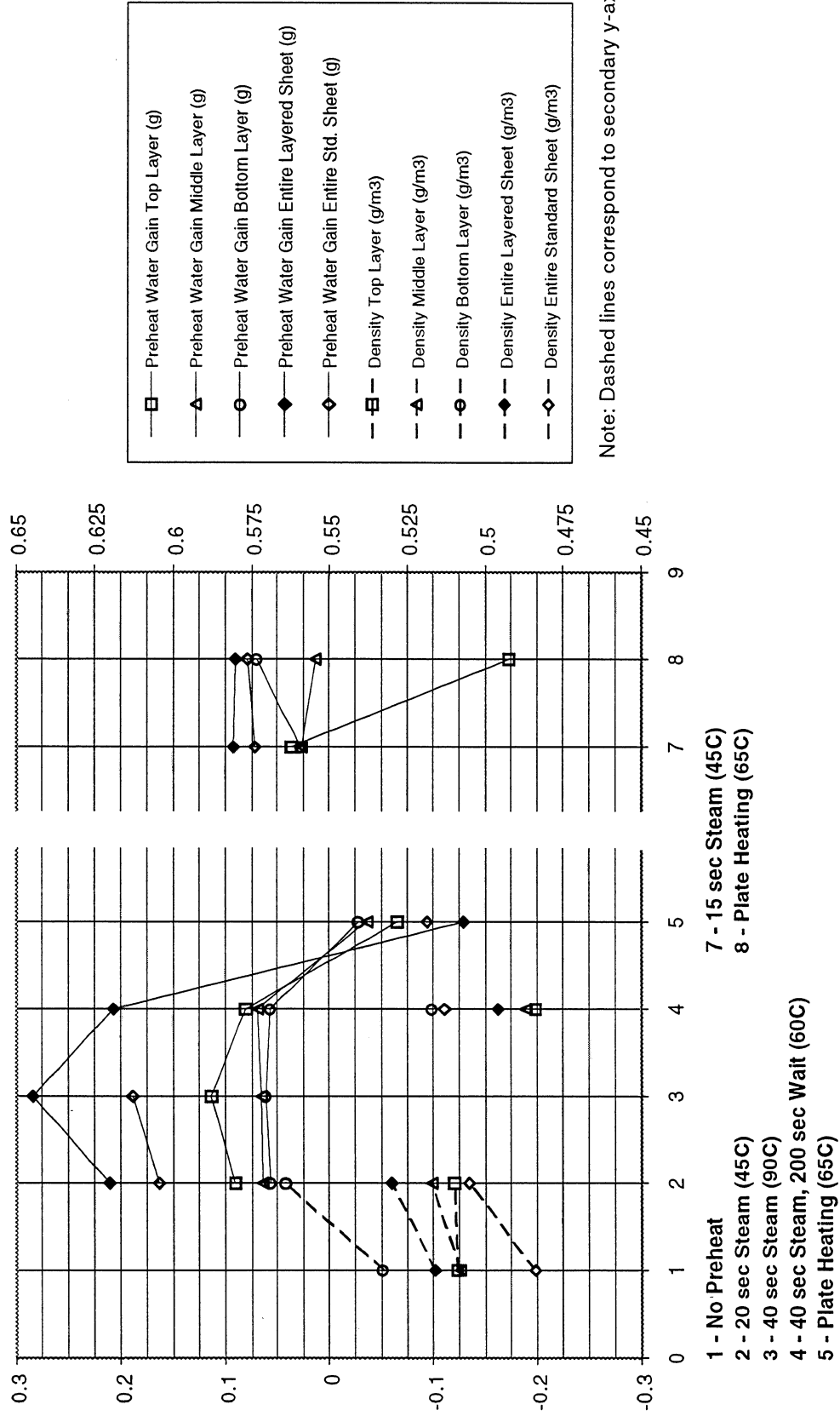


Note: Dashed lines correspond to secondary y-axis.

Figure 2.1 Results from Layered Pressing - Preheat Weight Change and Outgoing Press Dryness

Confidential Information - Not for Public Disclosure  
 (For IPST Member Company's Internal Use Only)

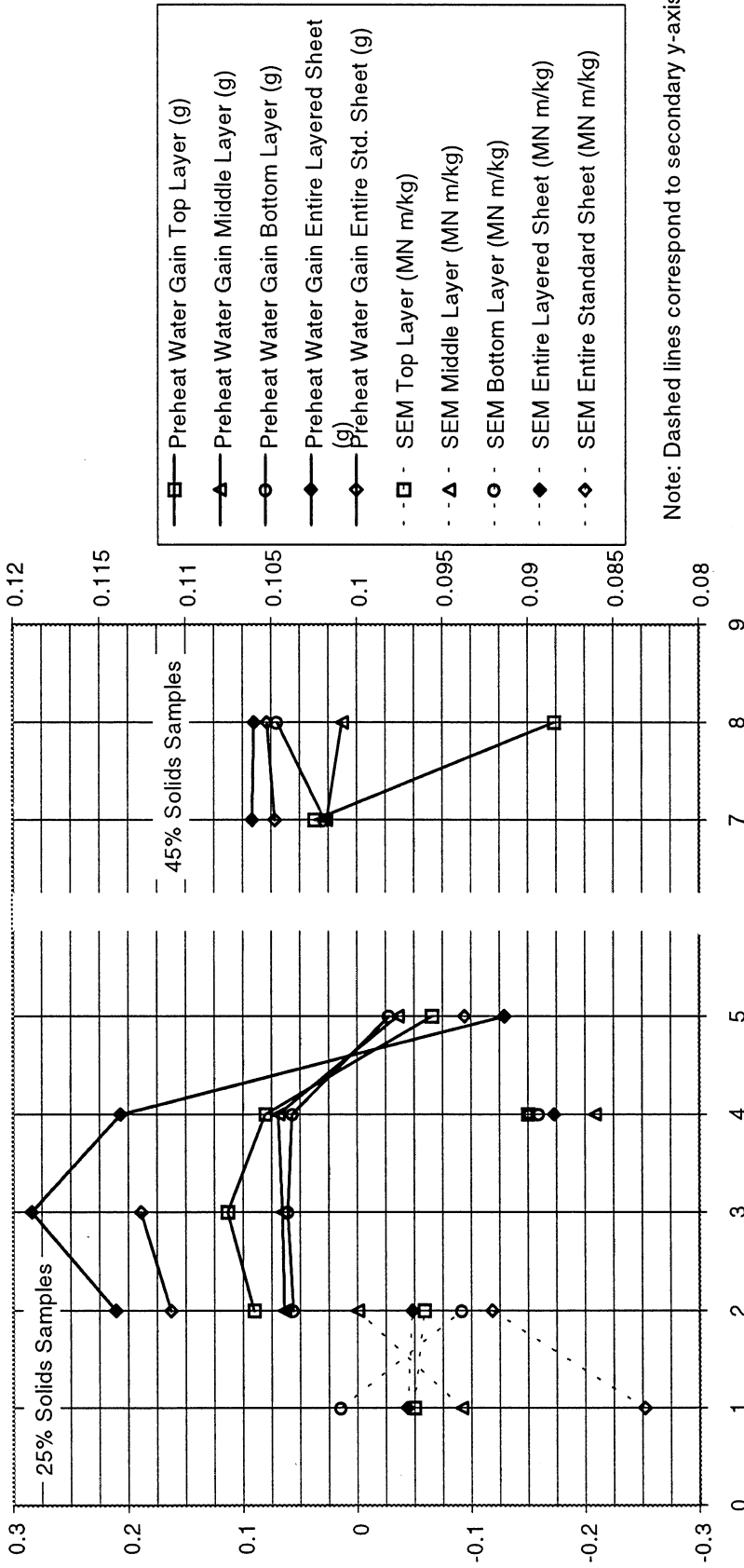
Summary of Layered Heating & Pressing Results



Note: Dashed lines correspond to secondary y-axis

Figure 2.2 Results from Layered Pressing - Preheat Weight Change and Conditioned Density

### Summary of Layered Heating & Pressing Results



- 1 - No Preheat
- 2 - 20 sec Steam (45C)
- 3 - 40 sec Steam (90C)
- 4 - 40 sec Steam, 200 sec Wait (60C)
- 5 - Plate Heating (65C)
- 7 - 15 sec Steam (45C)
- 8 - Plate Heating (65C)

Figure 2.3 Results from Layered Pressing - Preheat Weight Change and Conditioned Specific Elastic Modulus (SEM)

## 2.3 Single Stage Pressing

### 2.3.1 Single Stage Pressing - Results

The average water removal and mechanical strength properties produced by single stage pressing at ingoing solids of 25% and 45% are plotted in Figure 2.4 and Figure 2.5.

The results from the whole sheet, single stage pressing showed a difference as compared to the results from the layered pressing. In the whole sheet pressing, the case of 40-second steaming with 200-seconds waiting prior to pressing yielded slightly greater water removal than the 20-second steaming case (for 25% solids). This was contrary to what was found in the layered sheet pressing work. Thus, the layered structure apparently affected the water removal process to some extent. However, the whole sheet pressing data did support the conclusion that moisture profile has an effect on both water removal and sheet property development. The results also indicate the total moisture content is a factor, since similar preheating conditions produced different results for 25% and 45% solids sheets.

#### 25% Solids Sheets

The layered preheating results showed that as steaming time increased, more moisture was condensed in the top surface of the sheet and a steeper moisture profile resulted. The top of the sheet was wetter than the bottom of the sheet. The results also showed that as plate heating time increased, the top of the sheet became drier, resulting in a moisture profile that was the opposite of that produced by steaming. These trends should be the same for the whole sheet. Assuming that to be the case, the 25% solids results, particularly as shown by Figure 2.5, demonstrate that the sheets with the most water in the top portion of the sheet had the lowest water removal. Interestingly, the SEM results followed the same trend, but the density and CD STFI tended to follow the opposite trend.

Overall, the 15 second steaming, the 40-second steaming with 200-seconds waiting, and the two plate heating cases produced the highest water removal. The SEM results followed a similar trend. The density and CD STFI tended to follow a trend which increased with sheet temperature and then reached a plateau.

#### 45% Solids Sheets

In Figure 2.4 and Figure 2.5 there is an additional 45% solids case shown. This is the 45% solids, no preheating case which used the same pressure pulse as was used for the 25% solids sheets. The results show that the dewatering is significantly less than that for all the other 45% solids cases, i.e., the cases using the "standard" higher peak pressure and greater impulse 45% solids pressing pulse. This demonstrates the generally accepted concept that increasing peak pressure and impulse increases dewatering.

At an ingoing solids of 45%, the benefits of steaming were less pronounced than with the 25% solids sheets. This is again consistent with the results obtained in the 1<sup>st</sup> MTS Experiment.

In the 45% solids results, the case of 40-second steaming is somewhat exaggerated because the ingoing moisture was approximately 38% instead of the desired 45%. As with the 25% solids cases, SEM and water removal followed similar trends. Unlike the 25% solids cases, density and CD STFI did not follow a similar trend. This may be attributed to the limited changes in density. In the steaming cases, water removal increased as the moisture content

of the top of the sheet increased. The plate heating yielded results which were in general less than those for the no preheating case. Plate heating resulted in considerable drying out fibers in the top part of the sheet. It is believed this caused decreased bonding between fibers which resulted in a noticeable decrease of SEM and STFI data. There is the possibility that increasing the peak pressure pulse may result in an increase in some of these properties, however, as the fibers dry out there is a point at which increasing peak pressure has no effect on bonding.

### 2.3.2 Single Stage Pressing - Conclusions

The results support the concept that moisture profile as well as total moisture content affect both water removal and sheet property development. The relationship changes as sheet solids is increased.

In the case of 25% solids, increasing the moisture content of the top of the sheet beyond a certain level tended to decrease the water removal and SEM. Density and CD STFI tended to increase with sheet temperature, regardless of moisture profile, and then level off. Only a significant decrease in the moisture content of the top of the sheet caused a decrease in SEM or density. Heating, depending on the moisture profile produced, can have a positive impact on sheet properties.

In the case of 45% solids, dewatering increased with increasing moisture at the top surface of the sheet. Any decrease in the moisture at the top surface resulted in decreased water removal, SEM, and CD STFI. Heating in general did not have a significant positive impact on sheet properties.

25% and 45% Pressing Data

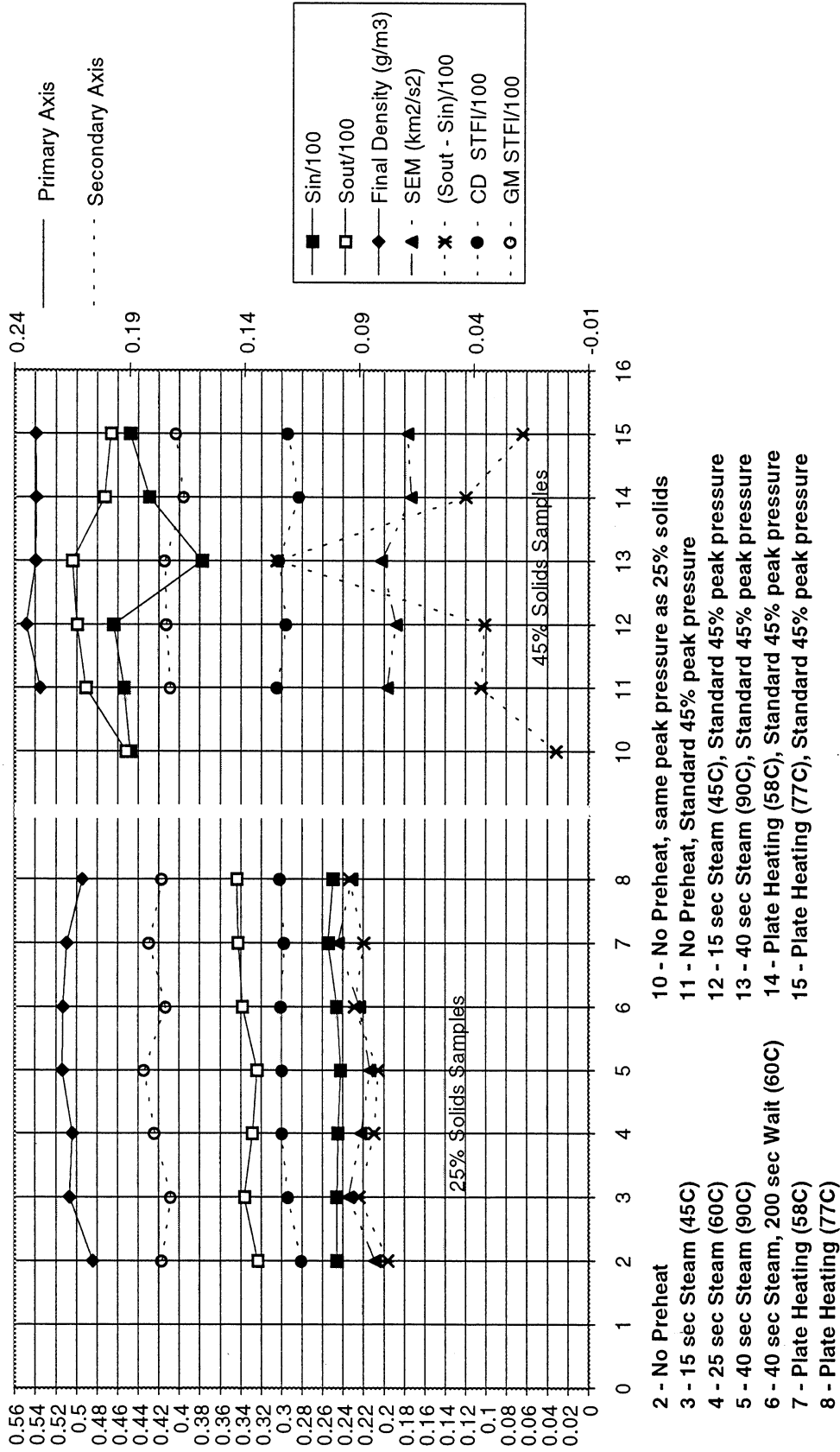


Figure 2.4 Results from Layered Sheet Pressing

Confidential Information - Not for Public Disclosure  
 (For IPST Member Company's Internal Use Only)

25% and 45% Pressing Data as a Percent Change from Unheated Case

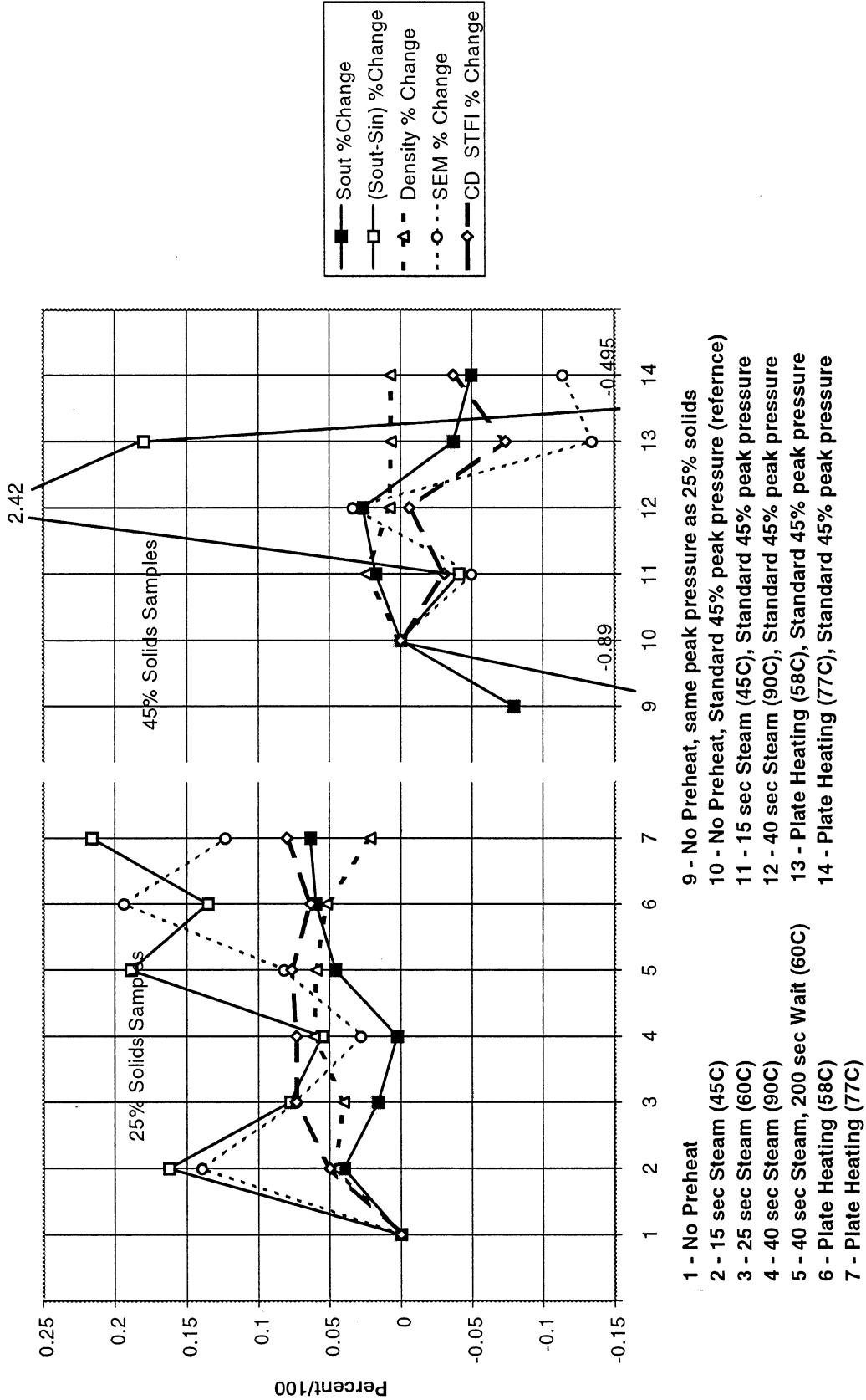


Figure 2.5 Results from Layered Pressing - Percent of Control Case

Confidential Information - Not for Public Disclosure  
 (For IPST Member Company's Internal Use Only)

## 2.4 Three Stage Pressing

Three stage pressing was performed to determine the potential of sheet preheating. It is an idealization of a three press configuration with preheating before each press. In this experiment ingoing solids were 25% prior to the first pressing and preheating was identical prior to each pressing.

Steaming was conducted for 15 seconds resulting in an average sheet temperature of 45-50°C. Plate heating was carried out for 20-seconds at a plate temperature 65°C resulting in an average sheet temperature of ~58°C. Data on water removal and mechanical strength are plotted in Figure 2.6.

The benefits of preheating are obvious both in terms of water removal and mechanical strength when compared with the case of no heating. Steaming is especially productive. Consolidation of the sheet is much higher. The increase in strength is on order of 12-14%. Apparent compression increased, which is assumed to have been caused by higher conformability of fibers and lower spring back at elevated sheet temperature. The advantages of plate heating are also significant but slightly lower than that of steam.

An attempt was made to select pressure pulses which were optimum for the ingoing solids contents. It was expected that as the solids increased, the total change in properties produced by each succeeding pressing would also decrease. However, the results consistently show the second pressing yielded a lesser change in properties than either the first or third pressing. This suggests that the pressure pulse used for the second pressing was not adequate; the peak pressure and impulse should have been higher.

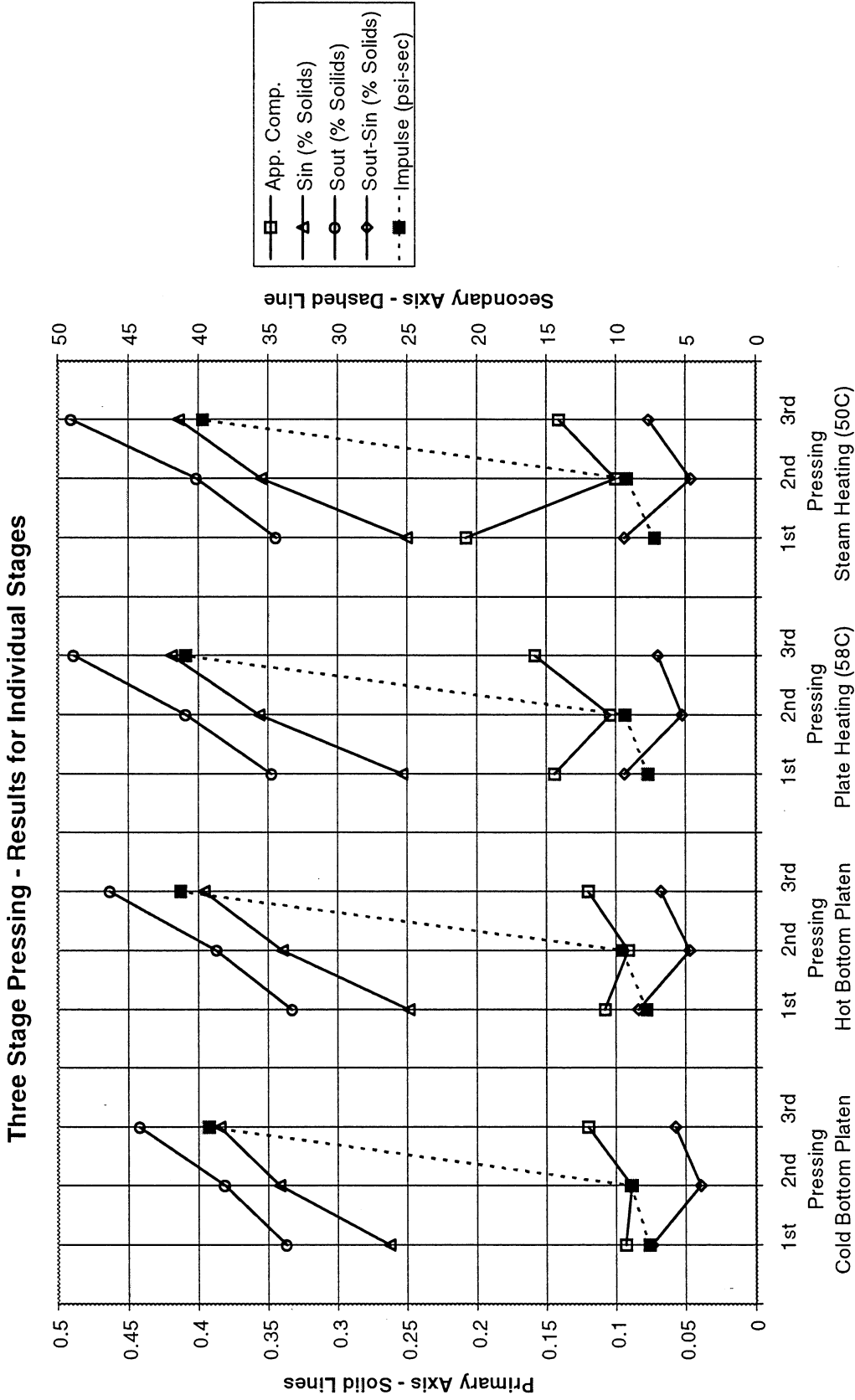


Figure 2.6 Three Stage Pressing - Results from Individual Stages

Confidential Information - Not for Public Disclosure  
(For IPST Member Company's Internal Use Only)

## 2.5 MTS Pressing - Conclusions

The effect of ingoing sheet solids and temperature on water removal and mechanical strength of paper using different preheating methods was addressed in this work. Single pressings were performed on layered and whole sheets using various preheating methods. Three-stage pressing was conducted using selected preheating methods to determine the potential of preheating in a three press configuration. The results make possible the following conclusions:

1. The beneficial effect of the sheet preheating is determined not only by increased sheet temperature but also by the changes in the solids profile during preheating. Accumulation of excessive moisture in the top part of steamed sheet may cause a decrease in water removal in spite of an increase in sheet temperature. Alternatively, excessive moisture evaporation in the top part of plate-preheated sheet may cause drying out of fibers, a deterioration of the sheet consolidation, and a drop in mechanical strength.
2. At an ingoing solids of 25%, moderate preheating by steam and hot plate resulted in an increase in water removal and mechanical strength. Strength characteristics were also high. Steam preheating could result in a decrease in dryness due to accumulation of condensate in the top part of the sheet.
3. At an ingoing solids of 45%, preheating by steam had less pronounced benefits than that at 25%. The same was true of plate heating. Plate heating also caused considerable drying of the top surface with a resultant detrimental effect on strength properties.
4. Three-stage preheating showed that steaming produces significantly improved water removal and strength of the sheet as compared with the no preheating case. The advantages of plate preheating were less pronounced, but were also significant.
5. Comparing the results from the 25% and 45% single stage pressing, the three stage pressing, and earlier work, there appears to be a threshold pressure pulse (peak pressure and/or impulse) required to obtain maximum benefit from preheating in a particular pressing application. If the pressing pulse is inadequate, little or no benefit will be obtained from preheating in terms of water removal. Sheet strength increases will also be affected.

It appears that the ideal preheating method for a low solids sheet is one which leads to a maximum increase in sheet temperature and a minimum or no decrease in solids in the top part of the sheet. At higher ingoing solids the ideal preheating method is one which leads to a maximum increase of sheet temperature and some decrease in solids in the top part of the sheet. It should be noted that the moisture profiles produced during the testing were in all likelihood extreme compared to those produced by commercial web heating systems.

### 3. Georgia Tech/IPST Seed Grant - Infrared Heating

#### 3.1 Summary

This research used a radiant infrared source to preheat a moist paper web on a felt. Using selective emission of radiant energy, it was expected that more uniform heating through the depth of the web could be obtained than through the use of contemporary steam boxes. Greybody spectra of resistance-heated SiC elements were incrementally shifted to shorter wavelengths, maintaining irradiance constant (constant incident energy on the paper web), by varying element temperature and spacing. As the majority of the spectral intensity shifted to wavelengths shorter than 2.7  $\mu\text{m}$ , heat penetration was expected to increase. Previous researchers had produced transmittance spectra for paper which indicated that moist paper was partially transmittive at the shorter wavelengths. Spectrally emitting coatings of ytterbium, erbium, and neodymium oxides on internally heated mullite tubes and on heated SiC elements were also to be investigated. Radiation emission/absorbtion were measured using a spectral radiometer along with fine thermocouple junctions imbedded in the web at known depths. The absorbance spectra of common pulp furnishes were statically evaluated using an infrared spectroradiometer. The data indicated that at selected infrared wavelengths, there should be some transmittance of infrared energy into the moist sheet. Transmittance of infrared energy into the sheet could produce more uniform heating through the thickness of the moist sheet. Previously published results showed that paper was almost completely infrared absorbant at wavelengths greater than 3  $\mu\text{m}$ , but was partially transmittive in the wavelength range of 1.5 to 2.7  $\mu\text{m}$  [4, 5].

The moist paper transmittance spectra obtained as part of this work were not the same as reported in the literature. The spectra depended on furnish type and moisture content. The furnish of interest OCC (Old Corrugated Container) showed lower than reported transmittance. The experimental results obtained using the greybody spectra produced by the SiC elements showed that there was no significant difference in temperature gradient in the web as the greybody spectra was shifted to shorter wavelengths or as the sample moisture content was changed. This indicated that there was not sufficient energy radiated at the relevant wavelengths. There was considerable difficulty in obtaining narrow band radiant energy emittance using the mullite tubing and the various coatings. It was not possible to obtain an emittance spectrum with only a narrow band peak at the desired wavelength. Plain SiC elements were coated with alumina and a spectrum which consisted of what was believed to be a narrow band emission peak superimposed on a greybody emission spectrum was obtained. This spectrum did not yield a significantly different temperature gradient as compared to the uncoated SiC greybody spectrum nor was there a significant difference based on sample moisture content. Increased moisture resulted in lower temperatures, but the shape of the temperature gradient was not significantly different. The conclusion was that the method employed for producing the narrow band spectrum was inadequate. It was interpreted that radiation/conduction of heat from the greybody SiC heating elements was not captured and reradiated spectrally by the coating materials. Rather, the coating was partially transmissive and acted as a window to the heating element greybody radiation. The transmittance/absorbtion spectra of the samples indicates that narrow band radiation should provide enhanced internal heating of the sample, alternate methods of producing the spectra are required if the hypothesis is to be validated. It is believed that gas heating of spectrally emitting surfaces will serve this purpose.

### 3.2 Purpose

In the case of broad band greybody radiation, most of the energy from a heating element is absorbed in a thin layer at the top of the suspension of paper (moist paper web), it is then conducted downward. This occurs because much of the radiation is emitted at frequencies which are readily absorbed by the paper. If a significant amount of the energy was emitted in the frequency range at which the paper was partially transmissive, then the radiation would penetrate into the sheet and result in a more even temperature gradient through the sheet. If the element could more evenly heat the suspension through out its thickness, the viscosity of water would be lowered and extrusion of the water during pressing would be more efficient. Therefore, the objective of this project is heating entire depth more evenly by shifting and or altering the maximum of greybody distribution without altering total heat flow.

The sheet type chosen for heating evaluation was OCC. This furnish is used to make linerboard, a heavier weight sheet on which steamboxes are routinely used. In recent years the effectiveness of steamboxes has decreased as the use of OCC has increased. OCC tends to be less permeable to steam than a virgin furnish. Thus an effective infrared heating system would have immediate applications. Two other sheet types were examined for absorbtion/transmission spectra, virgin kraft and glassine paper.

The intent of this work was to show that properly implemented infrared heating could produce a more even temperature gradient in the sheet by providing for transmission of some of the energy into the sheet. The objective of producing an infrared system with sufficient energy output to outperform a steambox was intended to be left for future work. This work was to demonstrate the concept.

### 3.3 Basic Experimental Plan

The experimental plan involved testing of two basic rod arrangements. The first used plain SiC rods and the second used SiC rods inserted into mullite tubes which were coated with inorganic powder. The coatings modified the emittance spectrum.

A plain SiC rod has a greybody emittance spectrum. As the temperature of the rod is increased, the emittance spectrum shifts to shorter wavelengths and higher frequencies. An increase in temperature also results in a change in rod electrical resistance and a change in the power output. The number, size, and spacing of the rod were varied to compensate for this effect. Thus, the spectrum of the incident radiation was shifted from low temperature, longer wavelength greybody radiation to high temperature, short wavelength radiation. The configurations were to be tested first using static samples and then the most effective configurations were to be tested using dynamic samples. The configurations which resulted in high temperature, short wavelength spectrums were anticipated to be the most effective, (i.e., provide for internal heating of the sheet) as this emittance spectrum should be partially transmitted into the sheet.

The second heater arrangement was to utilize a SiC rod inserted into mullite tubes. The mullite tubes were to be coated with one of three inorganic powders. These powders had narrow band emittance spectrums. The hypothesized operating mode was that the SiC rods would emit greybody radiation which would be completely absorbed by the internal surface of

the mullite tube, heating the tube. The powder on the external surface of the mullite tube would in turn be heated and it would re-radiate the energy in a narrow infrared band. The operation was one of re-radiation rather than filtering, thus little energy would be lost. As with the plain SiC rods, static tests would be used to identify the most efficient configurations which would then be employed with the dynamic tests.

### 3.4 Conclusions

The conclusions that can be drawn from this work are, in general, negative conclusions. None of the heater configurations produced significant internal heating of the sample, this however, does not disprove the hypothesis that focused infrared emitters potentially can provide for a more even temperature profile through the sheet..

The infrared transmittance and absorbance spectra showed that there are infrared frequencies (1  $\mu\text{m}$  to 2  $\mu\text{m}$  depending on conditions) at which there should be at least partial transmittance of infrared energy into the sheet. The type of pulp used and the moisture content of the sample effect the transmittance spectrum. As a comparison a sheet of glassine paper was analyzed for transmittance, it had a significantly different transmittance spectrum as compared to the OCC furnish tested. The glassine had a higher transmittance and that band of transmittance extended over a considerable range, 1  $\mu\text{m}$  to 3  $\mu\text{m}$ . Thus, one would expect infrared heating to extend to a greater depth in this type of sheet than it would in the OCC sheet. Glassine type papers were not subjected to infrared heating testing in this study. The fibers in these two furnishes undergo considerably different processing, resulting in considerably different internal structures. This structural difference apparently effected the transmission/absorbption properties of the sheets . This indicates that infrared heating effectiveness is probably dependent on both furnish and solids content.

The shifting of the greybody radiation spectrum of the heaters by increasing the rod temperature did not yield significantly different sample heating. While no definite conclusion can be drawn, this does suggest that the process does not yield a sufficient focused infrared spectrum. The emitted energy spans a wide frequency range and not enough energy is incident on the sample at the frequencies which would penetrate the sample.

The coated rods also did not yield significantly enhanced heating of the samples. The coating of the mullite tubes failed to yield a focused infrared emittance spectrum. The hypothesized explanation is as follows. The mullite tubes are greybody radiators when heated. The coatings were partially transparent to infrared. Therefore, when the underlying mullite tube was heated some of the radiation was absorbed by the coatings and re emitted at the desired frequencies. However, some of the radiation, wide band greybody radiation, was transmitted through the coatings. The coating was not the primary emitter, the underlying surface was. The result was either no narrow band peak in the emittance spectrum or a narrow band peak superimposed on a wide band greybody spectrum. The same result occurred when the coating was applied directly to the SiC rods. Thus, in none of the cases did the heater configuration emit large amounts of infrared radiation in a narrow wavelength band. The resultant test conditions were not adequate for evaluating if this was an effective means of enhancing sample heating. It is believed that a properly designed gas fired infrared heater would insure that the coating was the highest temperature element in the heater. The coating would then be the primary infrared emitter and the emitted radiation would be in a narrow wavelength range. An alternative device is an electrical infrared system in which the radiant elements are fabricated from the narrow spectral band emitting material.

## 4. Paper Machine Steambox Experiment

### 4.1 Rationale

The pilot paper machine located at the Industrial Research Facility (IRF) at IPST is a 30 cm (12 in) wide machine which is capable of making light weight paper (50 g/m<sup>2</sup>) at approximately 230 m/in (750 ft/min). The fourdriner of the machine is too short, and the drainage too limited to make heavy weight sheets such as linerboard. The machine does however, have a relatively open press section which can accommodate a steambox in several locations relative to the press. This provides the capability to test, in a non-continuous mode, a concept developed as a result of previous Steambox Comparator testing.

The literature on steamboxes uniformly recommends that the steambox be placed as close to the following press as possible. The rationale is that such a placement limits cooling of the top of the sheet by convection. In previous Steambox Comparator experiments the temperature profiles showed that the top surface of the sheet did indeed cool after the sheet left the steambox (Figure 4.1). However, the data also showed that the total energy content of the sheet remained relatively unchanged this was particularly true of the higher solids sheets (35% and 45%). As shown in Figure 4.2. The temperature change appeared to be due primarily to conduction of heat towards the bottom of the sheet. Since water is removed from the bottom of the sheet (in single feted pressing), and water removal is enhanced by heating the water in the sheet and thus lowering its viscosity, it would appear that allowing the conduction to occur should enhance water removal. A test of this hypothesis requires realistic timing between heating and pressing, pressing; must occur within a short time (0.5 - 2 seconds) after heating. This is not possible using the MTS press simulator; however, it is possible using the pilot paper machine.

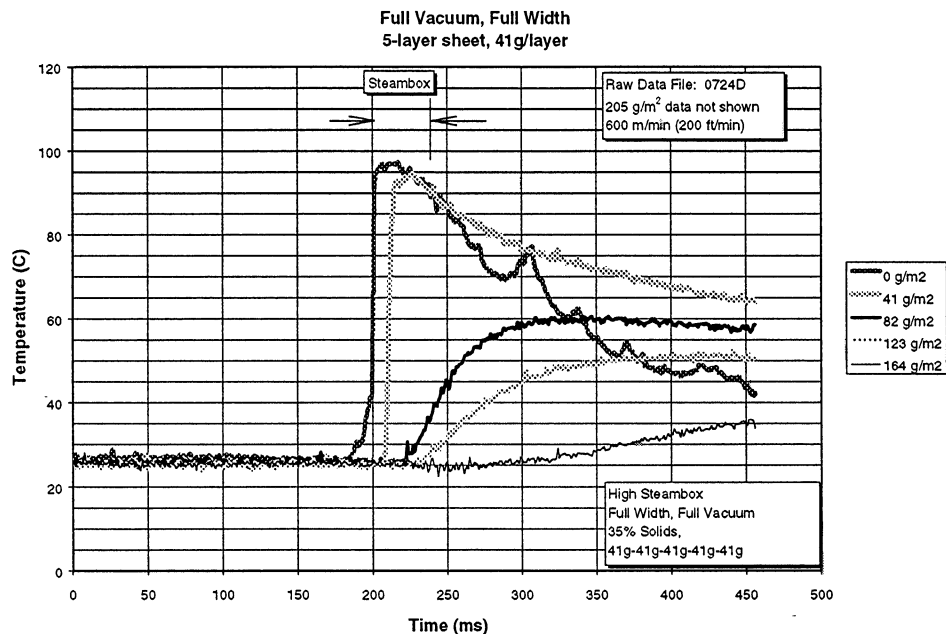


Figure 4.1 Temperature Profile After Exiting Steambox

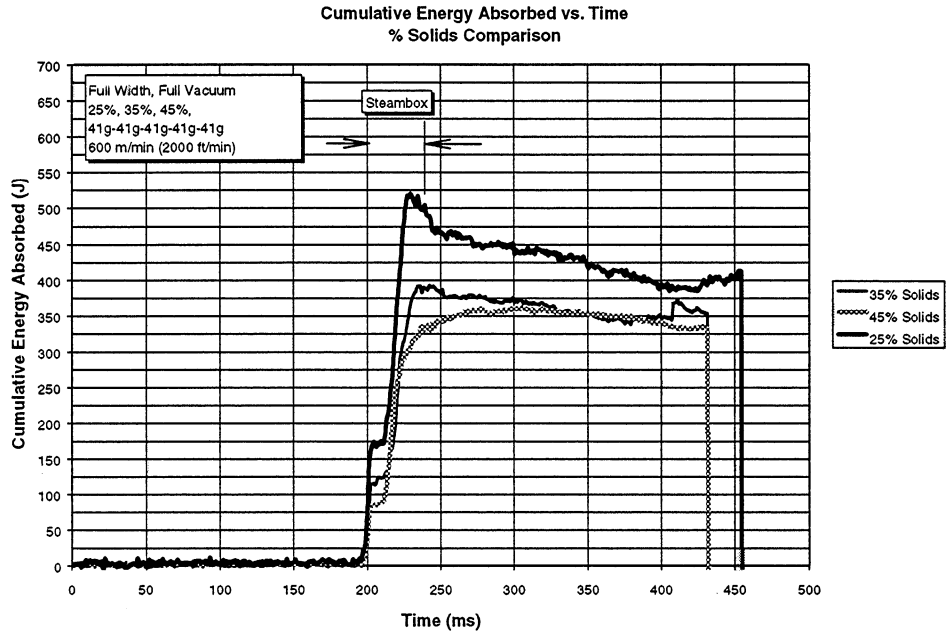


Figure 4.2 Energy Content After Exiting Steambox

4.2 Implementation

The hypothesis for the testing was that if conduction is allowed to occur after the sheet leaves the steambox, then water removal will be enhanced because of the more uniform temperature profile. Two steambox locations are to be tested, one as far from the press as possible 0.6 m (2 ft) and one as close to the press as possible. A schematic diagram is shown in Figure 4.3

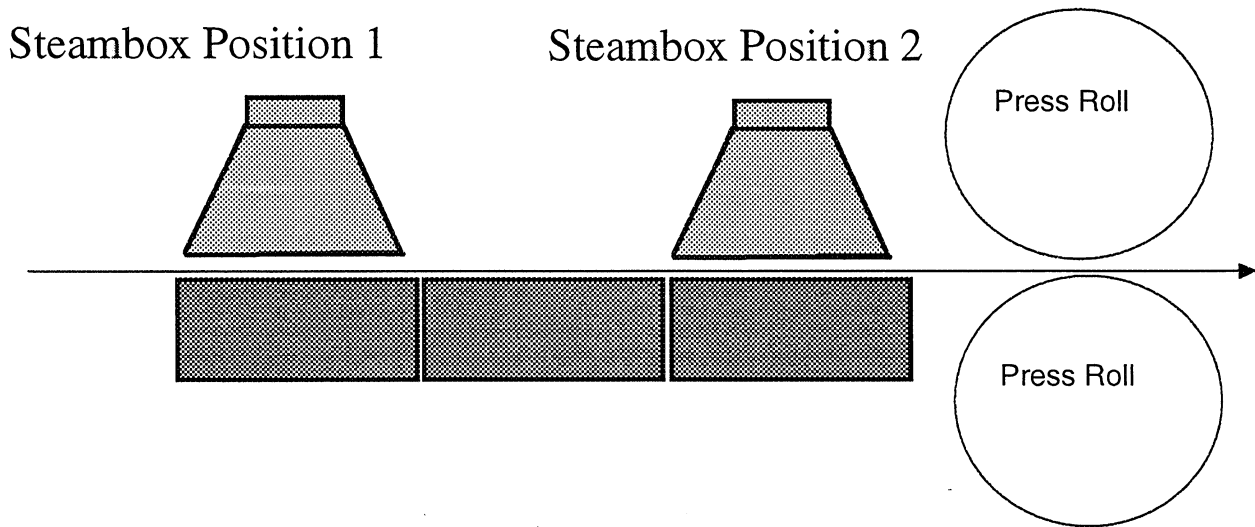


Figure 4.3 Steambox Position Test - Schematic Diagram

Preparation for the testing required:

- Removal of the standard top felt, allowing installation of a steambox.
- Installation of the steambox, including fabrication of a frame to support it.
- Extension of the steam line to the steambox.
- Repair of the felt tracking devices.
- Development of procedures for feeding handsheets through the pilot machine press section.
- Fabrication of samples.

These tasks are complete.

Testing is now in progress and results should be available at the Spring PAC meeting in March. If the results support the hypothesis, the concepts can be immediately applied.

## 5. Permeability of Wet Samples

### 5.1 Introduction

Previous research using the Steambox Comparator indicated that steam penetration into the sheet is linked with the degree of sheet openness or permeability. In the earlier work (F002 Member Report 4), the permeability of various wet sheets was compared to the amount of steam penetration which occurred during steaming tests. Those sheets with high permeability had significant steam penetration into the sheet during steaming tests. Those with low permeability had little or no steam penetration.

Since the permeability of the wet (or dry) sheet to the steam is difficult to measure; the openness of the sheet to the air flow was measured instead. The rationale behind this was that viscosity of the steam is close to that of air. For example, absolute (dynamic) viscosity of air at 20°C,  $\mu = 18.21 \times 10^{-6}$  kg/(s m). For the saturated steam,  $\mu = 12.28 \times 10^{-6}$  kg/(s m) at 100°C and  $\mu = 14.19 \times 10^{-6}$  kg/(s m) at 150°C .

In the paper industry there are several tests that are used to characterize the openness of sheets. In all of these methods the air flow rate through the sheet is measured at known pressure differential,  $\Delta P$ . The Bendtsen porosimeter (UM 535 in TAPPI Useful Methods) measures flow rate at three pressure differentials 75, 150, and 225 mm H<sub>2</sub>O (0.735 - 2.206 kPa). The standard TAPPI Gurley Porosity test T460 om-88, uses  $\Delta P = 123.4$  mm H<sub>2</sub>O (1.21 kPa). The Frazier permeability tester uses a relatively low air pressure (12.7 mm H<sub>2</sub>O or 124.5 Pa) to measure the air permeability of porous fabrics (TAPPI method T251 om-85).

The use of the Gurley, Bendtsen, and Frazier instruments to determine the air permeability of wet sheet is not a standard procedure. As part of an effort to validate the results relating steam penetration to wet sheet air permeability an evaluation of the applicability of these instruments was undertaken.

### 5.2 Air Permeability Measurements of Wet Sheets

In previous experiments investigating sheet steam heating, the Gurley Porosimeter was used to determine the permeability to air of wet sheets. Based on the characteristics of the Gurley Porosimeter permeability can be determined using Darcy's equation

$$\text{eq. 5.1} \quad K = \mu \ Q \ L / (A \ \Delta P)$$

where K is permeability (m<sup>2</sup>),  $\mu$  is dynamic viscosity (kg/(s m)), Q is flow rate (cm<sup>3</sup>/s), L is sheet thickness ( $\mu$ m) and A is the testing area (cm<sup>2</sup>). For the TAPPI Gurley Porosity test T460 om-88 pressure differential,  $\Delta P = 1.21$  kPa, and flow area,  $A = 6.47$  cm<sup>2</sup>. The Gurley Porosimeter measures the time in seconds for 100 cm<sup>3</sup> of air to flow through the sample. The volume flow rate is proportional to this measurement and is given by

$$\text{eq. 5.2} \quad Q = 100 / g$$

where g is the instrument measurement. By substituting known values into Darcy's equation, the following formula for calculating the air permeability from the Gurley Porosity is obtained

$$\text{eq. 5.3} \quad K = 2.326 \ * \ 10^{-15} \ * \ L / g$$

Since Darcy's equation only accounts for viscous resistance and neglects inertial resistance, the above approach for calculation of permeability to the air is valid only when inertial resistance is low, that is, at low Reynolds numbers. In [1], it is pointed out that the Darcy's equation should be valid if  $Re < 2$ .

In [2], Re number was defined as follows:

$$\text{eq. 5.4} \quad Re = \rho Q / (A m S_v)$$

where  $\rho$  is the density of fluid;  $S_v$  (Specific Surface) is surface area of fibers per unit volume of the bed,  $m^2/m^3$  and the other quantities are as previously defined. To calculate Re from eq. 5.4, it is necessary to know  $S_v$ . However,  $S_v$  can only be determined only after measuring the permeability and making some assumptions with regards to the Kozeny factor,  $k$ .

Fortunately, the applicability of Darcy's law can be verified by plotting pressure drop,  $\Delta P$ , as a function of volume flow rate  $Q$  (or superficial velocity). This dependence should be linear if Darcy's law is valid. In [3] this check was done for air flow through dry sheets using a Bendtsen porosimeter. Values of Re were also calculated using eq. 5.4, the results showed  $Re < 1$ .

In [4], the frictional pressure gradient for water permeability measurements is considered as the sum of a viscous resistance that is proportional to  $Q$  and an inertial resistance for water that is proportional to  $Q^2$ . In this case the Kozeny factor must be treated as a variable that is a function of inertial resistance. At a Reynolds number of unity, the inertial resistance was about 4% of the total filtration resistance. For most wood pulps, constant-rate filtration results in a water velocity of 1.4 cm/s. At that velocity the inertial resistance is only 1-2% of the total pressure drop.

Bendtsen and Gurley porosimeters were used to measure air flow through white copy paper (BW=75gsm; thickness  $L=95\text{mcm}$ ). The resultant Gurley reading was 11 s/100cc, which is close to the measurement obtained for some previously examined wet sheets. It represents one of the higher velocities obtained in the permeability testing performed during the steam heating test. It therefore represents one of the high Reynolds numbers that was obtained during that testing. Superficial velocities were calculated from the instrument readings, the results are shown in Table 5.1 and are plotted in Figure 5.1. Figure 5.1 shows a linear relationship between  $\Delta P$  and superficial velocity, verifying that Darcy's Law is applicable. This result also provides justification for using air permeability as a measure of wet sheet "openness" to steam penetration.

Tester Used	Pressure Differential mm H <sub>2</sub> O	Superficial Velocity of Air cm/s
Gurley Porosimeter	123.4	1.405
Bendtsen Porosimeter	75	1.057
Bendtsen Porosimeter	150	2.097
Bendtsen Porosimeter	225	3.089

Table 5.1 Gurley and Bendtsen Testing

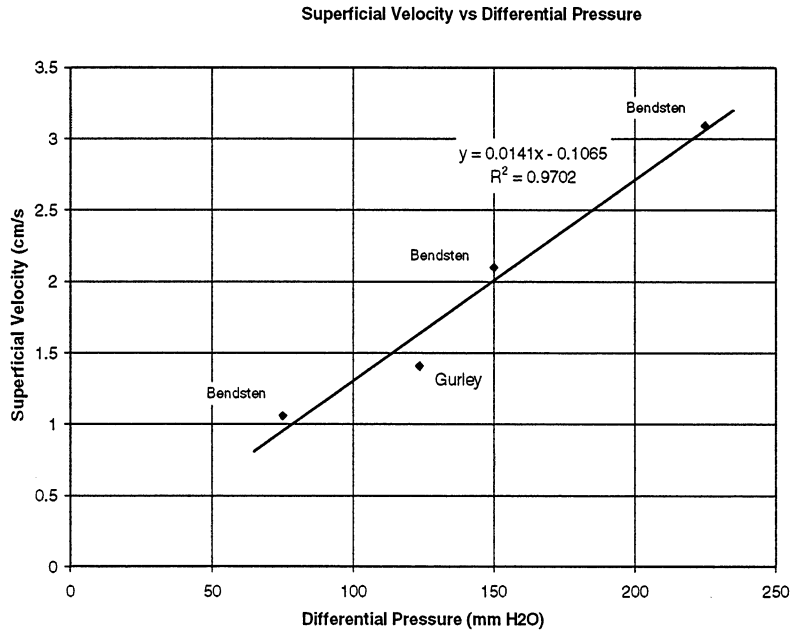


*Figure 5.1 Gurley and Bendtsen Testing*

### 5.3 Interrelation Between Water and Air Permeability

Work was initiated to develop a correlation between water and air permeability. Water permeability has been used extensively at IPST. However, water permeability testing is a complicated process. Developing a correlation between the two permeabilities has the potential of further validating air permeability as a measure of sheet openness for steaming. It also has the potential of providing an alternative test to water permeability. Preliminary results suggest that there is a correlation between the two permeabilities based on the porosity of the sheet. Additional testing is in progress.

### 5.4 References

1. Robertson, A.A., and Mason, S.G., Specific Surface of Cellulose Fibers by the Liquid Permeability Method. Pulp Paper Mag. Can., 50: 103-109. (Dec 1949).
2. Carlsson, G., Lindstrom, T., Floren, T., Permeability to Water of Compressed Pulp Fiber Mats. Svensk Papers., 86: R128-R134. (1983)
3. Knauf, G.H., Doshi, M.R., Calculation of Aerodynamic Porosity, Specific Surface Area, and Specific Volume from Gurley Second Measurements. IPC Tech. Ser. no.183: 7p. (June 1986).
4. Ingmanson, W.L., Andrews, B.D., High-Velocity Water Flow through Fiber Mats. Tappi J.,46(3): 150-155 (1963).

## 6. Jet Impingement Literature Search

### 6.1 Introduction

Impinging jets are widely used for their enhanced transport characteristics, primarily drying through evaporation. There is considerable literature on the use of impinging jets for that purpose. The steambox is also an example of a device which employs impinging jets. In the case of a steambox, the objective is not drying. However, the jets from a steambox are used for heat and mass transport. In the paper industry, there is little agreement on the jet types or configurations which are optimum for web heating. Thus, a literature search was undertaken to determine if the general literature on the subject of jet impingement could yield some insight. This work is the first step in developing an understanding of what occurs between the jet nozzles on the underside of the steambox and the top surface of the sheet. Understanding the fundamentals of this process will allow more efficient implementation of steamboxes and may also provide insight for enhanced steambox designs.

A typical impinging jet is illustrated in Figure 6.1, the nozzle with a diameter  $D$  (or slot width  $w$ ) issues steam (or gas) to an impinging surface. The distance from the nozzle to the surface is  $H$ . The flow field can be divided into three characteristic regions: free jet, stagnation flow, and wall jet.

The free jet may consist of a potential core, developing flow, and a developed flow region. In the stagnation region, flow makes a  $90^\circ$  turn. Here, static pressure first increases sharply with a corresponding drop in axial velocity, then drops as the flow accelerates along the impingement surface. Hence, in this region, there is significant favorable pressure gradient on the surface.

The end of stagnation region in the lateral direction, defined as the location where pressure gradient becomes zero, is reported to be around  $0.35\text{-}0.6H$  from the impingement point. Beyond the stagnation region, in the wall jet region, the pressure gradient in the lateral flow direction is essentially zero while the fluid boundary layer over the impingement surface grows.

For a multiple jet system, such as arrays of nozzles, there are secondary stagnation zones where the wall jets from adjacent jets impinge upon each other. Characteristics of this region are highly dependent on the spacing between the nozzles and the type of outflow used.

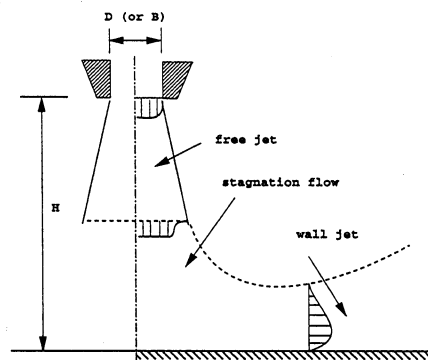


Figure 6.1 Impingement Jet

Many variables and effects need to be considered for proper design of such impinging jet systems: the steam flow rate, the diameter or slot width of the nozzle, nozzle-to-nozzle spacing, nozzle-to-surface distance, nozzle configuration, location of exhaust ports (used extensively in dryer applications), cross flow, jet exit velocity and surface motion, and the permeability of the impinging surface. For a permeable paper sheet, additional enhancement of heat and mass transfer occurs when a vacuum device is used under the paper sheet. Comprehension and quantification of these multiple effects is critical for an efficient design.

## 6.2 Jet Flow

Like any boundary layer flow, for a given set of geometric conditions, impingement heat transfer rates increase as jet flow increases. High jet flow implies a high Reynolds number and intensive turbulence. An approximate relation describing the dependency of an average Nusselt number on Reynolds number is expressed as  $Nu = b * Re^a$ , where the proportionally constant "b" and the exponent "a" are reported as functions of geometric parameters. Experimental results show that "a" is in the range of 0.5 to 0.8 for a single round nozzle [1]. For a single slot jet, "a" is close to 0.65 [2]. These results are for non steambox applications.

## 6.3 Nozzle Geometry

Since different nozzle designs produce different nozzle exit velocity profiles, it is generally believed that the nozzle design appreciably affects the impingement surface heat transfer profiles. The nozzle exit turbulence is also affected by the nozzle design. Pan et al. [3] studied the flow structure and heat transfer characteristics of turbulent and the effect of selected nozzle configurations on the local heat transfer in the stagnation zone. They employed four different nozzle configurations: pipe-type jet, sharp-edged orifice with screens, sharp-edged orifice without screen and contoured orifice. For the case of single, axisymmetric turbulent water jets, the sharp-edged orifice without turbulence-damping screens provided the highest heat transfer coefficients, followed by the sharp-edged orifice with screens, the fully developed pipe-type nozzle, and finally, the contoured orifice. To control the normal force on the impingement surface, Seyed-Yagoobi and his colleagues [4] studied the impinging heat transfer with radial jet reattachment nozzle and self-oscillating jet impinging nozzle. Lee et al [5] studied the impinging heat transfer by elliptic jets.

## 6.4 Nozzle-to-Plate Spacing

The effect on impingement heat transfer of the nozzle-to-plate distance is again related to the flow and turbulence characteristics of a free jet. Gardon and Akfirat [6] studied local as well as average heat transfer coefficients between an isothermal plate and impinging two-dimensional air jets for both single jets and arrays of jets. They derived a relation between heat transfer coefficients and nozzle-to-jet spacing. Saad [10] studied the contoured entry slot nozzles in a multiple jet system, he found that average heat transfer coefficients in the range of  $4w < H < 8w$  are almost independent of  $H/w$ . For single jets with contoured slot nozzle, Polat et al. [7] found that the average heat transfer coefficients increase with increasing distance from the nozzle exit for  $H/w$  values of up to 6.

Lytle and Webb [7] considered the heat transfer characteristic of air jet impingement at nozzle-plate spacings of less than one nozzle diameter. They found a power-law relationship between Nusselt number and nozzle-plate spacing of the form  $Nu \approx (H/D)^{-0.288}$ .

Gardon et al. [6] noted that the heat transfer in the impingement stagnation region is maximum when the nozzle is 6-7 diameters away from the plate.

According to Huber and Viskanta [9], the maximum Nusselt number at the stagnation point for a single jet occurs when the jet-to-plate spacing is roughly equal to the length of the potential core.

These different trends show that effect of nozzle-to-plate spacing on heat transfer could vary depending on the nozzle design and the jet medium.

### **6.5 Nozzle-to-Nozzle Spacing**

The effect of nozzle-to-nozzle separation distance is naturally coupled with other effects that exist in a multiple jet system. Saad et al. [10] classified multiple jets as "non-interacting" when the internozzle spacing was sufficiently wide, and "interacting" when the internozzle spacing was not wide enough. Their data indicated that in the case of multiple slot jets, for  $4 < H/w < 24$  when  $S/H > 1.5$  (where  $S$  is the spacing between adjacent jets), a multiple impinging jet system is without cross flow effects and single jet transfer data can be used effectively.

Huber and Viskanta [11] also conducted experimental studies on the effect of jet-jet spacing to heat transfer. For their particular case, it was found that, for an array jet with high nozzle-plate spacings, adjacent jet interference before impingement causes significant degradation of the convection coefficient when compared to a single jet. However, as the separation distance is decreased to one jet diameter, the adjacent jet interference before impingement is minimized and the Nusselt numbers for the array jet and single jet are similar. They also added spent air exits between the jet orifices which show increased heat transfer rate.

### **6.6 Surface Motion**

For the case of steambox preheating, the impingement plate is the fast moving paper sheet, very limited studies have been done about the effect of surface motion to the heat transfer rate. Polat and his colleagues [7], [12] provided the local heat transfer profiles at a rapidly moving surface under confined slot jets for interacting multiple jets and a single jet, respectively. Their results show that the net effect of surface motion on average heat transfer rates was found to decrease heat transfer. For both interacting and non-interacting jets, the overall effects are not large.

### **6.7 Permeable Surface with Through Flow**

For a permeable impingement surface such as paper sheet, the heat transfer rate can be enhanced further by withdrawing some of the jet flow through the surface. Research done by Polat and Douglas [12] shows enhancement is nearly uniform everywhere in the profiles. The increase is very significant. The actual effects also depend on other factors; correlations for the effect of impingement plate permeability have not been reported.

### **6.8 Other Factors**

There are many other factors that may affect the impinging jets heat transfer as well. Jet temperature will be a factor since the variation in fluid properties from nozzle exit to the surface can be substantial. In a paper by Chow and Chung [13], it was suggested the fluid properties

should be evaluated at a reference temperature given by the one-third rule, i.e., the reference temperature was chosen as one-third of steam jet temperature and two-thirds of surface temperature. However, since the superheated steam temperature is limited, so is enhancement by high jet temperature. Obot et al. [14], Goldstein and Seql [15] studied the cross flow effect on impingement heat transfer. Sparrow and Lovell [16], Chuang and Wei [17] studied the heat transfer characteristics of an obliquely impinging circular jet, which is the case when jet impinging the plate at an oblique angle.

Investigators have also tried to use novel designs and techniques to enhance heat transfer rate. For example, in a study done by Kum et al. [18], based on the fact that the area of enhanced heat transfer is limited to the neighborhood of the stagnation point, heat transfer is augmented remote from the stagnation point in an impinging plane jet system by putting a rod array located near the wall. Each square rod in the array was positioned normal to the flow direction and parallel to the flat plate surface. They found that for an optimum configuration, the average heat transfer coefficient is about 1.6 times greater compared to that without a rod array. Zumbrennen and Aziz [19] proposed a novel technique of enhancing heat transfer in impinging jet flows by briefly and repetitively interrupting the jet flow and thereby halting the development of the hydrodynamic and thermal boundary layers. Although little or no cooling (or heating) is available during a brief interval when the flow is interrupted, the thermal resistance due to the newly forming thermal boundary layers becomes much smaller each time the flow is resumed and a net enhancement can thereby arise.

## 6.9 References

1. Martin, H. Heat and Mass Transfer Between Impinging Gas Jets and Solid Surfaces. *Advances in Heat Transfer*, 13:1-60, 1977.
2. Polat, S., Heat and Mass Transfer In Impingement Drying. *Drying Technology*, 11(6):1147-1176, 1993.
3. Pan, Y., Stevens, J., Webb, B. W., Effect of Nozzle Configuration on Transport in the Stagnation Zone of Axisymmetric, Impinging Free-Surface Liquid Jets: Part 2 - Local Heat Transfer. *ASME Journal of Heat Transfer*, 114:880-886, 1992.
4. Seyed-Yagoobi, J., Enhancement of Heat and Mass Transfer with Innovative Impinging Jets. *Drying Technology*, 14(5):1173-1196, 1996.
5. Lee, S., Lee, J., Lee, D., Local Heat Transfer Measurements from and Elliptic Jet Impinging on a Plate Using Liquid Crystal. *International Journal of Heat and Mass Transfer*, 37(6):967-976, 1994.
6. Gardon, R., Akfirat, J.C., Heat Transfer Characteristics of Impinging Two-dimensional Air Jets. *ASME Journal of Heat Transfer*, 88:101-108, 1966.
7. Polat, S., Huang, B., Mujumdar, A. S., Douglas, W. J. M., Numerical Flow and Heat Transfer Under Impinging Jets: A Review. *Annual Review of Numerical Fluid-Mechanics and Heat Transfer Volume II*, Pages 157-197, 1991.
8. Ltyle, D., Webb, B. W., Air Jet Impingement Heat Transfer at Low Nozzle-plate Spacings. *International Journal of Heat and Mass Transfer*, 37(12): 1687-1697, 1994.

9. Huber, A. M., Viskanta, R., Effect of Jet-Spacing on Convective Heat Transfer to Confined, Impinging Arrays of Axisymmetric Air Jets. *International Journal of Heat and Mass Transfer*, 37(18):2859-2869, 1994.
10. Saad, N. R., Polat, S., Douglas, W. J. M., Confined Multiple Impinging Slot Jets without Cross Flow Effects. *International Journal of Heat and Fluid Flow*, 13:2-14, 1992.
11. Polat, S.,
12. Polat, S.,
13. Chow, L. C., Chung, J. N., Evaporation of Water into a Laminar Stream of Air and Superheated Steam. *International Journal of Heat and Mass Transfer*, 26(3):373-380, 1983.
14. Obot, N. T., Trabold, T. A., Impingement Heat Transfer Within Arrays of Circular Jets: Part I - Effects of Minimum, Intermediate, and Complete Cross Flow for Small and Large Spacings. *ASME Journal of Heat Transfer*, 109:872-879, 1987.
15. Goldstein, R. J., Seol, W. S., Heat Transfer to a Row of Impinging Circular Air Jets Including the Effect of Entrainment. *International Journal of Heat and Mass Transfer*, 34(8):2133-2147, 1991.
16. Sparrow, E., Lovell, B. J., Heat Transfer Characteristics of and Obliquely Impinging Wall Jet. *ASME Journal of Heat Transfer*, 102:202-209, 1980.
17. Chuang, S. H., Wei, C. Y., Computations for a Jet Impinging Oblique on a Flat Surface. *International Journal of Numerical Methods Fluids*, 12:637-653, 1991.
18. Kum S. M., Kawaguchi, Seo, J. Y., Study of Heat Transfer Enhancement by Square Rod Array in Impinging Jet System. *Japan Society of Mechanical Engineers, Part B*, 61:3289-3295, 1995.
19. Zumbrunnen, D. A., Aziz, M., Convective Heat Transfer Enhancement Due to Intermittancy in an Impinging Jet. *ASME Journal of Heat Transfer*, 115:91-98, 1993.

## 7. Plan for Third Steambox Experiment

### 7.1 Introduction

The primary objective of the third steambox experiment is to verify the permeability relationship that was developed as a result of the 2<sup>nd</sup> Steambox Comparator experiment. Specifically, the energy absorbed by the sheet through steam condensation is proportional to the permeability of the sheet and the vacuum level that is used. This relationship is shown in Figure 7.1. The data used to develop Figure 7.1 was obtained using the following sheet types

- Virgin Kraft softwood, 400 & 600 CSF, 25% & 45% solids, 123g/m<sup>2</sup> & 205 g/m<sup>2</sup>
- OCC, 400 & 600 CSF, 25% and 45% solids, 123g/m<sup>2</sup> & 205 g/m<sup>2</sup>.

While this represents a total of 16 different sheet types, the range of sheets tested was not great. The 3<sup>rd</sup> experiment is intended to remedy this lack of scope by testing a wider range of fibers types and basis weights. The hypothesis for this work is that fiber type will not alter the relationship; permeability is the primary factor determining steam energy absorbed by the sheet.

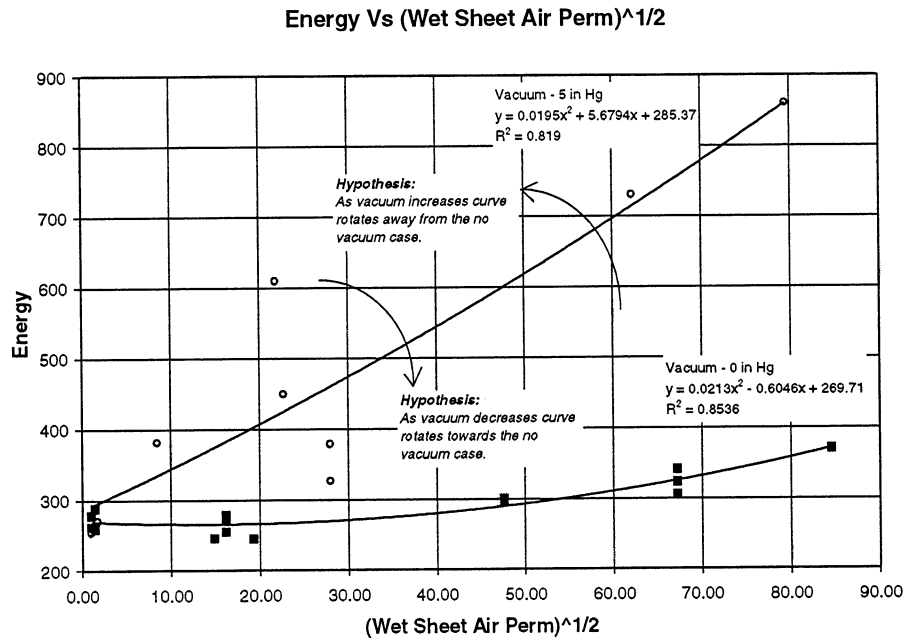


Figure 7.1 Energy Absorbed by the Sheet vs Sheet Permeability

### 7.2 Test Plan

The fiber types that will be tested are

- Softwood (southern pine), kraft, unbleached
- Softwood (non southern pine), kraft, unbleached
- OCC, unbleached
- Softwood kraft, bleached



intent is to demonstrate that the previously developed relationship is valid over a wide range of conditions. The experimental matrix for a single furnish is shown in Table 7.2.

Furnish	A																							
Permeability	High			Medium			Low																	
Basis Weight	High		Medium	Low		High		Medium	Low															
Vacuum	H	M	L	H	M	L	H	M	L	H	M	L	H	M	L	H	M	L	H	M	L	H	M	L

*Table 7.2 Part 3 Experimental Matrix*

If Part 2 of the experiment shows that the steam energy absorbed is not independent of furnish, then this matrix will be reexamined.

### 7.3 Related Pressing Study

The planned steambox experiment provides an opportunity to expand on the MTS pressing work reported on in Member Report 5 for this project. The reported work dealt exclusively with linerboard sheets made from OCC and the response of those sheets to heating. A similar set of experiments will be performed using the same furnishes as will be used for the steambox experiment. The objective will be to determine if there is a similar dependence of water removal and final sheet properties on both sheet moisture profile and sheet temperature. An additional aspect of the study will be a microscopic examination of selected sheets. The objective will be to determine if heating followed by pressing produces structural changes within the sheet which can be correlated with either the water removal or final sheet properties. Some work was done previously in this area, however the results were inconclusive. The reason for the lack of conclusive results is believed to have been due to the furnish and an inadequate pressing pulse.

### 8. Steambox Implementation Guidelines

A final product of this research is intended to be a set of guidelines/procedures for the implementation of steambox preheating. Such a set of guidelines, necessarily must address the following questions:

**Pressing Objective**

1. What is the objective of employing web steam heating, Water Removal, Improved Sheet Properties.

**Evaluation of Heating Potential and Prospective Steamboxes**

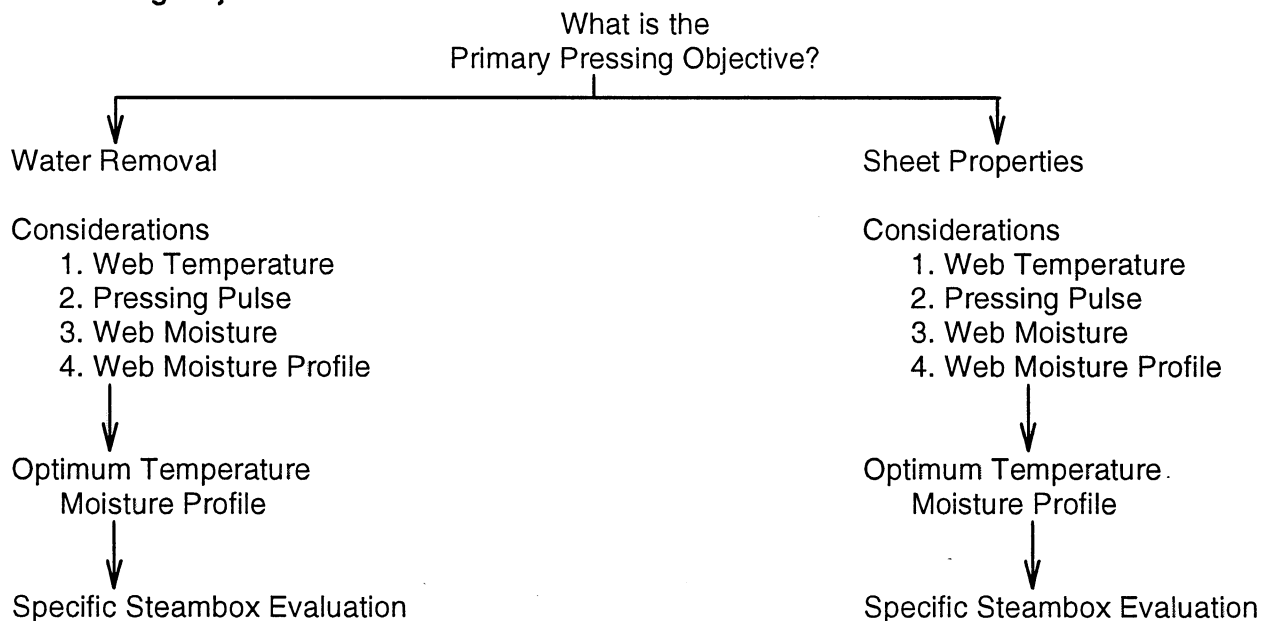
2. At press X in the machine, what temperature and moisture profile is required to obtain the desired water removal and sheet properties?
3. At press X in the machine, is there a steambox which can provide the desired temperature and moisture profiles?

**Evaluation of Total Machine Efficiency**

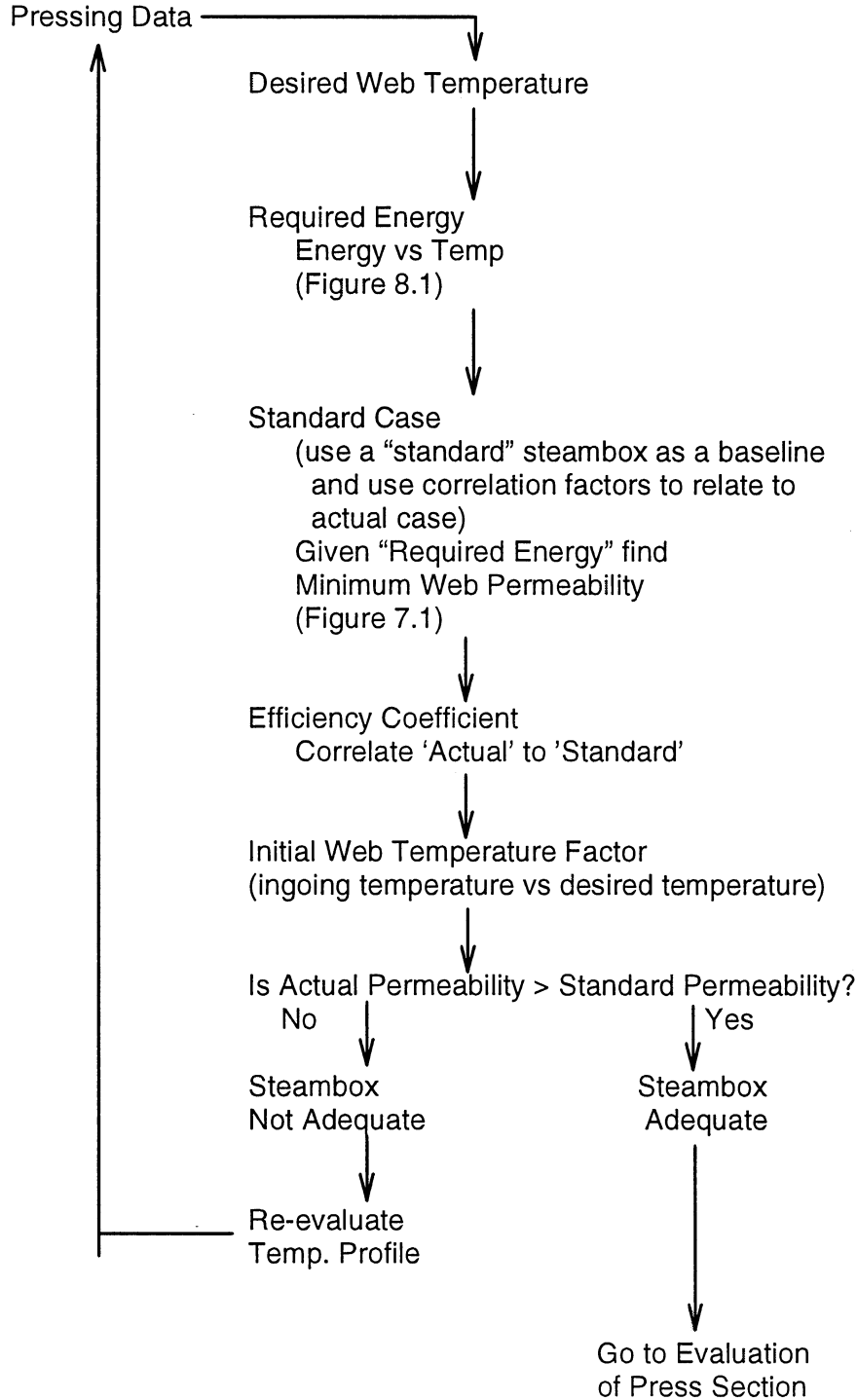
4. Assuming there are steamboxes which can provide the desired temperature/moisture profiles at presses X<sub>1</sub>, X<sub>2</sub>, and X<sub>3</sub>, what are the most effective/efficient places to place the steambox(es)?

A potential sequence for evaluation of steambox implementation is given in the following flow charts. The objective of the proposed guidelines is to fill in the blanks in those flow charts.

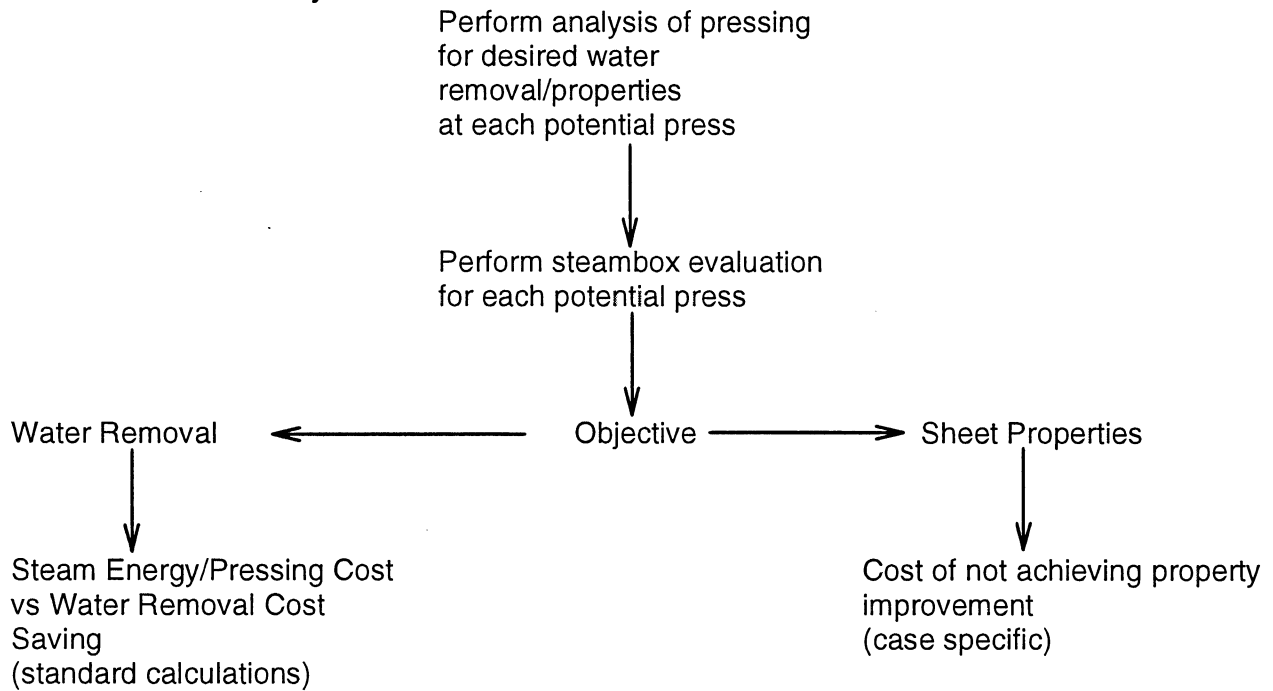
#### 1. Pressing Objective



**2. Evaluation of Specific Steambox at Specific Location**



### 3. Press Section Analysis



Energy Required for Temperature Rise at Various Basis Weights

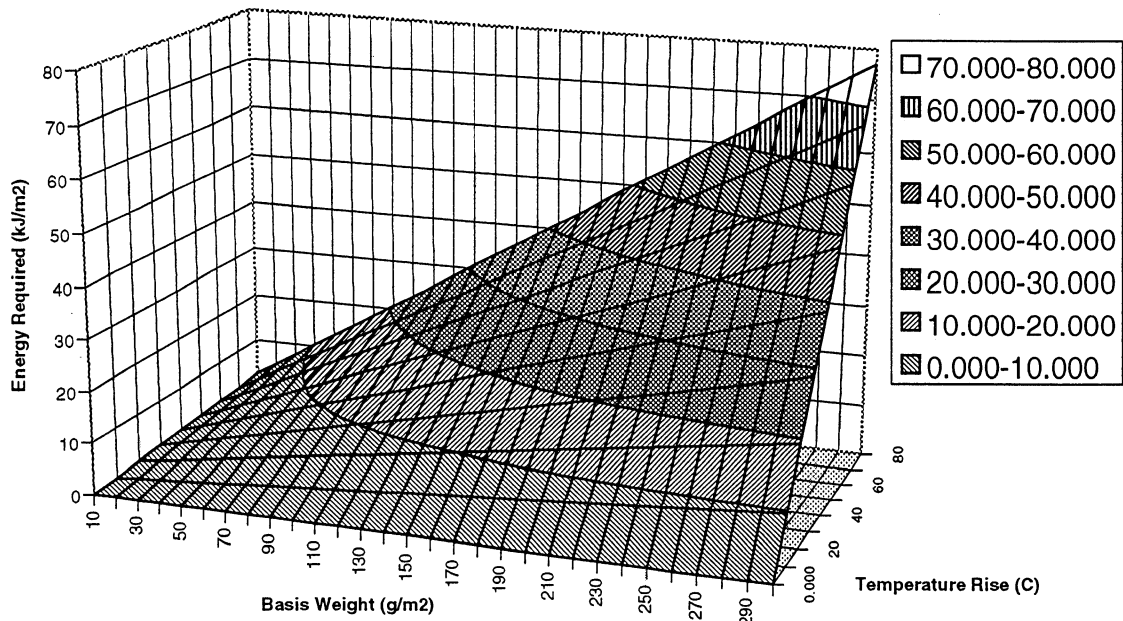


Figure 8.1 Energy vs Temperature Rise

Energy Vs (Wet Sheet Air Perm)<sup>1/2</sup>

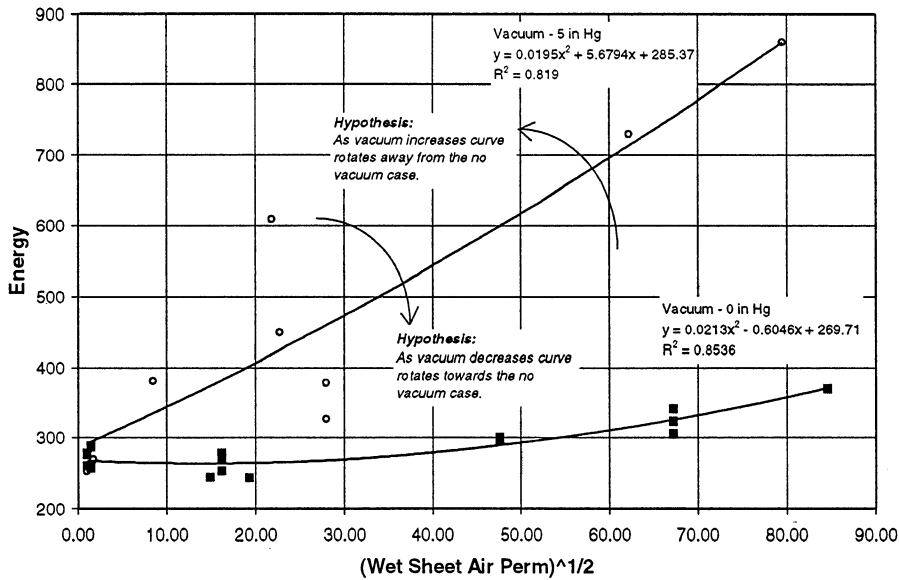


Figure 8.2 Energy Absorbed vs Permeability

